NSWCCR/RDTR-93/040

CHARACTERIZATION AND CALIBRATION OF THE AGEMA 880+ IMAGING RADIOMETER

Tim Bradley
Jeff Hendrixson (Comarco, Inc.)

PREPARED BY

ORDNANCE ENGINEERING DIRECTORATE

CRANE DIVISION, NAVAL SURFACE WARFARE CENTER

CRANE, INDIANA

23 AUGUST 1993

APPROVED FOR PUBLIC RELEASE; DISTRIBUTION IS UNLIMITED

THIS PAGE INTENTIONALLY LEFT BLANK.

REPORT DOCUMENTATION PAGE

Form Approved
OMB No. 0704-1088

1. AGENCY USE ONLY *(Leave blank)*	2. REPORT DATE 23 AUGUST 1993	3. REPORT TYPE AND DATES COVERED FINAL TEST 1 JANUARY - 23 AUGUST 1993

4. TITLE AND SUBTITLE

CHARACTERIZATION AND CALIBRATION OF THE AGEMA 880+ IMAGING RADIOMETER

5. FUNDING NUMBERS

6. AUTHOR(S)

TIM BRADLEY (Code 4072)
JEFF HENDRIXSON (COMARCO, INC.)

7. PERFORMING ORGANIZATION NAME(S) AND ADDRESS(ES)

COMMANDER
(CODE 40)
NAVSURFWARCENDIV
ORDNANCE ENGINEERING DIRECTORATE
OPERATIONS RESEARCH BRANCH
CRANE IN 47522-5001

8. PERFORMING ORGANIZATION REPORT NUMBER

NSWCCR/RDTR-93/040

9. SPONSORING/MONITORING AGENCY NAME(S) AND ADDRESS(ES)

NAVSURFWARCENDIV
ORDNANCE ENGINEERING DIRECTORATE
OPERATIONS RESEARCH BRANCH

10. SPONSORING/MONITORING AGENCY REPORT NUMBER

11. SUPPLEMENTARY NOTES

12a. DISTRIBUTION/AVAILABILITY STATEMENT

APPROVED FOR PUBLIC RELEASE;
DISTRIBUTION IS UNLIMITED

12b. DISTRIBUTION CODE

13. ABSTRACT ***(Maximum 200 words) WITH TRADITIONAL FLARE MEASUREMENTS, A FLARE IS ASSUMED TO BE A POINT SOURCE SINCE IT IS A RELATIVELY SMALL TARGET VIED AT A RELATIVELY LONG RANGE. HOWEVER, WHEN THE FLARE AREA BECOMES SUFFICIENTLY LARGE IN RELATION TO THE VIEWING RANGE THE FLARE MUST BE TREATED AS AN EXTENDED SOURCE AND THE SPATIAL CHARACTERISTICS OF THE FLARE MUST BE CONSIDERED. THE ABILITY OF AN IMAGING RADIOMETER TO PROVIDE SPATIAL INFORMATION MAKES THIS INSTRUMENT IDEAL FOR AREA TYPE FLARE MEASUREMENTS. THIS REPORT OUTLINES A SERIES OF CALIBRATION AND CHARACTERIZATION PROCEDURES PERFORMED ON THE AGEMA 880+ THERMAL IMAGER. THE PROJECT OBJECTIVES WERE TO 1) VERIFY THE ACCURACY OF 880+ MEASUREMENTS, 2) PERFORM AN EXTERNAL CALIBRATION OF THE 880+ SYSTEM, AND 3) REDUCE RADIOMETRIC DATA AND PRODUCE FALSE COLOR IMAGES. THE WORK WAS PERFORMED AT THE NAVAL SURFACE WARFARE CENTER - CRANE DIVISION (NSWC-CD).***

14. SUBJECT TERMS

CALIBRATION; IMAGES; IMAGE PROCESSING; INFRARED MEASUREMENTS; RADIOMETRY; THERMAL IMAGER

15. NUMBER OF PAGES
94

16. PRICE CODE

17. SECURITY CLASSIFICATION OF REPORT	18. SECURITY CLASSIFICATION OF THIS PAGE	19. SECURITY CLASSIFICATION OF ABSTRACT	20. LIMITATION OF ABSTRACT
UNCLASSIFIED	UNCLASSIFIED	UNCLASSIFIED	SAR

THIS PAGE INTENTIONALLY LEFT BLANK.

TABLE OF CONTENTS

LIST OF FIGURES

LIST OF TABLES

LIST OF APPENDICES

ACKNOWLEDGEMENTS

The success of this project is not the product of just the authors of this report. A project of this magnitude requires a great deal of technical support as well as planning and coordination. Therefore, the authors wish to express their appreciation to the following people: Mr. Eric Hillenbrand from the Naval Surface Warfare Center Crane Division, Crane , Indiana; Mr. Albert J. Bolander, Mr. Gary P. Hart, and Mr. Mark E. Halter from Comarco Inc., Bloomfield, Indiana; and special thanks to Mr. Douglas S. Fraedrich of the Naval Research Laboratory, Washington, D.C. for his pioneering work with the Agema 880 that shaped the testing of this project.

LIST OF ABBREVIATIONS

µm	micrometer
BRUT	Burst Recording Unit
CVF	Circular Variable Filter
FOV	Field Of View
InSb	Indium Antimonide
IR	Infrared
MS-DOS	MICROSOFT® Disk Operating System
OCLI	Optical Coating Laboratories, Inc.

1.0 INTRODUCTION.

1.1 Purpose. This report outlines a series of characterization tests and calibration procedures performed on the Agema 880+ Thermal Imager (880+). The purpose of these tests was to determine the feasibility of obtaining calibrated imagery of area sources. The 880+ will also be evaluated to determined the potential of measuring point sources. The objectives of this test are 1) verify the accuracy of 880+ measurements, 2) perform an external calibration of the 880+, and 3) reduce radiometric data and produce false color images.

1.2 Background. With traditional flare measurements, a flare is assumed to be a point source since it is a relatively small target viewed at a relatively long range. However, when the flare area becomes sufficiently large in relation to the viewing range, the flare must be treated as an extended source and the spatial characteristics of the flare must be considered. The ability of an imaging radiometer to provide spatial information makes this instrument ideal for area type flare measurements.

1.3 Scope. This report will cover characterization and calibration procedures performed in the laboratory. The work performed on this effort is similar to that of Fraedrich[1].

Section 2.0 is a description of the Agema 880+ Thermal Imager. Section 3.0 discusses the laboratory procedures and results. Sections 4.0 and 5.0 are the conclusions and references respectively. Appendix A provides a brief description of the apparatus used in the lab procedures. Appendix B contains all of the data collected in the laboratory. Appendix C contains a brief description of the computer programs that were used for this project.

THIS PAGE INTENTIONALLY LEFT BLANK.

2.0 DESCRIPTION OF THE AGEMA 880+ THERMAL IMAGER.

The 880+ imaging radiometer is a real-time infrared imaging system consisting of the Agema 880+ optical head, a Burst Recording Unit (BRUT), a cable connector, a high resolution video monitor, and a computer terminal. Infrared radiation is converted into a video signal by the optical head and the video signal is sent directly to the BRUT. The BRUT relays the signal, in real time, directly to the video monitor. The computer terminal provides the interface between the user and the BRUT. A brief description of the optical head and the BRUT follows.

2.1 Agema 880+ Optical Head. The optical head converts electromagnetic thermal energy into an electronic video signal. This video signal is then amplified and sent to the BRUT. The optical head consists of an electro-optical scanning mechanism, an infrared detector, a video interface, and the control electronics and microprocessor.

Figure 1 provides a cut-away view of the 880+ optical head[2]. The infrared radiation is focused by an infrared lens into an oscillating mirror. The optical output from the oscillating mirror is focused by three fixed mirrors onto a horizontal mirror polygon which rotates at 16000 rpm. The oscillating mirror provides vertical scan while the rotating polygon mirror provides horizontal scan. The on-board microprocessor controls both units. The two mirrors are synchronized such that a single image is actually comprised of four interlaced fields. Each field consists of 70 complete horizontal scans of 140 samples which creates a frame of 140 by 280 pixels.

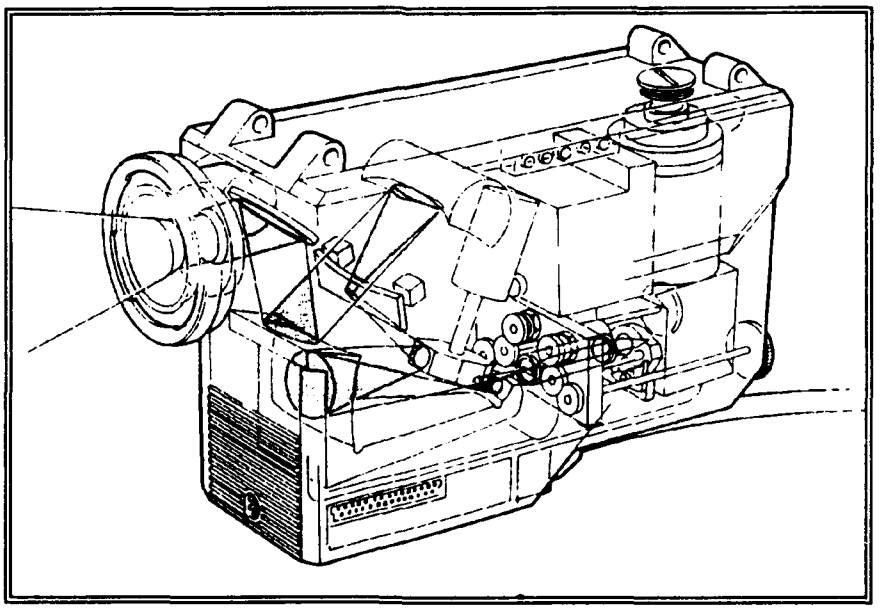

FIGURE 1. AGEMA 880+ OPTICAL SCANNING HEAD.
Thermovision 880 Operating Manual

The first scan of field number 1 is followed by the first scan of field number 2 and so forth. A total of 25 fields (or 6.25 frames) are scanned per second. The horizontal polygon mirror also periodically scans two internal "blackbody" sources to adjust for ambient temperature drift. This internal source allows for measurements of objects without an external reference, and also allows for good measurements over time with a single calibration.

The reflected beam from the polygon mirror is passed through a selectable filter and aperture. The apertures are designed so that "hot" objects can be measured without the use of neutral density filters. There are three possible filter selections: no filter, blue filter (2.0 - 2.5 μm), and yellow filter (3.8 - 4.6 μm). The filter response curves are included in Appendix A. The filter selection can be made in conjunction with any aperture setting.

After passing through the filter and aperture, the optical beam is focused onto the detector. The detector is a liquid nitrogen cooled Indium Antimonide (InSb) element (photovoltaic) covering the spectral band from 2.0 - 5.0 μm. Plots of the spectral response of the detector and optics appear in Appendix B. The InSb detector is operated in the photovoltaic mode and the voltage output is converted into a video signal. The video signal is sent, via cable, to the BRUT.

2.2 Burst Recording Unit (BRUT).[3] The BRUT provides control to the 880+ optical head and also provides the means of storing and reviewing data from the 880+. The video signal sent from the 880+ is collected by the BRUT and sent to an analog to digital converter. Utilizing the computer terminal, the user can instruct the BRUT to record the images. When in the RECORD mode, the digital data is continuously assembled to full frame images in the *frame* memory and sent through a *level & range* unit to the display monitor where they are presented, in real time, to the user. The *level & range* unit is user selectable and sets the range and level of temperatures to be displayed. Within the RECORD mode there is also a STOP mode and a GO mode. If in the GO mode, the assembled frames are sent to the *sequence* memory (a segmented Winchester hard-drive.) The recorded data can then be retrieved by the BRUT for playback. When in the PLAYBACK mode, the images are sent from *sequence* memory to the *frame* memory and then on to the display monitor via the *level & range* unit.

Image sequences in the *sequence* memory will be lost when the BRUT is powered down. However, these images can be permanently stored on either tape streamer or floppy disk. Sequences are dumped consecutively onto the tape streamer. Floppy disk storage is in MICROSOFT® Disk Operating System (MS-DOS) format and the sequence must be dumped as single frames, one at a time. Sequences on tape streamer can be reloaded onto the BRUT for later analysis.

Images that are located in the *frame* memory (either from the RECORD or PLAYBACK mode) can be measured for radiometric quantities. Measurements include temperature, radiance, and sample value (from the 13-bit data). These values can be measured either by performing an area paint or by setting a spot meter. With the area paint, the user "paints" an area of pixels. The spot meter simply provides measurements at the user selected "spot" in the image. Isotherms and histograms are also possible.

THIS PAGE INTENTIONALLY LEFT BLANK.

3.0 METHODS AND PROCEDURES.

Since the 880+ was not specifically designed to acquire radiometric measurements of infrared countermeasure flares, a series of characterization tests was developed to determine the feasibility of using the 880+ for such a task. These tests were designed to provide familiarity of the device to the end users, determine the accuracy of measurements with the 880+, acquire an external calibration of the system, and to exploit the image quality of the 880+ in the form of false color images, histograms, contour maps, etc. The testing was divided into three broad categories: System-Level Characterizations; Radiometric Measurements; and Data Reduction and Analysis.

3.1 System Level Characterizations. This section addresses the ability of the 880+ to accurately measure radiant energy from extended (area) infrared sources. Tests were conducted to determine the accuracy of temperature measurement in general, the spectral response of the 880+ system, and the transmission of the primary lenses.

3.1.1 Temperature Measurements and Error Determination. The InSb detector used in the 880+ system is not a temperature measuring device. It is actually a photon counter. However, an estimate can be made of the target temperature by evaluating the measured signal over the range from the imager to the target. The software provided with the BRUT is designed to estimate the target temperature and radiance. The following procedure was designed to determine the level of accuracy of the 880+ system to acquire a temperature estimate.

Several blackbody sources with varying aperture sizes were viewed by the 880+ through an off-axis reflecting collimator. The target area was controlled by varying the aperture size of the blackbody source. Over the period of the test, the temperature of the blackbody was varied from 300°C through 1200°C. This temperature range corresponds to the expected range of flare irradiances encountered in actual testing. At each blackbody temperature setting, the actual temperature was measured with a calibrated thermocouple and then this value was compared to the temperature reported by the 880+. Temperature measurement with the 880+ is accomplished by doing an area paint with the 880+ BRUT software (see section 2.0 for an explanation of the BRUT). These data are presented in Appendix B, Tables B1 - B7, along with radiance values calculated from the two temperatures.

Figures 2 and 3 (page 9) show the average error in temperature measurement as a function of blackbody aperture size. Each aperture was assigned a number with the aperture size presented in ascending order, (i.e., the higher the number the larger the actual aperture size). Figure 2 presents the error for measurements taken at 300°C. Figure 3 presents the error for measurements taken at 900°C.

As can be seen in Figures 2 and 3 the accuracy of temperature measurement of the 880+ decreases significantly as the target size decreases. For small distant targets where the target only fills one or two pixels (or less than one pixel) the 880+ may not produce an accurate measurement. However, for larger targets, the temperature measurement error is generally less than five percent (5%). Some measurement error can be attributed to possible errors in the use of the calibrated temperature probe. The probe was placed inside the blackbody cavity by lab personnel and there is no assurance that it was placed in the same position each time.

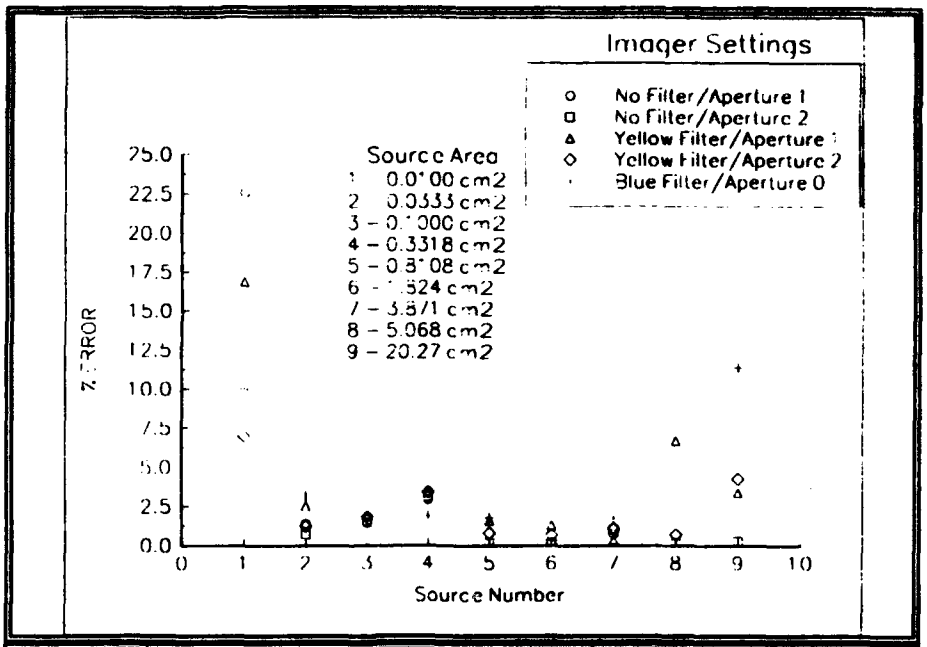

FIGURE 2. TEMPERATURE MEASUREMENT ERROR OF THE 880+ WITH A 300°C BLACKBODY SOURCE. THE APERTURE LISTED IN THE LEGEND REFERS TO THE APERTURE SELECTION OF THE 880+.

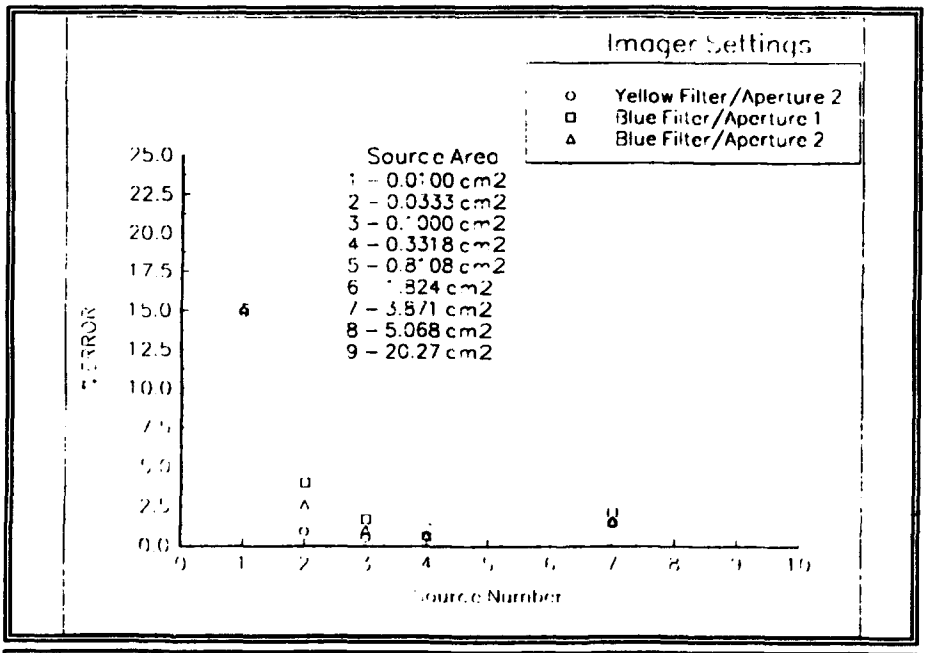

FIGURE 3. TEMPERATURE MEASUREMENT ERROR OF THE 880+ WITH A 900°C BLACKBODY SOURCE. THE APERTURE LISTED IN THE LEGEND REFERS TO THE APERTURE SELECTION OF THE 880+.

3.1.2 System Spectral Response. The response of a detector to radiant energy is known as the detector responsivity. Stated more directly, responsivity is the ability of the detector to convert electromagnetic radiation into an electrical current or voltage signal. When the absolute detector responsivity is plotted as a function of wavelength, the resultant curve is the "spectral response" of the detector. Figure 4 is the measured spectral response of the 880+ over the spectral range of the 880+ InSb detector. (There were no spectral filters in place.) This plot was constructed by dividing the measured signal of an 800°C blackbody at selected wavelengths by the calculated in-band radiance.

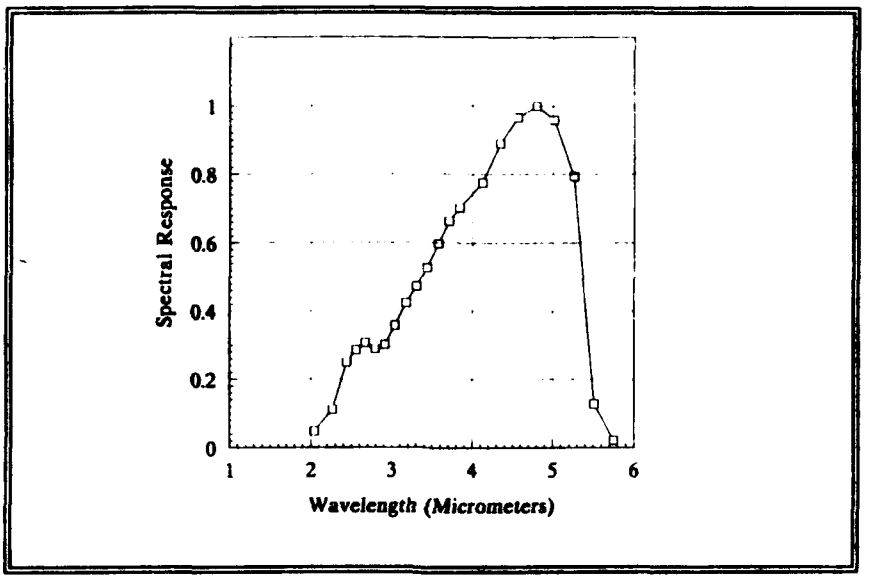

FIGURE 4. NORMALIZED SPECTRAL RESPONSE OF THE 880+ SYSTEM.

The wavelength selection was accomplished by using an Optical Coating Laboratories, Inc. (OCLI) circular variable filter (CVF) that spans the range of 2.38 to 5.95 micrometers. For each angular position, the CVF displays a specific spectral window. By measuring the signal for each "window" and then dividing the signal by the theoretical in-band radiance over that spectral band, an estimate of the spectral response can be made.

The CVF is divided into two segments. The first segment of the CVF (from 100 to 270 degrees) covers the spectral band from 2.380 to 4.650 micrometers. The second segment (from 280 to 350 degrees) covers the spectral band from 4.125 to 5.950 micrometers. The CVF was calibrated with a Perkin-Elmer 783 Infrared Spectrophotometer. Beginning at angular position 100 (degrees), the transmission of the CVF was measured at 10-degree intervals. The resultant digitized curves appear in Appendix B. Since the two segments of the CVF overlap

spectrally, they can be combined to produce a single filter that covers the spectral band from 2.380 to 5.950 micrometers. One method of combining the two segments joins segment 1 (in its entirety) with that portion of Segment 2 from 4.717 to 5.950 micrometers . The resultant curve is entitled CVF1. A second method combines the portion of segment 1 from 2.380 to 4.000 micrometers and all of segment 2. This combination is entitled CVF2. For the sake of comparison, both filters were used. The curves of the two filters are included in Appendix B.

The in-band radiance was calculated using the program PLRAD with the filters CVF1 and CVF2. In PLRAD, the in-band radiance is calculated by multiplying the normalized spectral response of the CVF (CVF1 and CVF2), the Planck function and the blackbody emissivity together. The blackbody spectral emissivity is assumed to be 1.0 (perfect blackbody) over all wavelengths. The total in-band radiance at each angular position is found by integrating the spectral radiance over the spectral band present at each CVF angular position.

The imager was then aligned so that it could observe the blackbody source through the CVF. The entire system was purged with dry nitrogen to reduce the effect of atmospheric attenuation. At each angular position, the signal from the 880+ was measured several times and averaged. The spectral response is calculated by dividing the measured signal at each angular position by the normalized theoretical in-band radiance calculated for the corresponding angular position with PLRAD. The resultant curve is then normalized and plotted.

Since the spectral transmission of the CVF cuts off below 2.38 micrometers, a pair of narrow band filters were utilized to measure the spectral response of the 880+ at wavelengths below 2.38 micrometers. The filters have spectral bands from 1.95 to 2.16 micrometers and 2.16 to 2.38 micrometers. Each was calibrated using the Perkin-Elmer spectrophotometer and their respective transmissions were normalized to the first segment of the CVF. The spectral response was then measured using the same procedure as above. These values are included in Figure 4.

Figures 5 and 6 are the spectral response of the 880+ with the yellow and blue filters respectively. These curves were created by simply multiplying the spectral response of the system and the filter transmission curve. Using the basic coded program, EVEN.EXE, values of the spectral response and the filter transmission were generated at corresponding wavelength intervals. These values were multiplied point- by-point to produce the spectral response of the 880+ with the yellow and blue filter in place.

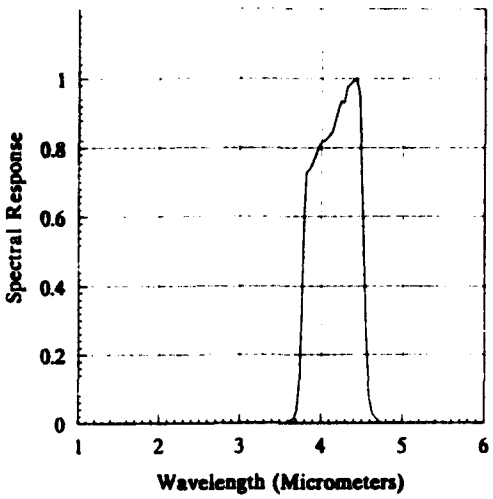

FIGURE 5. NORMALIZED SPECTRAL RESPONSE OF THE 880+ WITH THE YELLOW FILTER.

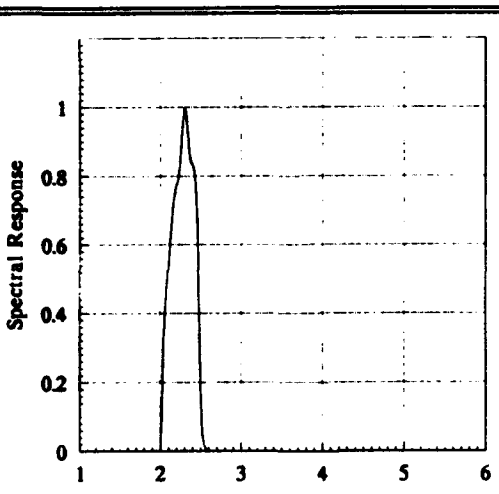

FIGURE 6. NORMALIZED SPECTRAL RESPONSE OF THE 880+ WITH THE BLUE FILTER.

3.1.3 Primary Lens Characterization. The 880+ optical system is comprised of the optical head and the primary light gathering lens. For the measurement of the spectral response of the system the 880+ was configured with a 7° FOV lens. To measure the optical transmission of the lens as a function of wavelength the spectral response measurements were repeated without the use of a primary lens. A comparison of the spectral response of the system with and without the primary lens will show the overall "flatness" of the optical coatings of the lens.

The imager head was placed approximately one inch from the CVF to obtain the optimum focus. The spectral response was then measured in the same manner as in the previous measurement. Due to physical constraints the system was not purged prior to testing. However, the range from the CVF to the imager was sufficiently small that the effects of atmospheric attenuation were quite small. The resultant spectral response of the imager minus the lens is presented in Figure 7 along with the spectral response of the system with the lens. From this plot it is evident that the spectral transmission of the lens is indeed quite flat.

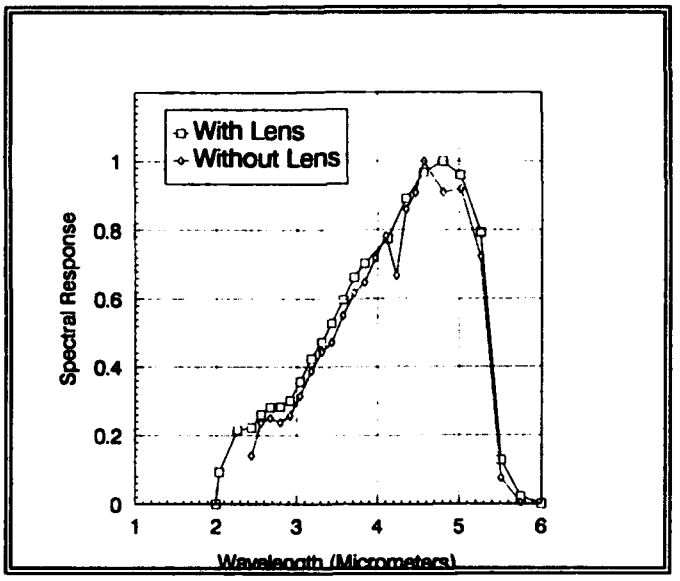

FIGURE 7. COMPARISON OF THE NORMALIZED SPECTRAL RESPONSE OF THE 880+ WITH AND WITHOUT THE PRIMARY LENS.

3.2 Radiometric Measurements. An infrared instrument, such as the 880+, collects the energy emitted by a "hot" object and focuses this energy onto a detector. The detector then converts the energy into an electrical voltage that can be accurately measured and ultimately expressed in radiometric units by utilizing well defined relationships between the voltage and the radiant energy exiting the object. Although radiometric measurement with the BRUT is possible, it is a tedious and cumbersome process that requires the user to "paint" each pixel of the desired target utilizing a mouse or keyboard. This time consuming process yields questionable results due to the large size of the paint brush and the small size of an individual pixel element.

The present section describes a method, external to the BRUT, of calculating radiometric quantities from the data. Formula derivations are included. This section also presents the methods utilized to acquire an external calibration of the 880+ and a comparison of the 880+ with other radiometers.

3.2.1 Theory. Measuring the spectral radiance of a thermal source can be an extremely difficult task. However, for a type of thermal source known as a "blackbody," the radiance can be calculated as a function of only the absolute temperature (T) and the wavelength of consideration. An object that is a perfect emitter (blackbody) of thermal electromagnetic radiation follows the Planck law:

$$M_{e,\lambda}(\lambda,T)=\frac{2\pi hc^2}{\lambda^5[e^{\frac{hc}{\lambda kT}}-1]} \qquad 3.2.1.1$$

where $M_{e,\lambda}(\lambda,T)$ = spectral radiant exitance in watts per square centimeter of area and micrometer of radiation bandwidth (W / cm^2 /micrometer),
λ = emitted wavelength in micrometers,
T = absolute temperature of the blackbody in Kelvins (K),
h = Planck's constant (6.626e-34 W sec^2),
c = speed of light (3.0e+10 cm/sec),
k = Boltzmann's constant (1.381e-23 W sec K^-1).

An object of radiant exitance M(λ,T) radiating into three-dimensional space, of solid angle Ω, can be defined by its radiance L:

$$L=\frac{M}{\Omega} \qquad 3.2.1.2$$

where the solid angle Ω is defined as the three-dimensional angular spread at the vertex of a cone, of angle θ, measured by the area intercepted by the cone on a unit sphere:

$$\Omega = 2\pi[1 - \cos(\theta)] \qquad 3.2.1.3$$

If the surface radiance of a hot object is independent of the angle of observation, that surface is known as a Lambertian radiator. By definition, the radiance emitted by a Lambertian radiator, into a detector of area dA_d, is the flux $d^2\Phi$ emitted into solid angle $d\Omega = dA_d \cos(\theta_d) / R^2$ by a source of projected area $Da_s \cos(\theta_s)$ where R is the range from the source to the detector.

$$d^2\Phi = \frac{L^s dA_s \cos(\theta_s) dA_d \cos(\theta_d)}{R^2} \qquad 3.2.1.4^4$$

The incremental radiant intensity I (W / sr) in the direction of the detector is found as:

$$dI = \frac{d^2\phi}{d\Omega_d} \qquad 3.2.1.5$$

Combining equations 3.2.1.4 and 3.2.1.5 yields:

$$dI = L^s dA_s \cos(\theta_s) \qquad 3.2.1.6$$

The total radiant intensity, I, is found by integrating equation 3.2.1.6 over the area of the source:

$$I = \int_{A_s} L^s \cos(\theta_s) dA_s (W/sr) \qquad 3.2.1.7$$

For an imaging radiometer, the radiance L^s over the surface area is not a continuous function. It is actually a summation of discrete radiance values. Each pixel represents an individual radiance value. If the radiance values over the entire image are sorted into individual bins of equal width ΔL (a histogram), the radiance then becomes a summation [Fraedrich[1]]:

$$L^s = \sum_i L_i n_i \qquad 3.1.2.8$$

where L_i is the average radiance value in bin i, and n_i is the number of pixels located in bin i. Combining equation 3.2.1.7 and 3.2.1.8 yields:

$$I = \omega R^2 \sum L_i n_i \qquad 3.2.1.9$$

where $dA_s = \omega R^2$ is the source area, ω is the average pixel solid angle, and R is the range from the detector to the source. The radiance L is related to the measured signal (S) from the source as:

$$L_i = \frac{S_i}{k\tau} \qquad 3.2.1.10$$

where k is the detector system responsivity, and τ is the atmospheric transmission across the range R. Substituting equation 3.2.1.10 into equation 3.2.1.9 and rearranging yields:

$$I = \frac{\omega R^2}{k\tau} \sum S_i n_i \qquad 3.2.1.11$$

In an arbitrary image there will always be areas of interest surrounded by areas of background noise. In the case of an infrared flare, the background generally consists of atmosphere, clouds, or possibly the carrier aircraft. The background is generally less radiant than the flare. One method of removing the background from the foreground is to segment the image. Segmentation effectively removes the cooler background from the target by setting a threshold value above which the target signature is located.

For a selected target above a threshold signal S_i, the summation in equation 3.2.1.11 becomes a simple product of S and n, where S is the average signal value of the pixels at or above the threshold, and n is the total number of pixels at or above the threshold. Therefore, the radiant intensity of a source above a threshold signal S_{th}, is found as

$$I = \frac{\omega R^2 n}{k\tau} S \qquad 3.2.1.12$$

The values S and n can be acquired directly from the frame of interest utilizing software developed specifically for this task (see section 3.2.3). The range R is acquired either from range radar data or from a laser ranger. The atmospheric transmission is calculated with PCTRAN, a personal computer version of LOWTRAN VII. The responsivity (k) and the pixel solid angle (ω) are acquired in an external system calibration.

3.2.2 External Calibration. In the paragraphs above, a relationship was derived between the signal acquired from a radiating object and the object's radiant intensity. This relationship must now be determined in the laboratory by performing a calibration of the system.

3.2.2.1 Responsivity. In doing an external calibration of the Agema 880+ Thermal Imager, there is a need for a measure of the system responsivity (k), or the system's sensitivity to radiant energy. The responsivity is defined as the ratio of the measured signal from a known source to the calculated in-band radiance of the source. The responsivity of the 880+ was determined by measuring the signal from a blackbody source over a range of temperatures from 300°C to 900°C. The testing was performed in an environmental control chamber filled with dry nitrogen to remove the effects of water vapor and CO_2 absorption. The blackbody aperture has an area of 0.3318 cm^2 and was observed by the imager through an off-axis reflecting collimator with a focal length of 65 cm. Measurements were taken for each 880+ aperture/filter combination. The temperatures and measured signals are presented in Appendix B.

The theoretical in-band radiance was calculated for each temperature using the basic coded program PLRAD. PLRAD performs an integration of the Planck function over a specified waveband. The Planck function is multiplied by the spectral emissivity of the blackbody and the spectral response of the imager system. Figure 7, presented here for illustration, is a plot of the responsivity of the 880+ with the yellow filter and aperture 2. A least-squares regression was performed on the data with the in-band radiance as the independent variable and the measured signal as the dependent variable (solid line in Figure 7). The slope of the line is the responsivity of the imager and its accompanying optics.

Table 1 lists the responsivity for each 880+ filter/aperture combination. See Appendix B for plots of responsivity for each filter/aperture combination.

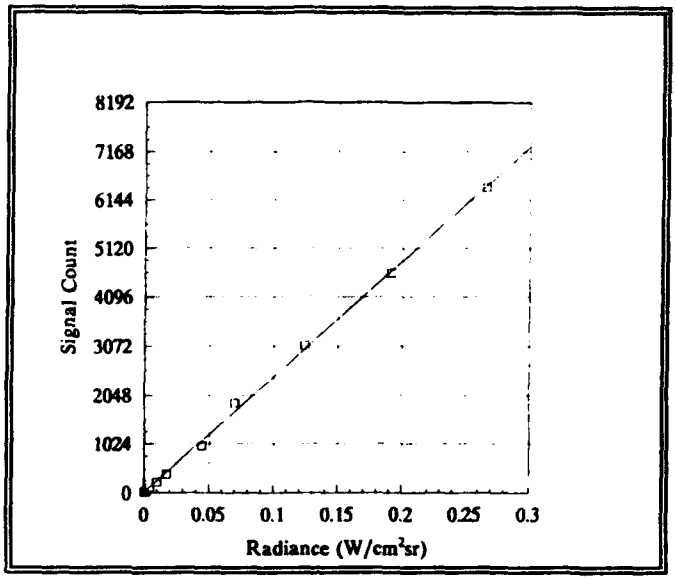

FIGURE 8. RESPONSIVITY OF THE 880+ WITH THE 7° LENS, YELLOW FILTER, AND APERTURE 2.

TABLE 1. RESPONSIVITY CONSTANTS (k) FOR THE 880+ FOR ALL COMBINATIONS OF FILTER AND APERTURE.

APERTURE	NO FILTER	YELLOW FILTER	BLUE FILTER
0	1.2821×10^{6}	1.0068×10^{6}	5.8522×10^{4}
1	1.5095×10^{5}	1.4128×10^{5}	8.2679×10^{3}
2	2.7801×10^{4}	2.4219×10^{4}	1.3114×10^{3}

3.2.2.2 Spatial Calibration. In equation 3.2.1.12, the area of the source was defined by the product of the unit solid angle of a pixel and the range to the target. Following the lead of Fraedrich[1], the unit solid angle of a pixel was found by viewing a set of square apertures and counting the number of pixels in the image of the aperture. The solid angle subtended by the aperture is divided by the number of pixels to yield the solid angle per pixel.

The apertures ranged in size from an area of 0.3325 cm^2 to 2.3226 cm^2 and were viewed at a range of 1.0 meters. The square aperture and the imager axis was aligned so that the aperture appeared in the center, top, and corner of the imager field-of-view with a measurement taken at each orientation. Utilizing the digital image software designed in-house (see section 3.2.3), the number of pixels in the image (N) of each aperture was counted. The data appear in Appendix B. A plot of the solid angle of each aperture versus N was constructed (see Figure 9) and a least-squares regression was performed on the data. The slope of this line is the average solid angle subtended by each pixel (ω).

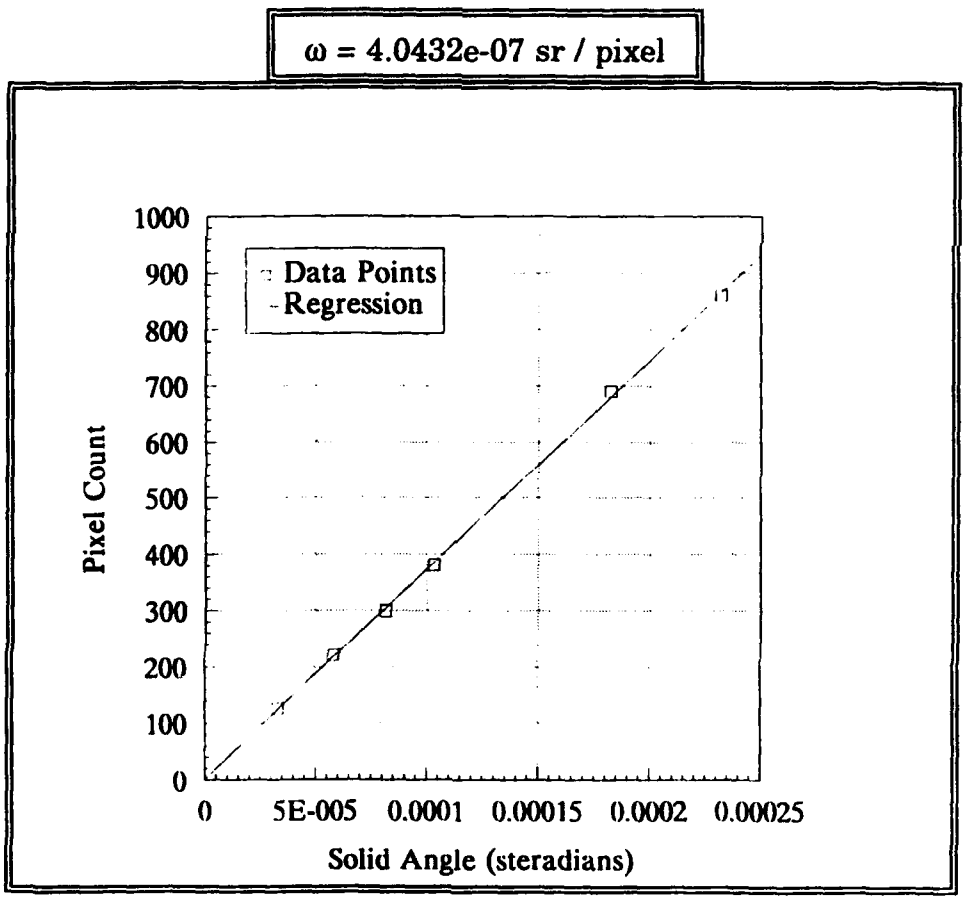

FIGURE 9. SOLID ANGLE PER PIXEL. THE SOLID LINE REPRESENTS THE LEAST-SQUARES REGRESSION OF THE DATA.

3.3 Image Analysis.

3.3.1 Image Dissection and Data Reduction. In section 3.2.1, it was shown that the radiant intensity from an infrared source could be found with the following equation:

$$I=\frac{\omega R^2 n}{k\tau}S \qquad (3.2.1.12)$$

where ω and k are calibration constants, R is the detector to target range, and τ is the atmospheric transmission. The quantities n and S (the number and average value of the pixels in the image respectively) must be obtained from the image raw data. The BRUT does allow access to the raw data for each frame or image. The data is in binary form and each frame is actually stored as four individual fields. The four fields must be interlaced to reconstruct the entire frame.

After the image is reconstructed, the image must also be dissected to locate and isolate the target from the background. This process is known as image segmentation. That is, the image is divided into disjointed regions of object and background where a region is defined as a connected set of pixels. One method of image segmentation, the method chosen for this project, divides the target object from the background by setting a numerical threshold above which the target is located. All pixels with a value at or above the threshold value are assigned to the target. Those pixels below the threshold are assigned to the background. In this way, the pixels contained within the target set can be operated on independent of the background. Much can be said about the method of selecting the threshold and there are a number of sources available that discuss optimal threshold selection[5]. This report will discuss one such method.

Since the 880+ will be used primarily to view single targets that are located on generally uniform backgrounds it is relatively simple to select the threshold. If viewed in three dimensions, the image of an infrared flare burning in the sky would look like a huge plane of relatively level ground with a mountain in the center. By locating the edge of the "mountain", one can isolate the flare from the background. To accomplish this, an image analysis software program, IMAGER.EXE, was created. The BASIC-coded program allows the user to select an image, set a threshold, and extract the number and average of the pixels above the threshold. An explanation of IMAGER.EXE appears in Appendix C. The program was tested by viewing a blackbody with the imager. With a blackbody of known temperature, a theoretical radiant intensity can be calculated and used as a comparison for the results of IMAGER.EXE.

The blackbody was placed 100 cm from the imager and used an aperture of 9.5mm. The blackbody and the imager were place in a sealed container and the atmosphere was purged from the container with dry nitrogen. Several frames were recorded onto floppy diskettes and subsequently analyzed with IMAGER.EXE. The theoretical radiant intensity was calculated with PLRAD (see Appendix C). Table 2 summarizes these results. No useable data was acquired for the no filter setting with aperture 0 and for the yellow filter setting and aperture 1.

The threshold was found as the mid-point between the mode (the pixel value with the most representative pixels) and the maximum pixel value. This decision was made on the assumption that 50% of the pixels above the background were due to diffraction at the blackbody aperture exit or from scattering. This assumption was loosely defined and has no scientific significance. It was chosen simply as a starting point for this effort.

The data errors, although not ideal, were not unreasonable. However, the variation in the error is cause for concern. Some of the error can no doubt be attributed to the method of thresholding. Other sources of error are the uncertainty of the temperature measurements, responsivity calibration errors, and spatial calibration errors.

The temperature measurement error is the result of human factors. The temperature of the blackbody was taken with a calibrated thermocouple for the calibration procedure. This process has errors due to the placement of the probe into the blackbody cavity. During the procedures of this test the temperature was taken directly from the blackbody control module. This difference in measurement techniques caused further uncertainty in the temperature measurements.

Errors in the responsivity calibration are due to temperature measurement error and to the small sample size of calibration data. Only one pixel count measurement was made for each temperature sample. In reality, a number of samples should have been taken at each temperature and the mean calculated. Also the value of the pixel count was taken as the maximum value in the image. An average taken around the peak would have been more accurate.

The error in the spatial calibration is due to the subpixel sampling. It is not a trivial task to determine if a pixel on the edge of the target is background or foreground. For this reason there is a certain amount of uncertainty associated with counting the number of pixels that appear to be in the foreground. Usage of contouring methods may help remove some of this uncertainty.

For the reasons stated above another calibration should be acquired using the knowledge gain in this effort thus far.

TABLE 3. RESULTS OF RADIANT INTENSITY MEASUREMENT TESTS.							
880+ Setup	k (cm^2 sr/W)	temp °C	Calculated I	n	S	Measured I	% Error
No filter 0	1.2821E+06	130	2.762E-03	na	na	na	na
No filter 1	1.5095E+05	300	3.027E-02	179	5339	2.560E-02	-22
No filter 2	2.7801E+04	300	3.027E-02	208	1022	3.090E-02	+5.5
Yellow 0	1.0068E+06	130	8.580E-04	456	410	7.700E-04	-13
Yellow 1	1.4128E+05	300	1.080E-02	na	na	na	na
Yellow 2	1.4219E+04	700	1.329E-01	228	3709	1.412E-01	+6
Blue 0	5.8522E+04	700	7.107E-02	212	3366	4.930E-02	-31
Blue 1	8.2679E+03	700	7.107E-02	206	718	7.230E-02	+1.7
Blue 2	1.3114E+03	900	2.691E-01	212	476	3.111E-01	+16

Constants used in the table above:

ω = 4.0432E-07 sr
τ = 1.0
R = 100.0 cm
S = average signal value
n = number of pixels above threshold

3.3.2 Image Enhancement and False Color Image Generation. One advantage the 880+ has over other radiometers is the ability to produce images. An image allows the user to "see" the spatial, temporal, and spectral characteristics of an emissive source. Although the BRUT cannot produce hard copy images, hard copies can be made by using the same raw data that is used to produce radiometric measurements. One such method is outlined below.

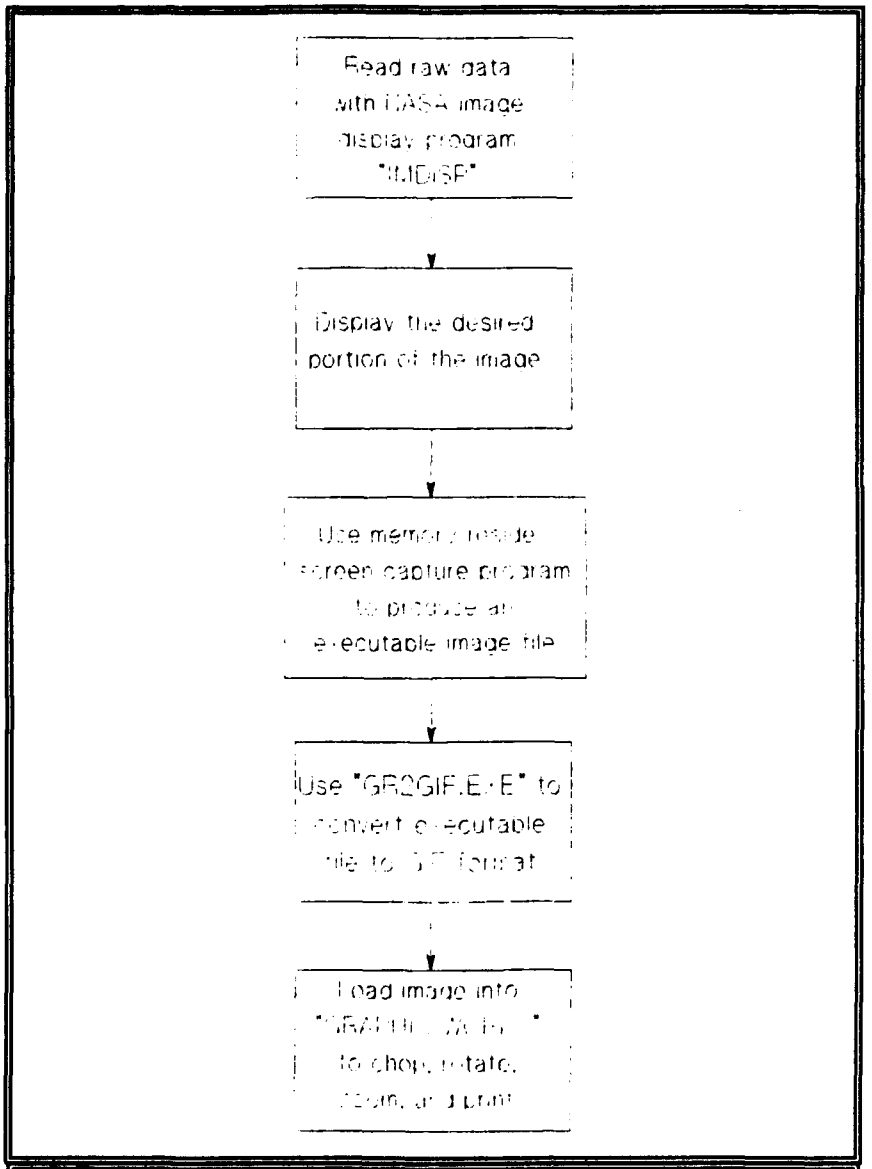

FIGURE 10. FALSE COLOR IMAGE HARD COPY METHODOLOGY.

This process was simply an initial effort at producing false color hard copies and is by no means the most expedient method available. A number of different software packages do exist that not only produce hard copy images but also do image enhancement and image analysis. An extensive survey was undertaken to find the best software package. In the end, the selection was made for OPTIMAS from Bioscan, Inc. Optimas is complete image processing toolbox that allows a user to acquire, enhance, identify, and present images.

Optimas works exclusively with 8-bit data and, therefore, an 880+ image must be mapped from a 13-bit word to an 8-bit word. This was accomplished by writing a special Optimas macro that would load the 880+ image, map the data from eight to 13 bits, and display the image in gray scale .

At the time of this writing the work with Optimas was still in progress. Work will continue in this area.

4.0 CONCLUSIONS.

At the onset of this effort three main objectives were outlined. The first objective was to verify that accurate measurements could be obtained using the 880+/BRUT system. In section 3.1 it was shown that the imaging system was indeed capable of acquiring accurate measurements at least for the blackbody case. This objective was also pursued to provide familiarization of the equipment to the end users.

The second objective was to perform an external calibration of the 880+. This effort included measurements of the system spectral response, the system responsivity, and the system spatial calibration. The results of the system spectral response measurements were encouraging in that they matched quite well with the results of previous work$_1$. The system responsivity and the system spatial resolution (solid angle per pixel) were measured within the constraints of available equipment. A check of these measurements (section 3.3.1) revealed that there may be some inaccuracy in these measurements. Uncertainties exist in the method of blackbody temperature measurement, collimator throughput, and the image pixel count estimation. For the spatial calibration uncertainties existed in the count of the pixels that are in the image and in the error associated with the projected solid angle for off-axis pixels (those pixels outside of the center of the field of view).

The third objective was to produce false-color images and radiometric measurements from images. This objective was achieved with moderate success. A method was constructed for producing false color image hardcopies. This method involved using several different programs to present an image onto the screen, capture the contents of the screen, convert the screen image into a GIF format, crop the unwanted portions of the screen image, and finally print the final image. This process was both time consuming and tedious. The end product was simply a color image with no scale to relate color to any radiometric quantity.

A BASIC coded program (IMAGER.EXE) was generated that would allow a user to decode an 880+ binary image and plot it to a computer screen. The image could be scaled or zoomed and a cross-hair was included that would allow the user to sample individual pixels for their value. The user can then select a threshold value and acquire a radiant intensity measurement of the pixels above the threshold. This program worked quite well with the exception of the inability to create contour or surface maps. The contour lines would be helpful in selecting a threshold value and would provide insight into the structure of area source flares.

Currently, work is in progress to generate a single program that will do all of the above mentioned tasks. The program will include all of the functions of IMAGER.EXE along with some new features. These features include functions to produce surface and contour plots, provide image enhancement, create a color scale,

and to automate the whole process. Any combination of false color images, contour maps, surface plots, scales, and radiometric measurements can be combined onto the screen and subsequently printed to a color printer. Further, the program will take entire data sets and produce plots of radiant intensity v. time. The program is being coded in the Interactive Data Language (IDL) format and will be a portable executable program.

RECOMMENDATIONS.

It is recommended that the calibration procedure be repeated. With a greater knowledge of the 880+ system in hand it will be a much easier and more accurate procedure. Careful measurement of the blackbody temperature and image pixel value is imperative. Pixel counting will be more accurate with the new software and will improve measurements of both the system responsivity and the system spatial calibration.

Other future activities will include the implementation of an Ethernet to expedite the transfer and storage of images. A calibration of the 880+ system with the 2.5° lens, a measure of the 880+ spectral filter transmission, an analysis of target shape factors, and a comparison of the 880+ versus other imaging radiometers and conventional radiometers will also be undertaken.

5.0 REFERENCES.

1. Fraedrich, D.S., "Methods in Calibration and Error Analysis for Infrared Imaging Radiometers", *Optical Engineering*, November 1991.

2. Agema Infrared Systems, *Thermovision 880 Operating Manual.*

3. Agema Infrared Systems, *Burst Recording Unit Introduction and Reference Manual.*

4. Dereniak, E. L. and Crowe, D. G. *Optical Radiation Detectors*, John Wiley & Sons, 1984.

5. Castleman, K. R. *Digital Image Processing*, Prentice-Hall, Inc., 1979

THIS PAGE INTENTIONALLY LEFT BLANK

APPENDIX A

INSTRUMENTATION

This appendix contains brief descriptions of the instrumentation used to support the characterization and calibration of the 880+. This is not intended to be a user's manual. Instrumentation described includes:

1) Barnes Engineering, Off-Axis Collimator
2) Barnes Engineering, 1" Blackbody Source
3) CI Industries, 1" Blackbody Source
4) Perkin-Elmer, 783 Spectrophotometer
5) Optical Coating Laboratories, Inc., Circular Variable Filter (CVF)
6) Agema 880+ Spectral Filters

BARNES ENGINEERING 4.5" REFLECTING COLLIMATOR

The Barnes Engineering collimator is an off-axis reflective collimator. The primary mirror is 4.5" in diameter and is spectrally flat in the spectral band covering the near IR. The optical throughput, measured in the near IR, was found to be approximately 94%. The system includes the seven aperture settings listed in Table A-1.

TABLE A-1. BARNES ENGINEERING COLLIMATOR APERTURE SETTINGS

APERTURE	DIAMETER (INCHES)	AREA (CM^2)
1	0.0080	3.2429E-04
2	0.0140	9.9315E-04
3	0.0256	3.2080E-03
4	0.0443	9.9441E-03
5	0.0811	3.3327E-02
6	0.1409	1.0060E-01
7	0.2559	3.3182E-01

BLACKBODY SOURCES

Two blackbody sources were used extensively during the laboratory portions of the testing: a Barnes Engineering, 1" blackbody source, and a CI Industries, 1" blackbody source. Both units consist of the 1" source head and a temperature control interface. The Barnes unit is capable of estimating a blackbody source across a temperature range from 50°C to 1000°C, while the CI source spans the temperature range from 50°C to 1200°C. Both units approximate a Lambertian radiator when used within a specified cone of approximately 30°C.

PERKIN-ELMER 783 SERIES SPECTROPHOTOMETER

The 783 spectrophotometer provides a continuous record of the infrared transmittance or absorbance of a sample as a function of frequency (expressed in wave number units). The resultant measurement is recorded versus wave number. The radiation emitted by the internal source is divided into two beams: a reference beam and a measurement beam. The measurement beam, of wave number cm^{-1}, passes through the sample and is absorbed as a function of the sample characteristic molecular vibrational frequency. The two beams are recombined to form a single beam consisting of alternating pulses of measurement and reference beam. The recombined beam converges onto a monochromator where it is refracted by the grating into its spectral components and scanned across the monochromator exit slit. The radiation exiting the monochromator slit passes through one of a set of optical filters (automatically selected) to reject any unwanted radiation and is finally focused onto a thermocouple. The resultant signal is characteristic of the sample transmittance or absorbance.

OPTICAL COATING LABORATORIES, INC. (OCLI)
CIRCULAR VARIABLE FILTER (CVF)

The OCLI CVF is a segmented optical filter that spans the spectral region from 2.380 to 5.950 μm. Table A-2 below lists the spectral bands present at specific CVF angular positions. A plot of transmission versus wavelength, obtained in a calibration of the CVF, is included in Appendix B.

TABLE A-2. OCLI CVF CALIBRATION

CVF Angle	Low λ	High λ	Peak λ
100	2.380	2.500	2.440
110	2.500	2.610	2.555
120	2.610	2.730	2.670
130	2.730	2.850	2.795
140	2.850	2.980	2.915
150	2.980	3.120	3.040
160	3.120	3.240	3.180
170	3.240	3.370	3.310
180	3.370	3.510	3.435
190	3.510	3.640	3.575
200	3.640	3.770	3.710
210	3.770	3.910	3.840
220	3.910	4.030	3.970
230	4.030	4.170	4.100
240	4.170	4.290	4.230
250	4.290	4.405	4.345
260	4.405	4.525	4.460
270	4.525	4.650	4.570
280	4.015	4.255	4.125
290	4.255	4.465	4.345
300	4.465	4.695	4.565
310	4.695	4.925	4.800
320	4.925	5.155	5.015
330	5.155	5.405	5.260
340	5.405	5.650	5.510
350	5.650	5.950	5.750

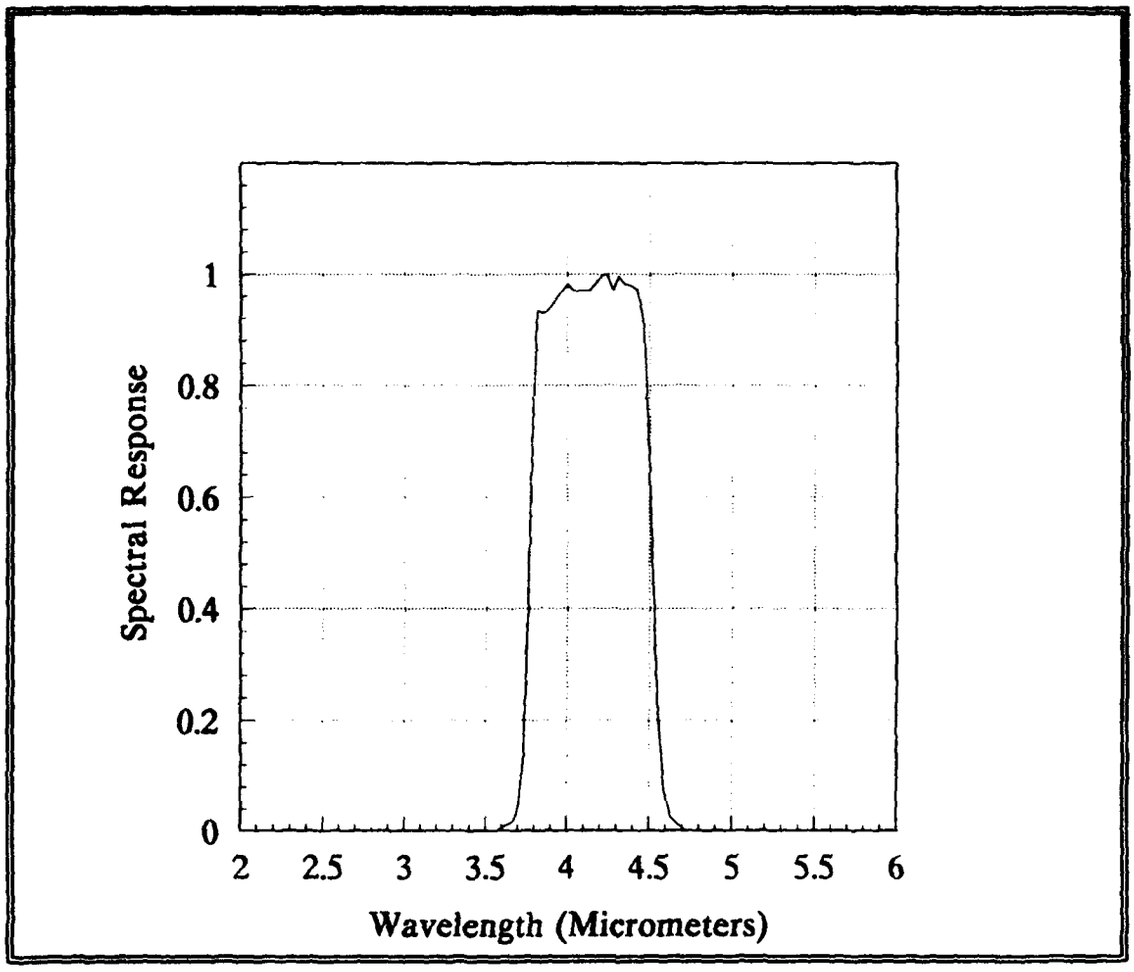

FIGURE A-1. NORMALIZED SPECTRAL TRANSMISSION OF THE 880+ YELLOW FILTER.

λ	RELATIVE TRANS.	λ	RELATIVE TRANS.
3.5714	0.0000	4.0984	0.9700
3.5971	0.0050	4.1322	0.9700
3.6232	0.0100	4.1667	0.9820
3.6496	0.0120	4.2017	0.9950
3.6765	0.0200	4.2373	1.0000
3.7037	0.0500	4.2735	0.9700
3.7313	0.1370	4.3103	0.9950
3.7594	0.4100	4.3478	0.9820
3.7879	0.7510	4.3860	0.9780
3.8168	0.9330	4.4248	0.9700
3.8462	0.9280	4.4643	0.9080
3.8760	0.9330	4.5045	0.5970
3.9063	0.9450	4.5455	0.2480
3.9370	0.9580	4.5872	0.0750
3.9683	0.9700	4.6296	0.0250
4.0000	0.9820	4.6729	0.0120
4.0323	0.9700	4.7170	0.0020
4.0650	0.9700	4.7619	0.0000

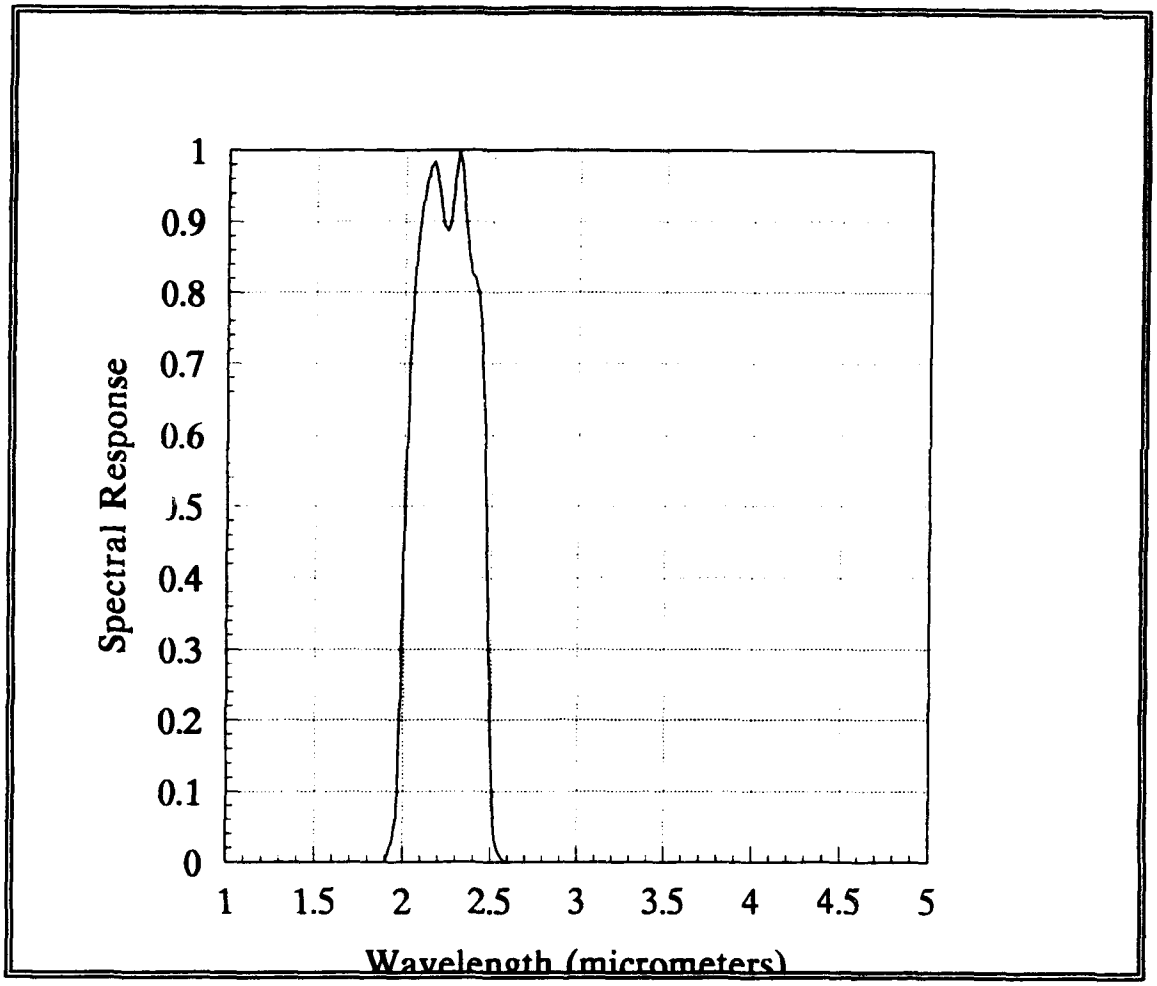

FIGURE A-2. NORMALIZED SPECTRAL TRANSMISSION OF THE 880+ BLUE FILTER.

λ	RELATIVE TRANS.	λ	RELATIVE TRANS.
1.900	0.000	2.260	0.902
1.920	0.015	2.280	0.962
1.940	0.030	2.300	1.000
1.960	0.060	2.320	0.977
1.980	0.203	2.340	0.917
2.000	0.439	2.360	0.857
2.020	0.606	2.380	0.827
2.040	0.752	2.400	0.820
2.060	0.834	2.420	0.797
2.080	0.887	2.440	0.737
2.100	0.925	2.460	0.601
2.120	0.955	2.480	0.361
2.140	0.977	2.500	0.135
2.160	0.985	2.520	0.037
2.180	0.962	2.540	0.015
2.200	0.932	2.560	0.007
2.220	0.895	2.580	0.001
2.240	0.887	2.600	0.000

APPENDIX B

DATA FROM LABORATORY TESTS

This appendix contains the data that were collected in the laboratory characterization and calibration of the 880+. The data are presented in accordance with the procedures outlined in the main report. The table on page A-2 lists the data in the order of appearance in this appendix. The page number generally refers to the figure unless there is no figure for that particular data set.

FIGURE	PAGE	TABLE	DATA FILENAME	DESCRIPTION
none	B-6	B-1	TABLES.WK1	Temperature measurements for no filter / aperture 1.
none	B-7	B-2	TABLES.WK1	Temperature measurements for no filter / aperture 2.
none	B-8	B-3	TABLES.WK1	Temperature measurements for yellow filter / aperture 1.
none	B-9	B-4	TABLES.WK1	Temperature measurements for yellow filter / aperture 2.
none	B-11	B-5	TABLES.WK1	Temperature measurements for blue filter / aperture 0.
none	B-12	B-6	TABLES.WK1	Temperature measurements for blue filter / aperture 1.
none	B-14	B-7	TABLES.WK1	Temperature measurements for blue filter / aperture 2.
none	B-15	B-8	ERROR.DAT	Temperature measurement error.
B-1	B-16	B-9	CVFSEG1.DAT	Digitized values of CVF segment 1 transmission.
B-1	B-16	B-10	CVFSEG2.DAT	Digitized values of CVF segment 2 transmission.
B-2	B-19	B-11	CVF1.DAT	Combination of complete CVFSEG1 and the portion of CVFSEG2 from 4.717 to 5.950 micrometers.
B-3	B-21	B-12	CVF2.DAT	Combination of complete CVFSEG2 and the portion of CVFSEG1 from 2.260 to 4.000 micrometers.
B-4	B-23	none	SYSINP1.DAT	Theoretical radiance (corrected and uncorrected) from an 805 degree blackbody using filter CVF1.DAT and program PLRAD.EXE.
B-5	B-24	none	SYSINP2.DAT	Theoretical radiance (corrected and uncorrected) from an 805 degree blackbody using filter CVF2.DAT and program PLRAD.EXE.
B-6	B-25	B-13	805RES1.DAT	Spectral response of the 880+ Thermal Imager detector and lens with radiance values taken from SYSINP1.DAT and no filter on the 880+.
B-6	B-25	B-14	805RES2.DAT	Spectral response of the 880+ Thermal Imager detector and lens with radiance values taken from SYSINP2.DAT and no filter on the 880+.

B-7	B-28	B-15	801RES1.DAT	Spectral response of the 880+ Thermal Imager detector and lens with radiance values taken from SYSINP3.DAT and no filter on the 880+.
B-7	B-28	B-16	801RES2.DAT	Spectral response of the 880+ Thermal Imager detector and lens with radiance values taken from SYSINP4.DAT and no filter on the 880+.
B-8	B-31	none	FILTER1.DAT	Spectral transmission of narrow band filter #1.
B-8	B-31	none	FILTER3.DAT	Spectral transmission of narrow band filter #3.
B-9	B-32	B-17	NOFRES.DAT	Average normalized spectral response from 805RES2.DAT and 801RES2.DAT.
B-10	B-34	none	YELRES.DAT	Spectral response of the 880+ Thermal Imager when the yellow filter is utilized. Created by multiplying the system spectral response (NOFRES.OUT) and the transmission curve of the yellow filter (880YEL.OUT).
none	N/A	none	NOFRES.OUT	Spectral response of the imager system from 2.0 to 5.750 micrometers with values at every 0.005 micrometers. This file is constructed using the program EVEN.EXE with the spectral response file NOFRES.IR. NOFRES.IR is a stripped version of NOFRES.DAT.
B-11	B-35 with plot		880YEL.OUT	Spectral response of the yellow filter from 2.0 to 5.750 micrometers with values at every 0.005 micrometers. This file is constructed using the program EVEN.EXE with the spectral response file 880YEL.IR. 880YEL.IR is the transmission of the yellow filter as a function of wavelength.
B-12	B-36	none	BLURES.DAT	Spectral response of the 880+ Thermal Imager when the blue filter is utilized. Created by multiplying the system spectral response (NOFRES.OUT) and the transmission curve of the blue filter (880BLU.OUT).
B-13	B-37 with plot		880BLU.OUT	Spectral response of the blue filter from 2.0 to 5.750 micrometers with values at every 0.005 micrometers. This file is constructed using the program EVEN.EXE with the spectral response file 880BLU.IR. 880BLU.IR is the transmission of the blue filter as a function of wavelength.
B-14	B-38	with plot	NOFILT0.DAT	Responsivity of the 880+ Thermal Imager with the 7° lens, no filter, and aperture 0. The radiance values were calculated with PLRAD.EXE using filter NOFRES.DAT.

B-15	B-39	with plot	NOFILT1.DAT	Responsivity of the 880+ Thermal Imager with the 7° lens, no filter, and aperture 1. The radiance values were calculated with PLRAD.EXE using filter NOFRES.DAT.
B-16	B-40	with plot	NOFILT2.DAT	Responsivity of the 880+ Thermal Imager with the 7° lens, no filter, and aperture 2. The radiance values were calculated with PLRAD.EXE using filter NOFRES.DAT.
B-17	B-41	with plot	YELLOW0.DAT	Responsivity of the 880+ Thermal Imager with the 7° lens, yellow filter, and aperture 0. The radiance values were calculated with PLRAD.EXE using filter YELRES.DAT
B-18	B-42	with plot	YELLOW1.DAT	Responsivity of the 880+ Thermal Imager with the 7° lens, yellow filter, and aperture 1. The radiance values were calculated with PLRAD.EXE using filter YELRES.DAT.
B-19	B-43	with plot	YELLOW2.DAT	Responsivity of the 880+ Thermal Imager with the 7° lens, yellow filter, and aperture 2. The radiance values were calculated with PLRAD.EXE using filter YELRES.DAT.
B-20	B-44	with plot	BLUE0.DAT	Responsivity of the 880+ Thermal Imager with the 7° lens, blue filter, and aperture 0. The radiance values were calculated with PLRAD.EXE using filter BLURES.DAT.
B-21	B-45	with plot	BLUE1.DAT	Responsivity of the 880+ Thermal Imager with the 7° lens, blue filter, and aperture 1. The radiance values were calculated with PLRAD.EXE using filter BLURES.DAT.
B-22	B-46	with plot	BLUE2.DAT	Responsivity of the 880+ Thermal Imager with the 7° lens, blue filter, and aperture 2. The radiance values were calculated with PLRAD.EXE using filter BLURES.DAT.
B-23	B-47	B-18	SPATIAL.DAT	Solid angle per pixel measurement. For each square aperture, the solid angle subtended by the aperture is plotted versus the number of pixels contained in the image. The slope of this line is the solid angle per pixel.

TEMPERATURE MEASUREMENT ERROR DATA

The data from the temperature error tests have been placed in a set of tables with one table for each aperture/filter combination. Data were collected over a range of temperatures utilizing three different blackbody sources and a variety of blackbody aperture sizes. The blackbody temperature was measured with a calibrated temperature probe (actual temp) and was then measured with the 880+ (measured temp). From these temperatures, the theoretical radiance was calculated. The radiance was also measured with the 880+ using an area paint.

NOTE: The following units apply to Tables B-1 through B-8.

Radiance - Watts / unit area / unit solid angle (W / cm^2 / Sr)
Wavelength (λ) - Micrometers (μm)
CVF Angle - Degrees
Signal - Digital Counts
Normalized Values - Normalized to the maximum value in that data set

BB1 - CI Industries 1" BlackBody
BB2 - Barnes Engineering 1" Blackbody
BB3 - E/O Systems 2" Blackbody
ND - No Data

TABLE B-1. TEMPERATURE MEASUREMENT DATA FOR NO FILTER APERTURE 1.

SOURCE	SOURCE APERTURE (CM^2)	ACTUAL TEMP (°C)	RADIANCE FROM ACTUAL TEMP	MEASURED TEMP (°C)	TEMP ERROR (%)	RADIANCE FROM MEASURED TEMP	RADIANCE FROM IMAGER
BB2	1.000e-02	298.2	4.61e+02	ND	ND	ND	ND
BB1	1.000e-02	303.5	4.90e+02	235.0	22.57	2.04e+02	1.51e+02
BB1	3.325e-02	303.5	4.90e+02	295.7	2.57	4.47e+02	3.34e+02
BB2	3.325e-02	298.2	4.61e+02	297.7	0.17	4.58e+02	4.21e+02
BB1	1.000e-01	303.5	4.90e+02	302.5	0.33	4.84e+02	4.07e+02
BB2	1.000e-01	298.2	4.61e+02	305.7	2.52	5.02e+02	4.62e+02
BB1	3.318e-01	303.5	4.90e+02	295.1	2.77	4.44e+02	4.31e+02
BB2	3.318e-01	298.2	4.61e+02	307.4	3.09	5.12e+02	4.71e+02
BB1	3.871e+00	299.8	4.69e+02	302.0	0.73	4.81e+02	4.70e+02

TABLE B-2. TEMPERATURE MEASUREMENT DATA FOR NO FILTER APERTURE 2.

SOURCE	SOURCE APERTURE (CM^2)	ACTUAL TEMP (°C)	RADIANCE FROM ACTUAL TEMP	MEASURED TEMP (°C)	TEMP ERROR (%)	RADIANCE FROM MEASURED TEMP	RADIANCE FROM IMAGER
BB2	1.000e-02	298.2	4.61e+02	ND	ND	ND	ND
BB1	1.000e-02	303.5	4.90e+02	274.0	9.72	3.44e+02	2.69e+02
BB1	3.325e-02	303.5	4.90e+02	303.1	0.13	4.87e+02	3.03e+02
BB2	3.325e-02	298.2	4.61e+02	302.1	1.31	4.82e+02	4.43e+02
BB1	1.000e-01	303.5	4.90e+02	304.0	0.16	4.92e+02	4.24e+02
BB2	1.000e-01	298.2	4.61e+02	307.3	3.05	5.11e+02	4.70e+02
BB1	3.318e-01	303.5	4.90e+02	294.7	2.90	4.42e+02	4.27e+02
BB2	3.318e-01	298.2	4.61e+02	308.1	3.32	5.16e+02	4.75e+02
BB3	8.108e-01	314.0	5.51e+02	313.5	0.16	5.48e+02	5.31e+02
BB3	1.824e+00	314.0	5.51e+02	313.6	0.13	5.48e+02	5.31e+02
BB1	3.871e+00	299.8	4.69e+02	302.8	1.00	4.87e+02	4.72e+02
BB3	5.068e+00	314.0	5.51e+02	313.5	0.16	5.48e+02	5.29e+02
BB3	2.027e+01	329.0	6.49e+02	328.1	0.27	6.43e+03	ND
BB2	1.000e-02	395.5	1.24e+03	ND	ND	ND	ND
BB2	3.325e-02	395.5	1.24e+03	391.3	1.06	1.20e+03	1.16e+03
BB2	1.000e-01	395.5	1.24e+03	399.7	1.06	1.29e+03	1.25e+03
BB2	3.318e-01	395.5	1.24e+03	401.1	1.42	1.31e+03	1.27e+03
BB1	3.871e+00	401.5	1.31e+03	399.3	0.55	1.28e+03	1.25e+03
BB2	1.000e-02	506.8	2.98e+03	447.9	11.62	1.93e+03	1.87e+03
BB2	3.325e-02	506.8	2.98e+03	478.8	5.52	2.44e+03	2.37e+03
BB2	1.000e-01	506.8	2.98e+03	492.3	2.86	2.69e+03	2.48e+03
BB2	3.318e-01	506.8	2.98e+03	493.5	2.62	2.71e+03	2.50e+03
BB1	3.871e+00	506.6	2.97e+03	489.7	3.34	2.64e+03	2.56e+03

TABLE B-3. TEMPERATURE MEASUREMENT DATA FOR YELLOW FILTER APERTURE 1.

SOURCE	SOURCE APERTURE (CM^4)	ACTUAL TEMP (°C)	RADIANCE FROM ACTUAL TEMP	MEASURED TEMP (°C)	TEMP ERROR (%)	RADIANCE FROM MEASURED TEMP	RADIANCE FROM IMAGER
BB1	1.000e-02	303.5	1.91e+02	235.0	22.57	8.55e+01	3.57e+01
BB2	1.000e-02	298.2	1.80e+02	264.9	11.17	1.24e+02	1.15e+02
BB2	3.325e-02	298.2	1.80e+02	295.4	0.94	1.75e+02	1.61e+02
BB1	3.325e-02	303.5	1.91e+02	291.0	4.12	1.67e+02	1.30e+02
BB1	1.000e-01	303.5	1.91e+02	298.5	1.65	1.81e+02	1.47e+02
BB2	1.000e-01	298.2	1.80e+02	304.5	2.11	1.93e+02	1.77e+02
BB1	3.318e-01	303.5	1.91e+02	290.9	4.15	1.67e+02	1.62e+02
BB2	3.318e-01	298.2	1.80e+02	306.4	2.75	1.97e+02	1.81e+02
BB3	8.108e-01	314.0	2.12e+02	309.0	1.59	2.02e+02	1.96e+03
BB3	1.824e+00	314.0	2.12e+02	310.0	1.27	2.04e+02	1.98e+02
BB1	3.871e+00	299.8	1.84e+02	300.8	0.33	1.85e+02	1.80e+02
BB3	5.068e+00	314.0	2.12e+02	293.0	6.69	1.71e+02	1.65e+02
BB3	2.027e+01	329.0	2.46e+02	317.9	3.37	2.21e+02	2.12e+02
BB2	1.050e-02	395.5	4.34e+02	324.7	17.90	2.36e+02	2.29e+02
BB2	3.325e-02	395.5	4.34e+02	389.5	1.52	4.14e+02	4.02e+02
BB2	1.000e-01	395.5	4.34e+02	397.8	0.58	4.42e+02	4.29e+02
BB2	3.318e-01	395.5	4.34e+02	399.7	1.06	4.48e+02	4.35e+02
BB1	3.871e+00	401.5	4.54e+02	396.2	1.32	4.36e+02	4.23e+02

TABLE B-4. TEMPERATURE MEASUREMENT DATA FOR YELLOW FILTER APERTURE 2.

SOURCE	SOURCE APERTURE (CM^2)	ACTUAL TEMP (°C)	RADIANCE FROM ACTUAL TEMP	MEASURED TEMP (°C)	TEMP ERROR (%)	RADIANCE FROM MEASURED TEMP	RADIANCE FROM IMAGER
BB2	1.000e-02	298.2	1.80e+02	285.6	4.23	1.58e+02	1.45e+02
BB1	1.000e-02	303.5	1.91e+02	274.0	9.72	1.38e+02	3.65e+01
BB1	3.325e-02	303.5	1.91e+02	301.1	0.79	1.86e+02	1.58e+02
BB2	3.325e-02	298.2	1.80e+02	303.2	1.68	1.90e+02	1.75e+02
BB2	1.000e-01	298.2	1.80e+02	308.7	3.52	2.01e+02	1.85e+02
BB1	1.000e-01	303.5	1.91e+02	303.7	0.07	1.91e+02	1.63e+02
BB2	3.318e-01	298.2	1.80e+02	308.2	3.35	2.00e+02	1.84e+02
BB1	3.318e-01	303.5	1.91e+02	293.0	3.46	1.71e+02	1.66e+02
BB3	8.108e-01	314.0	2.12e+02	311.5	0.80	2.07e+02	2.01e+02
BB3	1.824e+00	314.0	2.12e+02	311.9	0.67	2.08e+02	2.01e+02
BB1	3.871e+00	299.8	1.84e+02	303.0	1.07	1.90e+02	1.85e+02
BB3	5.068e+00	314.0	2.12e+02	311.8	0.70	2.08e+02	2.00e+02
BB3	2.027e+01	329.0	2.46e+02	315.0	4.26	2.14e+02	2.09e+02
BB2	1.000e-02	395.5	4.34e+02	362.2	8.42	3.31e+02	3.20e+02
BB2	3.325e-02	395.5	4.34e+02	394.5	0.25	4.31e+02	4.18e+02
BB2	1.000e-01	395.5	4.34e+02	399.8	1.09	4.49e+02	4.35e+02
BB2	3.318e-01	395.5	4.34e+02	401.5	1.52	4.54e+02	4.41e+02
BB1	3.871e+00	401.5	4.59e+02	397.5	1.00	4.41e+02	4.27e+02
BB2	1.000e-02	506.8	9.10e+02	459.3	9.37	6.82e+02	6.27e+02
BB2	3.325e-02	506.8	9.10e+02	499.8	1.38	8.74e+02	7.86e+02
BB2	1.000e-01	506.8	9.10e+02	504.9	0.37	9.00e+02	8.10e+02
BB2	3.318e-01	506.8	9.10e+02	507.1	0.06	9.12e+02	8.20e+02
BB1	3.871e+00	506.6	9.09e+02	496.4	2.01	0.00	8.31e+02
BB1	1.000e-02	612.2	1.55e+03	505.3	17.46	9.02e+02	7.67e+02
BB2	1.000e-02	603.6	1.49e+03	535.1	11.35	1.07e+03	9.79e+02
BB2	3.325e-02	603.6	1.49e+03	590.8	2.12	1.41e+03	1.29e+03
BB1	3.325e-02	612.2	1.55e+03	593.2	3.10	1.42e+03	1.21e+03
BB1	1.000e-01	612.2	1.55e+03	605.0	1.18	1.50e+03	1.26e+03
BB2	1.000e-01	603.6	1.49e+03	599.6	0.66	1.47e+03	1.35e+03
BB1	3.318e-01	612.2	1.55e+03	606.5	0.93	1.51e+03	1.28e+03
BB2	3.318e-01	603.6	1.49e+03	600.7	0.48	1.47e+03	1.35e+03
BB1	3.871e+00	610.9	1.54e+03	595.4	2.54	1.44e+03	1.39e+03
BB2	1.000e-02	700.1	2.23e+03	603.5	13.80	1.49e+03	1.37e+03
BB2	3.325e-02	700.1	2.23e+03	612.7	12.48	1.56e+03	1.91e+03

BB2	1.000e-01	700.1	2.23e+03	693.0	1.01	2.17e+03	1.99e+03
BB2	3.318e-01	700.1	2.23e+03	695.1	0.71	2.19e+03	2.01e+03
BB1	3.871e+00	715.6	2.36e+03	697.0	2.60	2.20e+03	2.13e+03
BB2	1.000e-02	801.0	3.15e+03	705.0	11.99	2.27e+03	2.08e+03
BB2	3.325e-02	801.0	3.15e+03	782.1	2.36	2.96e+03	2.72e+03
BB2	1.000e-01	801.0	3.15e+03	793.4	0.95	3.07e+03	2.82e+03
BB2	3.318e-01	801.0	3.15e+03	797.5	0.44	3.11e+03	2.86e+03
BB1	3.871e+00	817.6	3.31e+03	799.2	2.25	3.13e+03	3.02e+03
BB1	1.000e-02	911.6	4.31e+03	775.7	14.91	2.90e+03	2.46e+03
BB2	1.000e-02	899.5	4.18e+03	ND	ND	ND	ND
BB2	3.325e-02	899.5	4.18e+03	905.4	0.66	4.24e+03	3.89e+03
BB1	3.325e-02	911.6	4.31e+03	901.5	1.11	4.20e+03	3.56e+03
BB1	1.000e-01	911.6	4.31e+03	914.8	0.35	4.35e+03	3.68e+03
BB2	1.000e-01	899.5	4.18e+03	893.4	0.68	4.11e+03	3.77e+03
BB2	3.310e-01	899.5	4.18e+03	897.1	0.27	4.15e+03	3.81e+03
BB1	3.318e-01	911.6	4.31e+03	917.0	0.59	4.37e+03	3.71e+03
BB1	3.871e+00	917.0	4.37e+03	904.0	1.42	4.23e+03	4.08e+03

TABLE B-5. TEMPERATURE MEASUREMENT DATA FOR BLUE FILTER APERTURE 0.

SOURCE	SOURCE APERTURE (CM^2)	ACTUAL TEMP (°C)	RADIANCE FROM ACTUAL TEMP	MEASURED TEMP (°C)	TEMP ERROR (%)	RADIANCE FROM MEASURED TEMP	RADIANCE FROM IMAGER
BB1	3.325e-02	303.5	1.63e+01	295.1	2.77	1.39e+01	1.49e+01
BB2	3.325e-02	298.2	1.47e+01	287.8	3.49	1.20e+01	1.10e+01
BB1	1.000e-01	303.5	1.63e+01	302.4	0.36	1.60e+01	1.58e+01
BB2	1.000e-01	298.2	1.47e+01	306.5	2.78	1.72e+01	1.58e+01
BB2	3.318e-01	298.2	1.47e+01	307.2	3.02	1.75e+01	1.69e+01
BB1	3.318e-01	303.5	1.63e+01	301.4	0.69	1.57e+01	1.51e+01
BB3	8.108e-01	314.0	1.98e+01	308.5	1.75	1.79e+01	1.73e+01
BB3	1.824e+00	314.0	1.98e+01	315.1	0.35	2.02e+01	1.93e+01
BB1	3.871e+00	299.8	1.52e+01	305.0	1.73	1.67e+01	1.62e+01
BB3	2.027e+01	329.0	2.58e+03	291.6	11.37	1.30e+01	1.25e+01
BB2	1.000e-02	395.5	7.30e+01	330.3	16.49	2.64e+01	2.57e+01
BB2	3.325e-02	395.5	7.30e+01	380.2	3.87	5.85e+01	5.69e+01
BB2	1.000e-01	395.5	7.30e+01	401.8	1.59	7.97e+01	7.76e+01
BB2	3.318e-01	395.5	7.30e+01	406.5	2.78	8.50e+01	8.28e+01
BB1	3.871e+00	401.5	7.93e+01	404.0	0.62	8.20e+01	8.00e+01
BB2	1.000e-02	506.8	2.81e+02	ND	ND	ND	ND
BB2	3.325e-02	506.8	2.81e+02	463.9	8.46	1.75e+02	1.59e+02
BB2	1.000e-01	506.8	2.81e+02	503.6	0.63	2.72e+02	2.47e+02
BB2	3.318e-01	506.8	2.81e+02	510.0	0.63	2.91e+02	2.70e+02
BB1	3.871e+00	506.6	2.81e+02	508.2	0.32	2.85e+02	2.79e+02
BB2	1.000e-02	603.6	6.91e+02	ND	ND	ND	ND
BB1	1.000e-02	612.2	7.42e+02	512.0	16.37	2.97e+02	2.54e+02
BB2	3.325e-02	603.6	6.91e+02	549.1	9.03	4.28e+02	3.97e+02
BB1	3.325e-02	612.2	7.42e+02	590.0	3.63	6.17e+02	5.29e+02
BB1	1.000e-01	612.2	7.42e+02	612.1	0.02	7.41e+02	6.30e+02
BB2	1.000e-01	603.6	6.91e+02	599.1	0.75	6.66e+02	6.18e+02
BB1	3.318e-01	612.2	7.42e+02	616.7	0.74	7.75e+02	6.63e+02
BB2	3.318e-01	603.6	6.91e+02	609.3	0.94	7.25e+02	6.73e+02
BB1	3.871e+00	610.9	7.34e+02	611.4	0.08	7.37e+02	7.20e+02
BB2	1.000e-02	700.1	1.42e+03	ND	ND	ND	ND
BB2	3.325e-02	700.1	1.42e+03	631.20	9.84	8.63e+02	8.01e+02
BB2	1.000e-01	700.1	1.42e+03	690.50	1.37	1.33e+03	1.24e+03
BB2	3.318e-01	700.1	1.42e+03	702.10	0.29	1.44e+03	1.34e+03
BB1	3.871e+00	715.6	1.58e+03	709.5	0.85	1.51e+03	1.48e+03

TABLE B-6. TEMPERATURE MEASUREMENT DATA FOR BLUE FILTER APERTURE 1.

SOURCE	SOURCE APERTURE (CM^2)	ACTUAL TEMP (°C)	RADIANCE FROM ACTUAL TEMP	MEASURED TEMP	TEMP ERROR	RADIANCE FROM MEASURED TEMP	RADIANCE FROM IMAGER
BB2	1.000e-02	506.8	2.81e+02	448.2	11.56	1.46e+02	1.35e+02
BB2	3.325e-02	506.8	2.81e+02	492.1	2.90	2.41e+02	2.23e+02
BB2	1.000e-01	506.8	2.81e+02	501.1	1.12	2.65e+02	2.46e+02
BB2	3.318e-01	506.8	2.81e+02	505.0	0.36	2.76e+02	2.56e+02
BB1	3.871e+00	506.6	2.81e+02	502.9	0.73	2.70e+02	2.63e+02
BB1	1.000e-02	612.2	7.42e+02	506.7	17.23	2.81e+02	7.73e+02
BB2	1.000e-02	603.6	6.91e+02	522.9	13.37	3.32e+02	3.07e+02
BB1	3.325e-02	612.2	7.42e+02	591.4	3.40	6.24e+02	5.35e+02
BB2	3.325e-02	603.6	6.91e+02	581.8	3.61	5.75e+02	5.33e+02
BB2	1.000e-01	603.6	6.91e+02	596.6	1.16	6.52e+02	6.05e+02
BB1	1.000e-01	612.2	7.42e+02	600.9	1.85	6.78e+02	5.80e+02
BB1	3.318e-01	612.2	7.42e+02	604.9	1.19	6.99e+02	5.96e+02
BB2	3.318e-01	603.6	6.91e+02	599.9	0.61	6.70e+02	6.20e+02
BB1	3.871e+00	610.9	7.34e+02	600.1	1.77	6.72e+02	6.58e+02
BB2	1.000e-02	700.1	1.42e+03	ND	ND	ND	ND
BB2	3.325e-02	700.1	1.42e+03	662.3	5.40	1.09e+03	1.01e+03
BB2	1.000e-01	700.1	1.42e+03	688.2	1.70	1.31e+03	1.22e+03
BB2	3.318e-01	700.1	1.42e+03	692.3	1.11	1.35e+03	1.25e+03
BB1	3.871e+00	715.6	1.58e+03	699.0	2.32	1.41e+03	1.38e+03
BB2	1.000e-02	801.0	2.64e+03	ND	ND	ND	ND
BB2	3.325e-02	801.0	2.64e+03	761.9	4.88	2.10e+03	1.96e+03
BB2	1.000e-01	801.0	2.64e+03	781.7	2.41	2.36e+03	2.20e+03
BB2	3.318e-01	801.0	2.64e+03	786.6	1.80	2.43e+03	2.26e+03
BB1	3.871e+00	817.6	2.89e+03	799.5	2.21	2.62e+03	2.56e+03
BB1	1.000e-02	911.6	4.61e+03	773.5	15.15	2.25e+03	1.94e+03
BB2	1.000e-02	899.5	4.36e+03	ND	ND	ND	ND
BB2	3.325e-02	899.5	4.36e+03	855.9	4.85	3.53e+03	3.28e+03
BB1	3.325e-02	911.6	4.61e+03	883.3	3.10	4.03e+03	3.47e+03
BB1	1.000e-01	911.6	4.61e+03	901.7	1.09	4.40e+03	3.78e+03
BB2	1.000e-01	899.5	4.36e+03	879.3	2.25	3.96e+03	3.68e+03
BB2	3.318e-01	899.5	4.36e+03	886.1	1.49	4.09e+03	3.80e+03
BB1	3.318e-01	911.6	4.61e+03	905.7	0.65	4.48e+03	3.85e+03
BB1	3.871e+00	917.0	4.73e+03	898.0	2.07	4.33e+03	4.24e+03
BB2	1.000e-02	981.1	6.23e+03	ND	ND	ND	ND

BB2	3.325e-02	981.1	6.23e+03	920.0	6.23	4.79e+03	4.45e+03
BB2	1.000e-01	981.1	6.23e+03	952.0	2.97	5.51e+03	5.12e+03
BB2	3.318e-01	981.1	6.23e+03	956.8	2.48	5.63e+03	5.23e+03
BB1	3.871e+00	1017.0	7.19e+03	995.5	2.11	6.60e+03	6.46e+03
BB1	1.000e-02	1187.1	1.29e+04	ND	ND	ND	ND
BB1	3.325e-02	1187.1	1.29e+04	1133.7	4.50	1.09e+04	9.36e+03
BB1	1.000e-01	1187.1	1.29e+04	1180.5	0.56	1.27e+04	1.90e+04
BB1	3.318e-01	1187.1	1.29e+04	1192.8	0.48	1.31e+04	1.13e+04

TABLE B-7. TEMPERATURE MEASUREMENT DATA FOR BLUE FILTER APERTURE 2.

SOURCE	SOURCE APERTURE (CM^2)	ACTUAL TEMP (°C)	RADIANCE FROM ACTUAL TEMP	MEASURED TEMP (°C)	TEMP ERROR (%)	RADIANCE FROM MEASURED TEMP	RADIANCE FROM IMAGER
BB1	1.000e-02	612.2	7.42e+02	ND	ND	ND	ND
BB1	3.325e-02	612.2	7.42e+02	607.9	0.70	7.16e+02	6.14e+02
BB1	1.000e-01	612.2	7.42e+02	614.5	0.38	7.56e+02	6.48e+02
BB1	3.318e-01	612.2	7.42e+02	625.4	2.16	8.25e+02	7.07e+02
BB1	3.871e+00	610.9	7.34e+02	620.0	1.49	7.90e+02	7.72e+02
BB2	1.000e-02	700.1	1.42e+03	620.7	11.34	7.94e+02	7.38e+02
BB2	3.325e-02	700.1	1.42e+03	691.5	1.23	1.34e+03	1.25e+03
BB2	1.000e-01	700.1	1.42e+03	702.0	0.27	1.44e+03	1.34e+03
BB2	3.318e-01	700.1	1.42e+03	704.1	0.57	1.46e+03	1.36e+03
BB1	3.871e+00	715.6	1.58e+03	711.5	0.57	1.53e+03	1.50e+03
BB2	1.000e-02	801.0	2.64e+03	704.1	12.10	1.46e+03	1.36e+03
BB2	3.325e-02	801.0	2.64e+03	781.1	2.48	2.36e+03	2.19e+03
BB2	1.000e-01	801.0	2.64e+03	793.8	0.90	2.53e+03	3.35e+03
BB2	3.318e-01	801.0	2.64e+03	799.6	0.17	2.62e+03	3.43e+03
BB1	3.871e+00	817.6	2.89e+03	807.0	1.30	2.73e+03	2.67e+03
BB1	1.000e-02	911.6	4.61e+03	774.1	15.08	2.26e+03	1.94e+03
BB2	1.000e-02	899.5	4.36e+03	ND	ND	ND	ND
BB1	3.325e-02	911.6	4.61e+03	896.1	1.70	4.29e+03	3.68e+03
BB2	3.325e-02	899.5	4.36e+03	868.3	3.47	3.75e+03	3.49e+03
BB2	1.000e-01	899.5	4.36e+03	885.7	1.53	4.08e+03	3.79e+03
BB1	1.000e-01	911.6	4.61e+03	907.1	0.49	4.51e+03	3.88e+03
BB1	3.318e-01	911.6	4.61e+03	914.6	0.33	4.67e+03	4.01e+03
BB2	3.318e-01	899.5	4.36e+03	891.0	0.94	4.19e+03	3.89e+03
BB1	3.871e+00	917.0	4.73e+03	903.0	1.53	4.43e+03	4.34e+03
BB2	1.000e-02	981.1	6.23e+03	ND	ND	ND	ND
BB2	3.325e-02	981.1	6.23e+03	937.7	4.42	5.18e+03	4.82e+03
BB2	1.000e-01	981.1	6.23e+03	956.4	2.52	5.62e+03	5.22e+03
BB2	3.318e-01	981.1	6.23e+03	963.6	1.78	5.79e+03	5.38e+03
BB1	3.871e+00	1017.0	7.19e+03	998.5	1.82	6.68e+03	6.54e+03
BB1	1.000e-02	1187.1	1.29e+04	ND	ND	ND	ND
BB1	3.325e-02	1187.1	1.29e+04	1145.4	3.51	1.13e+04	4.72e+03
BB1	1.000e-01	1187.1	1.29e+04	1187.6	0.04	1.29e+04	1.11e+04
BB1	3.318e-01	1187.1	1.29e+04	1196.5	0.79	1.33e+04	1.14e+04

TABLE B-8. TEMPERATURE MEASUREMENT ERROR DATA. VALUES LISTED ARE PERCENTAGES.

APERTURE (CM^2)	B.B. TEMP = 300°C					900°C		
	NOF/AP 1	NOF/AP 2	YEL/AP 1	YEL/AP 2	BLU/AP 0	YEL/AP 2	BLU/AP 1	BLU/AP 2
0.0100	22.57	9.72	16.87	6.98	NS	14.91	15.15	15.08
0.0333	1.37	0.72	2.53	1.24	3.13	0.89	3.98	2.59
0.1000	1.42	1.61	1.88	1.80	1.24	0.52	1.67	1.01
0.3318	2.93	3.11	3.45	3.41	1.86	0.59	1.07	0.64
0.8108	NT	0.16	1.59	0.80	1.75	NT	NT	NT
1.8240	NT	0.13	1.27	0.67	0.35	NT	NT	NT
3.8710	0.73	1.00	0.33	1.07	1.73	1.42	2.07	1.53
5.0680	NT	0.16	6.69	0.70	NS	NT	NT	NT
20.270	NT	0.27	3.37	4.26	11.37	NT	NT	NT

NOTE:
NS - no signal detected
NT - no test
NOF - no filter
YEL - yellow filter
BLU - blue filter
AP - 880+ aperture

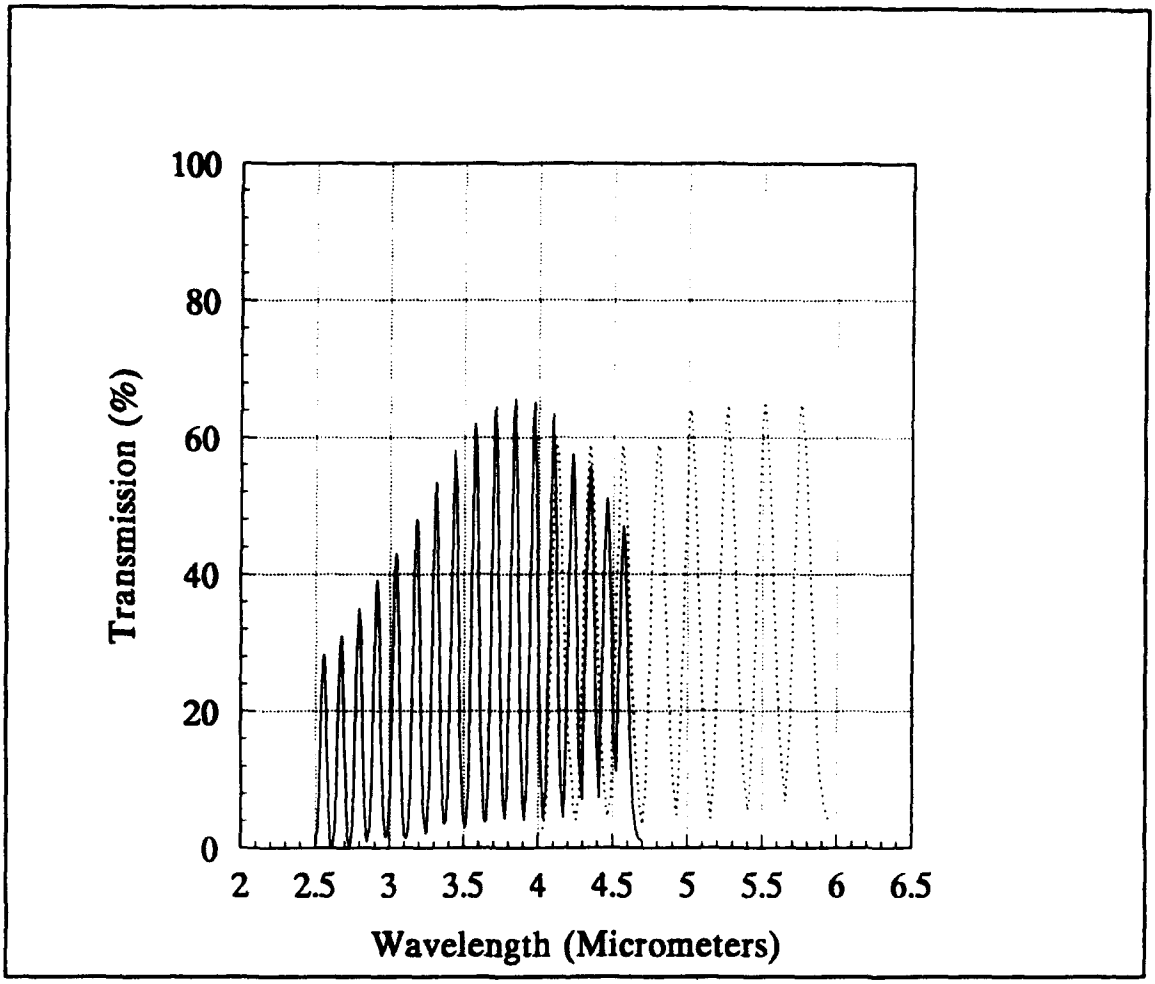

FIGURE B-1. TWO SEGMENTS OF THE OCLI CVF. SOLID LINE IS SEGMENT 1. DOTTED LINE IS SEGMENT 2.

TABLE B-9. CVFSEG1.DAT - TRANSMISSION OF CVF SEGMENT 1 AS A FUNCTION OF WAVELENGTH.

λ	%T	λ	%T	λ	%T	λ	%T
2.500	0.0	2.841	1.8	3.279	23.1	3.861	43.0
2.506	0.8	2.849	0.8	3.289	37.1	3.876	20.5
2.513	3.0	2.857	1.8	3.300	50.0	3.891	7.5
2.519	6.2	2.865	3.2	3.309	53.5	3.906	4.0
2.525	9.9	2.874	7.1	3.311	53.4	3.922	10.7
2.532	15.0	2.882	13.0	3.322	45.0	3.937	28.0
2.538	20.7	2.890	22.0	3.333	30.0	3.953	52.2
2.545	25.4	2.899	30.3	3.344	15.0	3.968	65.3
2.551	27.9	2.907	37.1	3.356	6.5	3.970	65.3
2.555	28.3	2.915	39.1	3.367	3.5	3.984	55.5
2.558	28.1	2.917	39.2	3.378	4.0	4.000	31.0
2.564	24.5	2.924	35.9	3.390	8.9	4.016	11.5
2.571	19.7	2.933	27.4	3.401	19.0	4.032	4.2
2.577	13.0	2.941	17.8	3.413	34.5	4.049	9.1
2.584	7.9	2.950	9.0	3.425	50.0	4.065	26.5
2.591	3.3	2.959	4.1	3.436	58.2	4.082	51.3
2.597	1.5	2.967	2.0	3.448	52.0	4.098	63.5
2.604	0.3	2.976	1.5	3.460	34.5	4.115	50.5
2.611	0.0	2.985	2.0	3.472	17.8	4.132	25.8
2.618	0.2	2.994	5.0	3.484	8.0	4.149	8.9
2.625	1.8	3.003	10.0	3.497	3.9	4.167	4.4
2.632	4.5	3.012	17.8	3.509	3.0	4.184	14.5
2.639	9.0	3.021	28.0	3.521	6.0	4.202	35.0
2.646	14.1	3.030	38.0	3.534	13.9	4.219	54.7
2.653	20.5	3.040	42.8	3.546	30.0	4.230	57.6
2.660	26.1	3.043	43.1	3.559	48.2	4.237	55.5
2.667	30.5	3.049	41.7	3.571	61.3	4.255	36.5
2.672	31.1	3.058	32.9	3.577	62.2	4.274	13.1
2.674	31.0	3.067	21.5	3.584	58.5	4.292	7.0
2.681	28.2	3.077	11.2	3.597	40.0	4.310	23.1
2.688	22.5	3.086	5.2	3.610	20.0	4.329	46.1
2.695	15.9	3.096	2.0	3.623	8.0	4.344	55.7
2.703	9.1	3.106	1.5	3.636	3.8	4.348	55.6
2.710	4.6	3.115	1.4	3.650	4.0	4.367	42.2
2.717	1.7	3.125	3.4	3.663	10.4	4.386	21.0
2.725	0.4	3.135	7.4	3.676	25.0	4.405	7.3
2.732	0.2	3.145	16.2	3.690	46.5	4.425	23.4
2.740	1.0	3.155	27.2	3.704	63.1	4.444	45.0
2.747	3.3	3.165	39.5	3.709	64.6	4.460	51.1
2.755	7.2	3.175	47.2	3.717	61.5	4.464	50.9
2.762	13.2	3.180	48.1	3.731	42.0	4.484	37.0
2.770	20.8	3.185	47.1	3.745	20.0	4.505	17.1
2.778	28.0	3.195	37.6	3.759	7.5	4.525	11.2
2.786	33.0	3.205	25.1	3.774	4.2	4.545	31.5
2.793	35.0	3.215	12.5	3.788	8.6	4.566	47.0
2.801	32.3	3.226	5.6	3.802	22.2	4.570	47.1
2.809	25.9	3.236	2.7	3.817	44.0	4.587	40.8
2.817	17.1	3.247	2.0	3.831	63.0	4.608	22.6
2.825	9.5	3.257	5.7	3.840	65.9	4.630	7.4
2.833	4.2	3.268	12.0	3.846	63.0	4.651	2.8
						4.673	1.4

TABLE B-10. CVFSEG2.DAT - TRANSMISSION OF CVF SEGMENT 2 AS A FUNCTION OF WAVELENGTH.

λ	%T	λ	%T	λ	%T
4.000	2.0	4.525	37.3	5.181	13.0
4.016	2.0	4.545	54.0	5.208	33.7
4.032	3.0	4.562	59.0	5.236	56.5
4.049	6.0	4.566	59.0	5.260	64.9
4.065	15.2	4.587	51.0	5.263	64.8
4.082	30.0	4.608	37.8	5.291	55.0
4.098	47.0	4.630	24.8	5.319	39.5
4.115	58.2	4.651	14.3	5.348	22.0
4.122	59.1	4.673	7.1	5.376	10.2
4.132	57.3	4.695	3.4	5.405	5.5
4.149	46.3	4.717	8.0	5.435	17.0
4.167	34.1	4.739	21.7	5.464	42.0
4.184	23.5	4.762	41.5	5.495	61.7
4.202	16.5	4.785	56.5	5.51	64.9
4.219	12.0	4.798	59.0	5.525	62.7
4.237	5.8	4.808	58.5	5.556	48.3
4.255	4.1	4.831	48.0	5.587	30.0
4.274	8.0	4.854	33.4	5.618	15.6
4.292	22.6	4.878	20.2	5.65	6.8
4.310	40.0	4.902	9.6	5.682	17.0
4.329	54.2	4.926	4.8	5.714	43.5
4.344	59.0	4.950	15.8	5.747	64.8
4.348	59.0	4.975	35.0	5.754	65.0
4.367	51.0	5.000	56.4	5.78	60.1
4.386	38.0	5.013	64.2	5.814	44.0
4.405	25.8	5.025	62.9	5.848	26.5
4.425	15.5	5.051	50.8	5.882	10.5
4.444	8.5	5.076	35.0	5.917	6.0
4.464	4.5	5.102	19.6	5.952	3.2
4.484	7.2	5.128	9.4		
4.505	19.1	5.155	4.3		

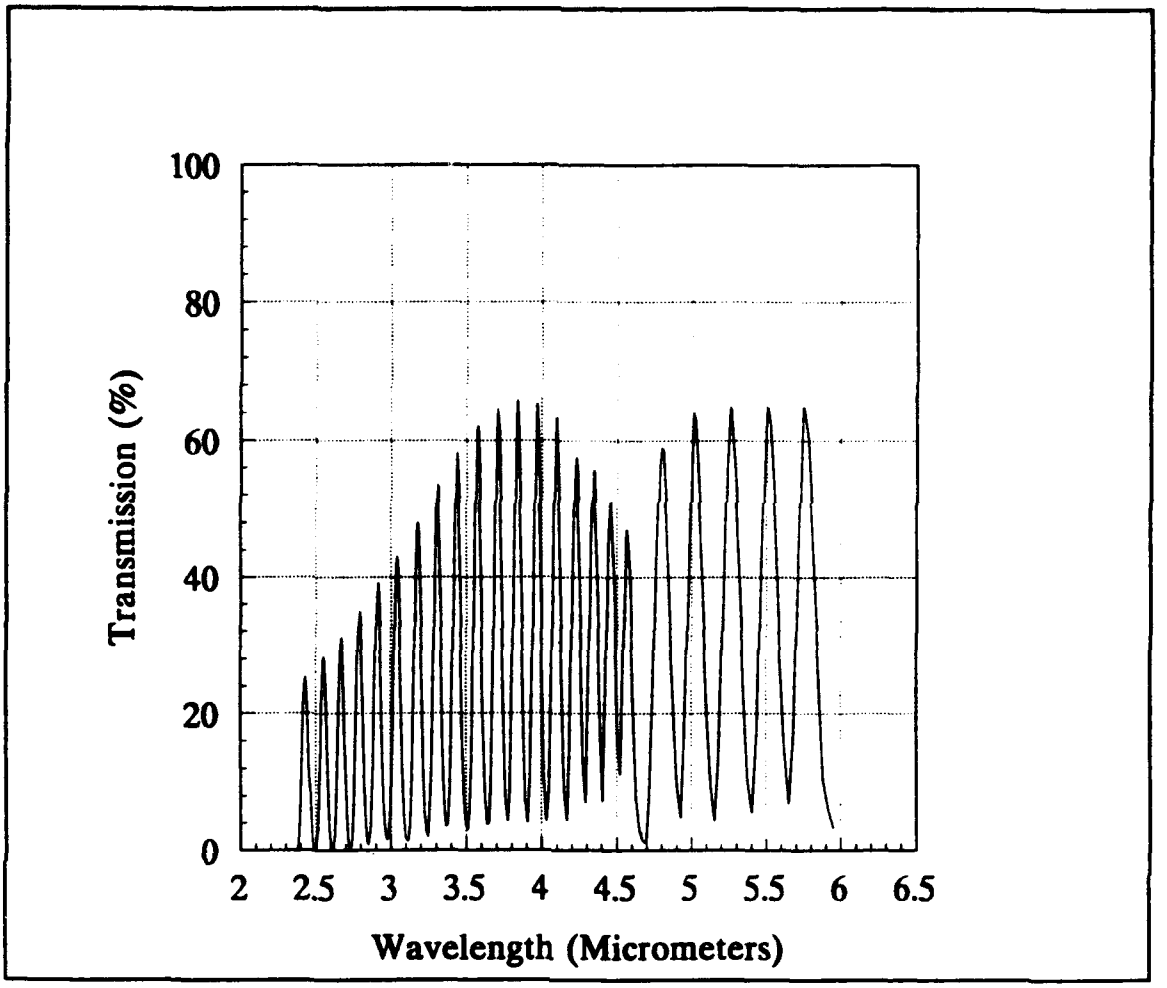

FIGURE B-2. COMBINATION OF COMPLETE CVF SEGMENT 1 AND THE PORTION OF CVF SEGMENT 2 FROM 4.717 TO 5.950 μm.

TABLE B-11. CVF1.DAT - COMBINATION OF COMPLETE CVF SEGMENT 1 AND THE PORTION OF CVF SEGMENT 2 FROM 4.717 TO 5.950 µm.

λ	%T	λ	%T	λ	%T	λ	%T	λ	%T
2.375	0.0	2.725	0.4	3.175	47.2	3.774	4.2	4.608	22.6
2.382	0.6	2.732	0.2	3.180	48.1	3.788	8.6	4.630	7.4
2.388	2.5	2.740	1.0	3.185	47.1	3.802	22.2	4.651	2.8
2.395	5.6	2.747	3.3	3.195	37.6	3.817	44.0	4.673	1.4
2.402	9.5	2.755	7.2	3.205	25.1	3.831	63.0	4.695	1.0
2.408	14.5	2.762	13.2	3.215	12.5	3.840	65.9	4.717	8.0
2.414	20.6	2.770	20.8	3.226	5.6	3.846	63.0	4.739	1.7
2.421	22.9	2.778	28.0	3.236	2.7	3.861	43.0	4.762	41.5
2.427	24.9	2.786	33.0	3.247	2.0	3.876	20.5	4.785	56.5
2.434	25.5	2.793	35.0	3.257	5.7	3.891	7.5	4.798	59.0
2.440	22.5	2.801	32.3	3.268	12.0	3.906	4.0	4.808	58.5
2.447	18.7	2.809	25.9	3.279	23.1	3.922	10.7	4.831	48.0
2.453	12.2	2.817	17.1	3.289	37.1	3.937	28.0	4.854	33.4
2.460	10.0	2.825	9.5	3.300	50.0	3.953	52.2	4.878	20.2
2.466	8.6	2.833	4.2	3.309	53.5	3.968	65.3	4.902	9.6
2.473	4.3	2.841	1.8	3.311	53.4	3.970	65.3	4.926	4.8
2.480	1.6	2.849	0.8	3.322	45.0	3.984	55.5	4.950	15.8
2.486	0.3	2.857	1.8	3.333	30.0	4.000	31.0	4.975	35.0
2.493	0.0	2.865	3.2	3.344	15.0	4.016	11.5	5.000	56.4
2.500	0.0	2.874	7.1	3.356	6.5	4.032	4.2	5.013	64.2
2.506	0.8	2.882	13.0	3.367	3.5	4.049	9.1	5.025	62.9
2.513	3.0	2.890	22.0	3.378	4.0	4.065	26.5	5.051	50.8
2.519	6.2	2.899	30.3	3.390	8.9	4.082	51.3	5.076	35.0
2.525	9.9	2.907	37.1	3.401	19.0	4.098	63.5	5.102	19.6
2.532	15.0	2.915	39.1	3.413	34.5	4.115	50.5	5.128	9.4
2.538	20.7	2.917	39.2	3.425	50.0	4.132	25.8	5.155	4.3
2.545	25.4	2.924	35.9	3.436	58.2	4.149	8.9	5.181	13.0
2.551	27.9	2.933	27.4	3.448	52.0	4.167	4.4	5.208	33.7
2.555	28.3	2.941	17.8	3.460	34.5	4.184	14.5	5.236	56.5
2.558	28.1	2.950	9.0	3.472	17.8	4.202	35.0	5.260	64.9
2.564	24.5	2.959	4.1	3.484	8.0	4.219	54.7	5.263	64.8
2.571	19.7	2.967	2.0	3.497	3.9	4.230	57.6	5.291	55.0
2.577	13.0	2.976	1.5	3.509	3.0	4.237	55.5	5.319	39.5
2.584	7.9	2.985	2.0	3.521	6.0	4.255	36.5	5.348	22.0
2.591	3.3	2.994	5.0	3.534	13.9	4.274	13.1	5.376	10.2
2.597	1.5	3.003	10.0	3.546	30.0	4.292	7.0	5.405	5.5
2.604	0.3	3.012	17.8	3.559	48.2	4.310	23.1	5.435	17.0
2.611	0.0	3.021	28.0	3.571	61.3	4.329	46.1	5.464	42.0
2.618	0.2	3.030	38.0	3.577	62.2	4.344	55.7	5.495	61.7
2.625	1.8	3.040	42.8	3.584	58.5	4.348	55.6	5.510	64.9
2.632	4.5	3.043	43.1	3.597	40.0	4.367	42.2	5.525	62.7
2.639	9.0	3.049	41.7	3.610	20.0	4.386	21.0	5.556	48.3
2.646	14.1	3.058	32.9	3.623	8.0	4.405	7.3	5.587	30.0
2.653	20.5	3.067	21.5	3.636	3.8	4.425	23.4	5.618	15.6
2.660	26.1	3.077	11.2	3.650	4.0	4.444	45.0	5.650	6.8
2.667	30.5	3.086	5.2	3.663	10.4	4.460	51.1	5.682	17.0
2.672	31.1	3.096	2.0	3.676	25.0	4.464	50.9	5.714	43.5
2.674	31.0	3.106	1.5	3.690	46.5	4.484	37.0	5.747	64.8
2.681	28.2	3.115	1.4	3.704	63.1	4.505	17.1	5.754	65.0
2.688	22.5	3.125	3.4	3.709	64.6	4.525	11.2	5.780	60.1
2.695	15.9	3.135	7.4	3.717	61.5	4.545	31.5	5.814	44.0
2.703	9.1	3.145	16.2	3.731	42.0	4.566	47.0	5.848	26.5
2.710	4.6	3.155	27.2	3.745	20.0	4.570	47.1	5.882	10.5
2.717	1.7	3.165	39.5	3.759	7.5	4.587	40.8	5.917	6.0
								5.952	3.2

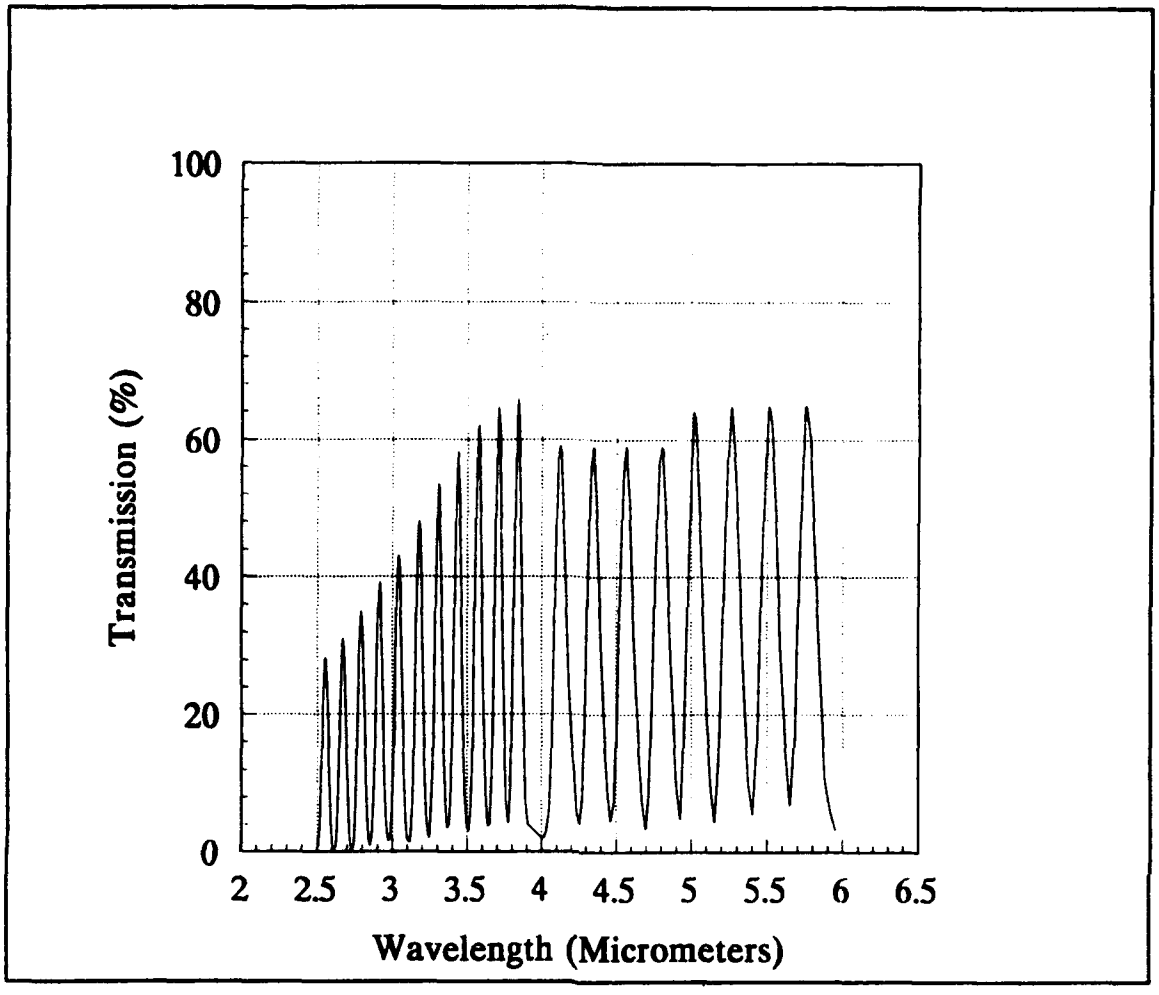

FIGURE B-3. COMBINATION OF COMPLETE CVF SEGMENT 2 AND THE PORTION OF CVF SEGMENT 1 FROM 2.380 TO 4.000 µm.

TABLE B-12. CVF2.DAT - COMBINATION OF COMPLETE CVF SEGMENT 2 AND THE PORTION OF CVFSEGMENT 1 FORM 2.380 TO 4.000 μm.

λ	%T	λ	%T	λ	%T	λ	%T	λ	%T
2.500	0.0	2.833	4.2	3.257	5.7	3.831	63.0	4.739	21.7
2.506	0.8	2.841	1.8	3.268	12.0	3.840	65.9	4.762	41.5
2.513	3.0	2.849	0.8	3.279	23.1	3.846	63.0	4.785	56.5
2.519	6.2	2.857	1.8	3.289	37.1	3.861	43.0	4.798	59.0
2.525	9.9	2.865	3.2	3.300	50.0	3.876	20.5	4.808	58.5
2.532	15.0	2.874	7.1	3.309	53.5	3.891	7.5	4.831	48.0
2.538	20.7	2.882	13.0	3.311	53.4	3.906	4.0	4.854	33.4
2.545	25.4	2.890	22.0	3.322	45.0	4.000	2.0	4.878	20.2
2.551	27.9	2.899	30.3	3.333	30.0	4.016	2.0	4.902	9.6
2.555	28.3	2.907	37.1	3.344	15.0	4.032	3.0	4.926	4.8
2.558	28.1	2.915	39.1	3.356	6.5	4.049	6.0	4.950	15.8
2.564	24.5	2.917	39.2	3.367	3.5	4.065	15.2	4.975	35.0
2.571	19.7	2.924	35.9	3.378	4.0	4.082	30.0	5.000	56.4
2.577	13.0	2.933	27.4	3.390	8.9	4.098	47.0	5.013	64.2
2.584	7.9	2.941	17.8	3.401	19.0	4.115	58.2	5.025	62.9
2.591	3.3	2.950	9.0	3.413	34.5	4.122	59.1	5.051	50.8
2.597	1.5	2.959	4.1	3.425	50.0	4.132	57.3	5.076	35.0
2.604	0.3	2.967	2.0	3.436	58.2	4.149	46.3	5.102	19.6
2.611	0.0	2.976	1.5	3.448	52.0	4.167	34.1	5.128	9.4
2.618	0.2	2.985	2.0	3.460	34.5	4.184	23.5	5.155	4.3
2.625	1.8	2.994	5.0	3.472	17.8	4.202	16.5	5.181	13.0
2.632	4.5	3.003	10.0	3.484	8.0	4.219	12.0	5.208	33.7
2.639	9.0	3.012	17.8	3.497	3.9	4.237	5.8	5.236	56.5
2.646	14.1	3.021	28.0	3.509	3.0	4.255	4.1	5.260	64.9
2.653	20.5	3.030	38.0	3.521	6.0	4.274	8.0	5.263	64.8
2.660	26.1	3.040	42.8	3.534	13.9	4.292	22.6	5.291	55.0
2.667	30.5	3.043	43.1	3.546	30.0	4.310	40.0	5.319	39.5
2.672	31.1	3.049	41.7	3.559	48.2	4.329	54.2	5.348	22.0
2.674	31.0	3.058	32.9	3.571	61.3	4.344	59.0	5.376	10.2
2.681	28.2	3.067	21.5	3.577	62.2	4.348	59.0	5.405	5.5
2.688	22.5	3.077	11.2	3.584	58.5	4.367	51.0	5.435	17.0
2.695	15.9	3.086	5.2	3.597	40.0	4.386	38.0	5.464	42.0
2.703	9.1	3.096	2.0	3.610	20.0	4.405	25.8	5.495	61.7
2.710	4.6	3.106	1.5	3.623	8.0	4.425	15.5	5.510	64.9
2.717	1.7	3.115	1.4	3.636	3.8	4.444	8.5	5.525	62.7
2.725	0.4	3.125	3.4	3.650	4.0	4.464	4.5	5.556	48.3
2.732	0.2	3.135	7.4	3.663	10.4	4.484	7.2	5.587	30.0
2.740	1.0	3.145	16.2	3.676	25.0	4.505	19.1	5.618	15.6
2.747	3.3	3.155	27.2	3.690	46.5	4.525	37.3	5.650	6.8
2.755	7.2	3.165	39.5	3.704	63.1	4.545	54.0	5.682	17.0
2.762	13.2	3.175	47.2	3.709	64.6	4.562	59.0	5.714	43.5
2.770	20.8	3.180	48.1	3.717	61.5	4.566	59.0	5.747	64.8
2.778	28.0	3.185	47.1	3.731	42.0	4.587	51.0	5.754	65.0
2.786	33.0	3.195	37.6	3.745	20.0	4.608	37.8	5.780	60.1
2.793	35.0	3.205	25.1	3.759	7.5	4.630	24.8	5.814	44.0
2.801	32.3	3.215	12.5	3.774	4.2	4.651	14.3	5.848	26.5
2.809	25.9	3.226	5.6	3.788	8.6	4.673	7.1	5.882	10.5
2.817	17.1	3.236	2.7	3.802	22.2	4.695	3.4	5.917	6.0
2.825	9.5	3.247	2.0	3.817	44.0	4.717	8.0	5.952	3.2

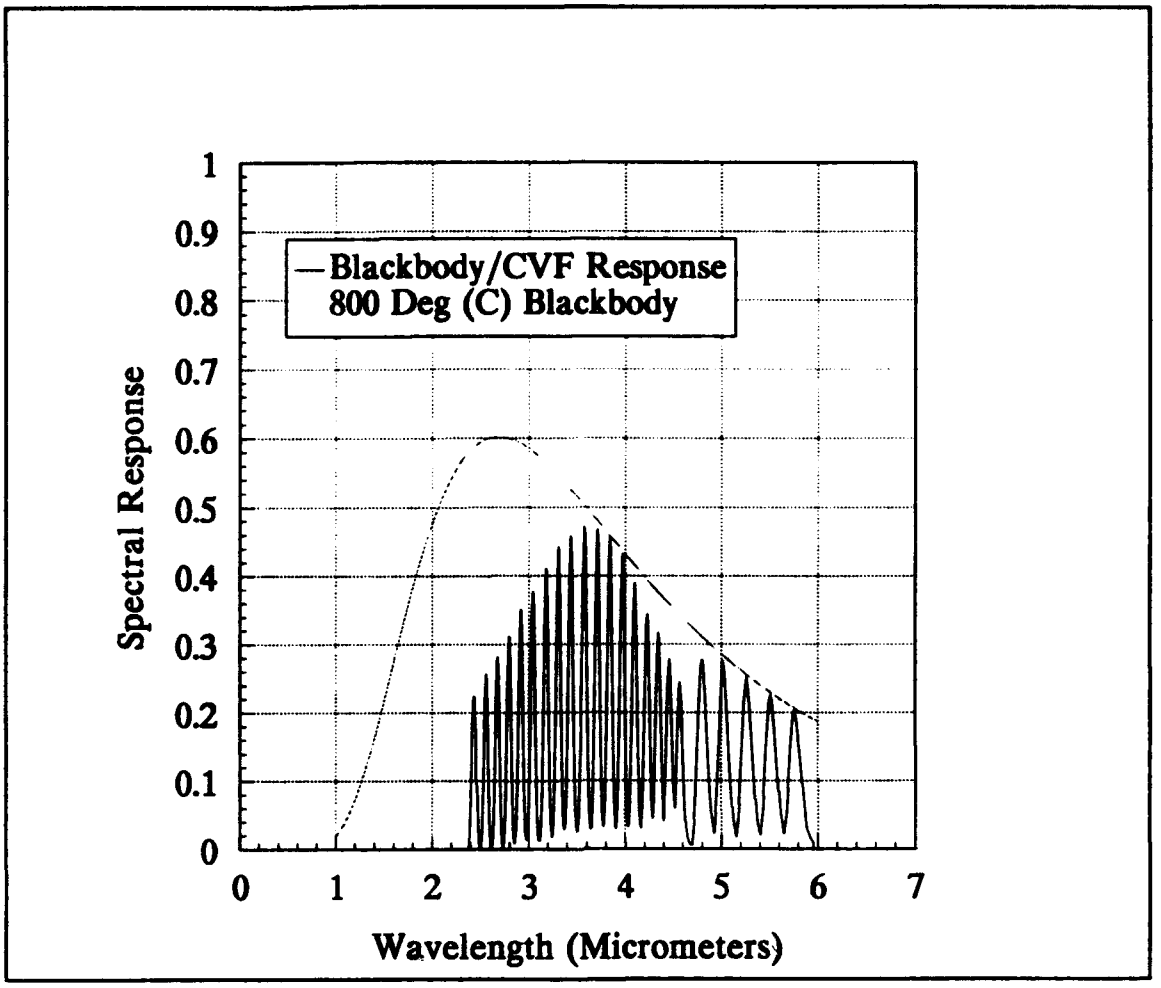

FIGURE B-4. CALCULATED IN-BAND RADIANCE FOR A 800 BLACKBODY (SOLID LINE). THEORETICAL PLANCK CURVE (DOTTED LINE) IS MULTIPLIED BY THE FILTER CVF1 TO GET THE IN-BAND RADIANCE.

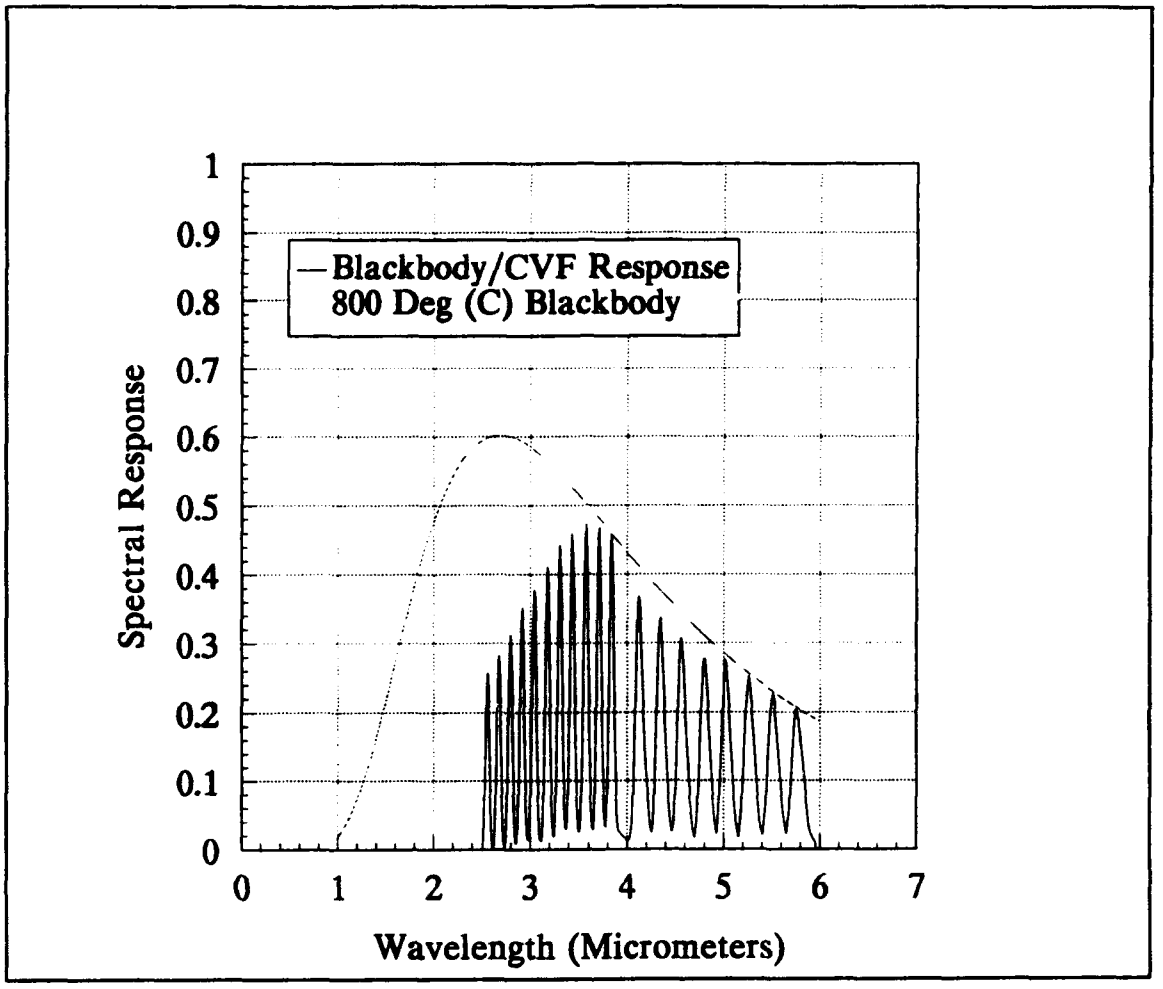

FIGURE B-5. CALCULATED IN-BAND RADIANCE FOR A 800 BLACKBODY (SOLID LINE). THEORETICAL PLANCK CURVE (DOTTED LINE) IS MULTIPLIED BY THE FILTER CVF2 TO GET THE IN-BAND RADIANCE.

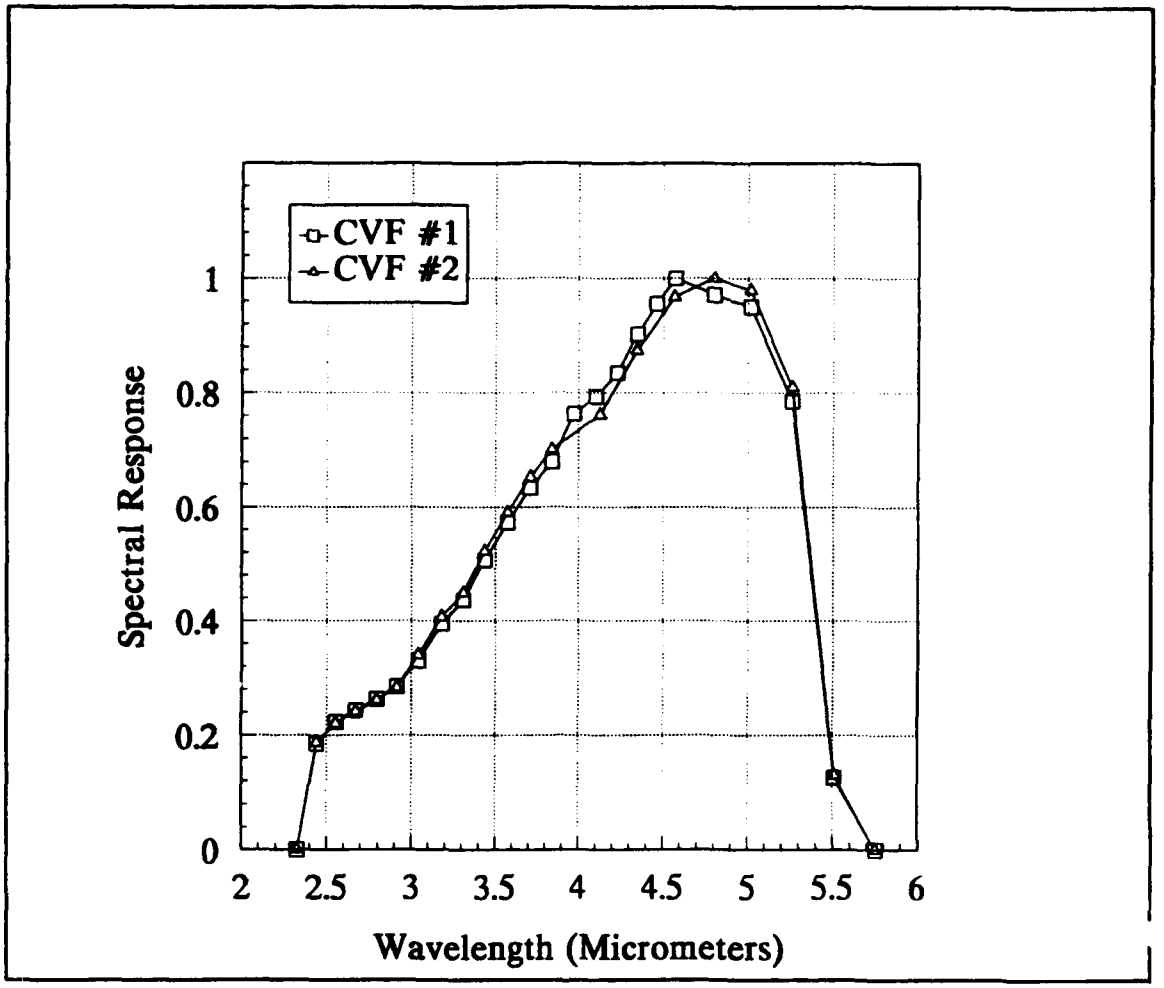

FIGURE B-6. SPECTRAL RESPONSE OF THE 880+ SYSTEM. AN 805°C BLACKBODY IS VIEWED AT EACH CVF ANGULAR POSITION AND THE MEASURED SIGNAL IS DIVIDED BY THE IN-BAND RADIANCE CALCULATED WITH FILTERS CVF1 AND CVF2.

TABLE B-13. 805RES1.DAT - SPECTRAL RESPONSE OF THE 880+. CALCULATED WITH A 805°C BLACKBODY AND FILTER CVF1.

CVF	λ	RADIANCE	SIGNAL	NORMALIZED RADIANCE	NORMALIZED RESPONSE
0	2.000	0.000000	0.00	0.000000	0.000000
100	2.440	0.011845	264.82	0.363332	0.184850
110	2.555	0.012251	306.54	0.375786	0.222840
120	2.670	0.014188	382.78	0.435201	0.243402
130	2.795	0.016504	413.25	0.506242	0.263026
140	2.915	0.019040	499.44	0.584031	0.285544
150	3.040	0.021020	660.14	0.644765	0.329897
160	3.180	0.023304	875.89	0.714824	0.394816
170	3.310	0.025606	1062.97	0.785436	0.436068
180	3.435	0.027305	1317.22	0.837551	0.506747
190	3.575	0.028276	1543.33	0.867335	0.573345
200	3.710	0.028228	1703.82	0.865863	0.634043
210	3.840	0.028714	1858.60	0.880770	0.679935
220	3.970	0.026739	1942.92	0.820189	0.763282
230	4.100	0.025084	1926.11	0.782310	0.793316
240	4.230	0.022889	1818.94	0.702095	0.834770
250	4.345	0.021246	1825.67	0.651697	0.902653
260	4.460	0.019818	1802.69	0.607895	0.955513
270	4.570	0.017126	1630.35	0.525321	1.000000
310	4.800	0.032601	3010.99	1.000000	0.970182
320	5.015	0.031633	2859.98	0.970307	0.949725
330	5.260	0.032132	2403.63	0.985613	0.785788
340	5.510	0.030153	362.11	0.924910	0.126149
350	5.750	0.028834	0.00	0.884451	0.000000

TABLE B-14. 805RES2.DAT - SPECTRAL RESPONSE OF THE 880+. CALCULATED WITH A 805°C BLACKBODY AND FILTER CVF2.

CVF	λ	RADIANCE	SIGNAL	NORMALIZED RADIANCE	NORMALIZED RESPONSE
0	2.000	0.000000	0.00	0.000000	0.000000
100	2.440	0.011845	264.82	0.363332	0.187670
110	2.555	0.012251	306.54	0.322386	0.220918
120	2.670	0.014188	382.78	0.373358	0.242112
130	2.795	0.016504	413.25	0.434304	0.261110
140	2.915	0.019040	499.44	0.501039	0.284013
150	3.040	0.021020	660.14	0.553143	0.340036
160	3.180	0.023304	875.89	0.613247	0.406949
170	3.310	0.025606	1062.97	0.673824	0.449470
180	3.435	0.027305	1317.22	0.718533	0.522321
190	3.575	0.028276	1543.33	0.744085	0.590966
200	3.710	0.028228	1703.82	0.742822	0.653529
210	3.840	0.028714	1858.60	0.755611	0.700832
280	4.125	0.038001	2672.37	1.000000	0.761417
290	4.345	0.035271	2847.32	0.928159	0.874058
300	4.565	0.034266	3061.89	0.901713	0.967492
310	4.800	0.032601	3010.99	0.857898	1.000000
320	5.015	0.031633	2859.98	0.832425	0.978913
330	5.260	0.032132	2403.63	0.845556	0.809937
340	5.510	0.030153	362.11	0.793479	0.130026
350	5.750	0.028834	0.00	0.758769	0.000000

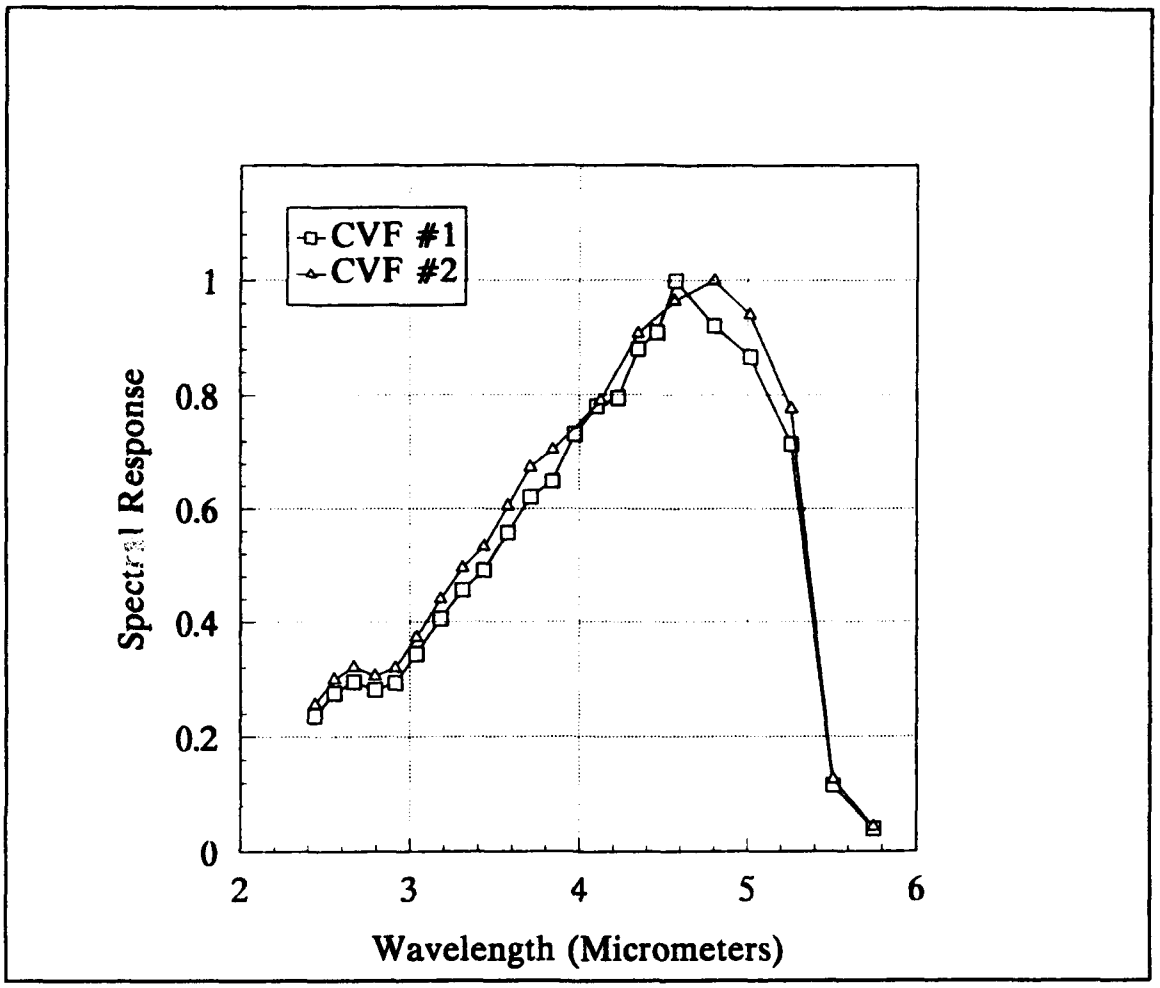

FIGURE B-7. SPECTRAL RESPONSE OF THE 880+ SYSTEM. AN 801°C BLACKBODY IS VIEWED AT EACH CVF ANGULAR POSITION AND THE MEASURED SIGNAL IS DIVIDED BY THE IN-BAND RADIANCE CALCULATED WITH FILTERS CVF1 AND CVF2.

TABLE B-15. 801RES1.DAT - SPECTRAL RESPONSE OF THE 880+. CALCULATED WITH A 801°C BLACKBODY AND FILTER CVF1.

CVF	λ	RADIANCE	SIGNAL	NORMAL. RADIANCE	RESPONSE	NORMALIZED RESPONSE
0	2.000	0.000000	0.0	0.000000	0.000	0.0000
100	2.440	0.011575	258.0	0.359472	717.719	0.2363
110	2.555	0.011977	312.0	0.371957	838.808	0.2761
120	2.670	0.013893	388.0	0.431460	899.273	0.2960
130	2.795	0.016175	430.5	0.502329	857.008	0.2821
140	2.915	0.018823	522.5	0.584565	893.827	0.2942
150	3.040	0.020898	678.5	0.649006	1045.445	0.3441
160	3.180	0.022892	875.5	0.710932	1231.483	0.4054
170	3.310	0.025170	1083.5	0.781677	1386.122	0.4563
180	3.435	0.027124	1256.0	0.842360	1491.049	0.4908
190	3.575	0.027828	1463.0	0.864224	1692.849	0.5572
200	3.710	0.027795	1628.0	0.863199	1886.008	0.6208
210	3.840	0.028287	1732.0	0.878478	1971.591	0.6490
220	3.970	0.026353	1819.0	0.818416	2222.586	0.7316
230	4.100	0.025065	1845.5	0.778416	2370.840	0.7804
240	4.230	0.022576	1692.0	0.701118	2413.288	0.7944
250	4.345	0.020962	1738.5	0.650994	2670.532	0.8791
260	4.460	0.019559	1678.5	0.607422	2763.316	0.9096
270	4.570	0.016906	1595.5	0.525031	3038.868	1.0000
310	4.800	0.032200	2798.5	1.000000	2798.500	0.9212
320	5.015	0.031258	2554.0	0.970745	2630.968	0.8660
330	5.260	0.031765	2141.5	0.986491	2170.826	0.7146
340	5.510	0.029820	326.0	0.926087	352.019	0.1159
350	5.750	0.028526	106.0	0.885901	119.652	0.0394

TABLE B-16. 801RES2.DAT - SPECTRAL RESPONSE OF THE 880+. CALCULATED WITH A 801°C BLACKBODY AND FILTER CVF2.

CVF	λ	RADIANCE	SIGNAL	NORMAL. RADIANCE	RESPONSE	NORMALIZED RESPONSE
0	2.000	0.000000	0.0	0.000000	0.000	0.000000
100	2.440	0.011575	258.0	0.308906	835.207	0.256500
110	2.555	0.011977	312.0	0.319634	976.117	0.299700
120	2.670	0.013893	388.0	0.370767	1046.480	0.321300
130	2.795	0.016175	430.5	0.431667	997.296	0.306200
140	2.915	0.018823	522.5	0.502335	1040.140	0.319400
150	3.040	0.020898	678.5	0.557711	1216.580	0.373600
160	3.180	0.022892	875.5	0.610926	1433.070	0.440100
170	3.310	0.025170	1083.5	0.671719	1613.030	0.495300
180	3.435	0.027124	1256.0	0.723866	1735.130	0.532800
190	3.575	0.027828	1463.0	0.742654	1969.960	0.604900
200	3.710	0.027795	1628.0	0.741774	2194.740	0.673900
210	3.840	0.028287	1732.0	0.754904	2294.330	0.704500
280	4.125	0.037471	2572.0	1.000000	2572.000	0.789800
290	4.345	0.034800	2742.5	0.928718	2953.000	0.906800
300	4.565	0.033827	2835.5	0.902751	3140.950	0.964500
310	4.800	0.032200	2798.5	0.859331	3256.600	1.000000
320	5.015	0.031258	2554.0	0.834192	3061.650	0.940100
330	5.260	0.031765	2141.5	0.847722	2526.180	0.775700
340	5.510	0.029820	326.0	0.795815	409.643	0.125800
350	5.750	0.028526	106.0	0.761282	139.239	0.042800

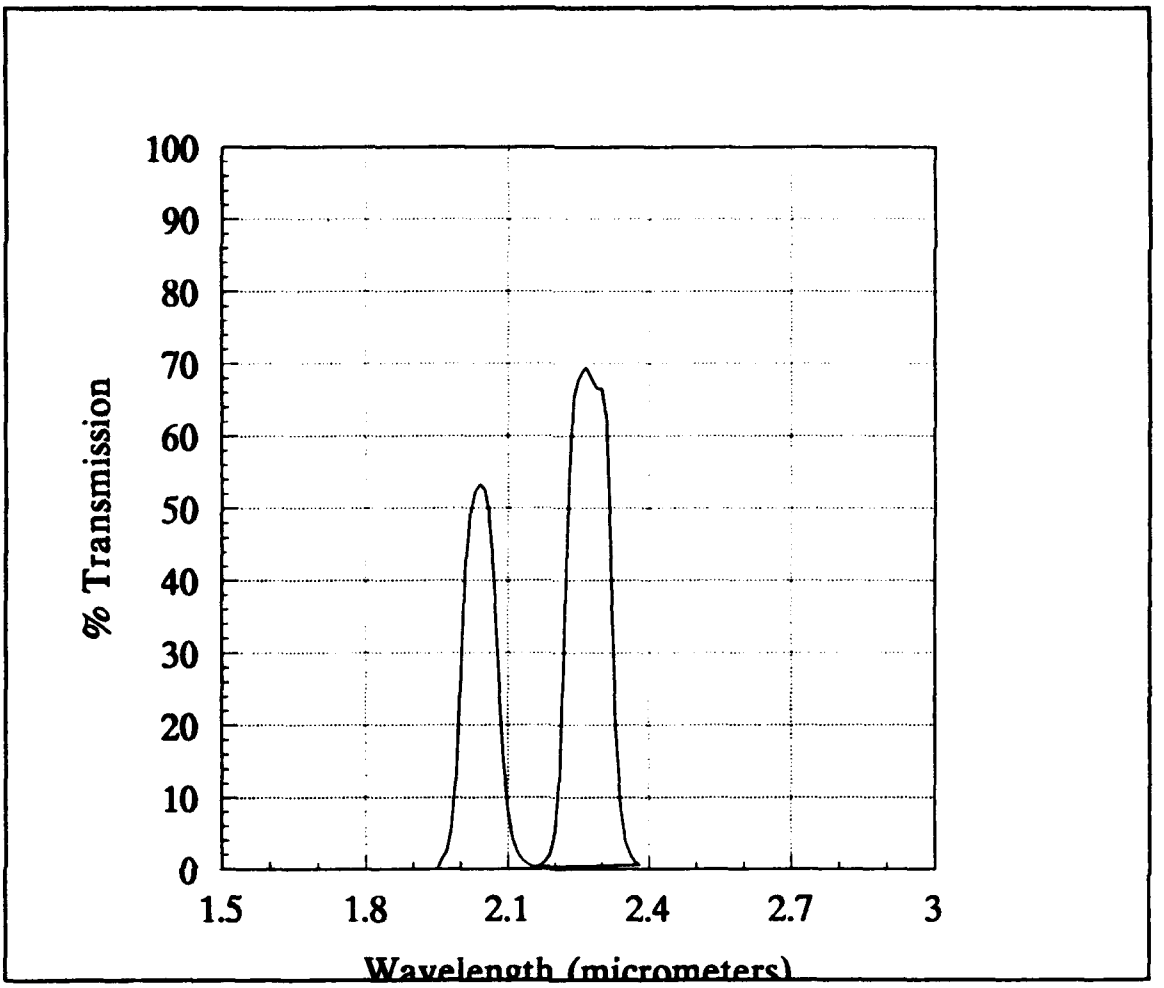

FIGURE B-8. SPECTRAL TRANSMISSION CURVES OF TWO NARROW BAND FILTERS THAT WERE USED TO MEASURE THE SPECTRAL RESPONSE OF THE 880+ AT WAVELENGTHS BELOW THOSE POSSIBLE FROM THE CVF.

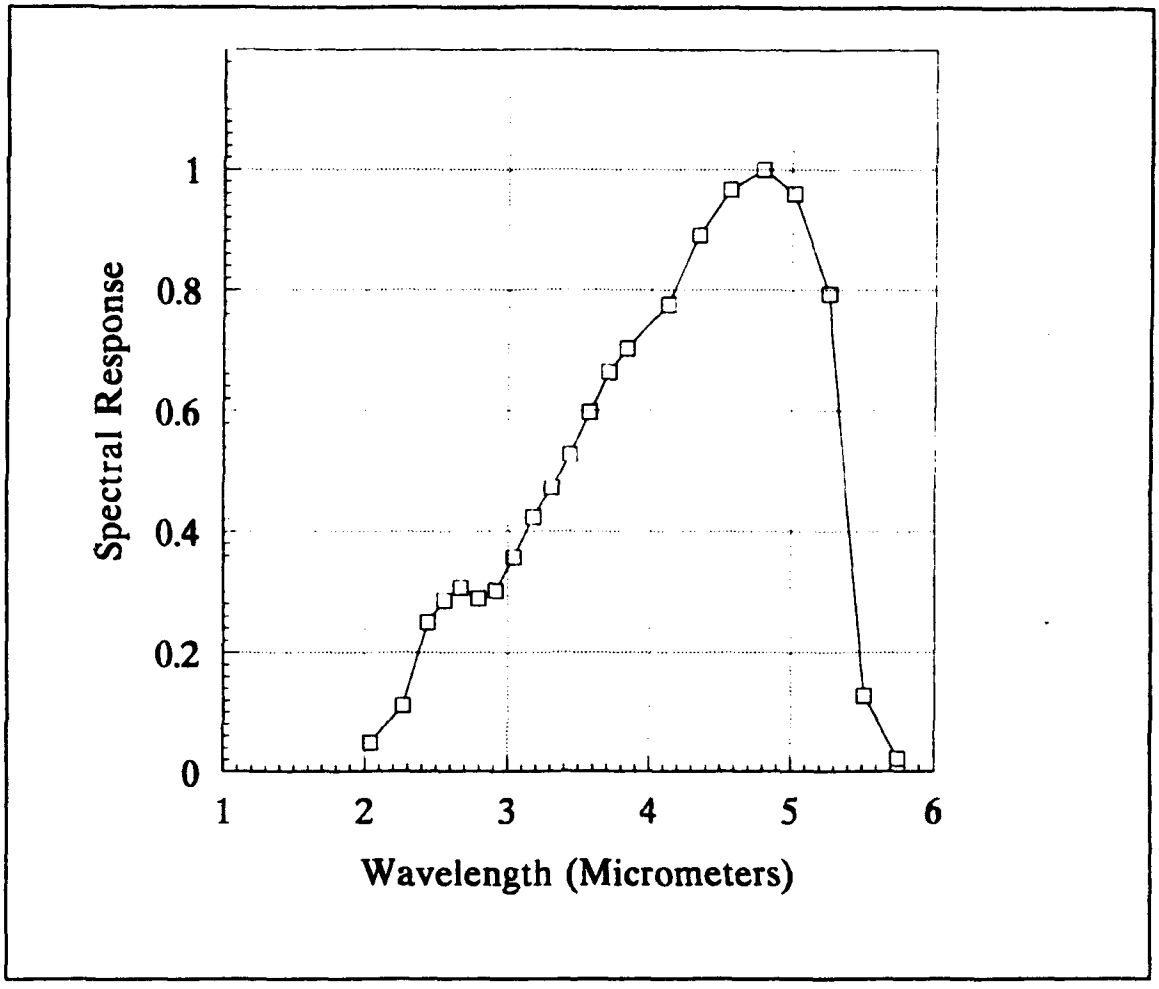

FIGURE B-9. AVERAGED NORMALIZED SPECTRAL RESPONSE OF THE 880+ SYSTEM. THIS CURVE WAS CONSTRUCTED BY TAKING THE AVERAGE VALUE OF THE SPECTRAL RESPONSE FROM 805RES2.DAT AND 801RES2.DAT. FILTER CVF2 WAS SELECTED DUE TO ITS SMOOTH RESPONSE OVER THE ENTIRE SPECTRUM OF INTEREST.

TABLE B-17. NOFRES.DAT - AVERAGE NORMALIZED SPECTRAL RESPONSE FROM 805RES2.DAT AND 801RES1.DAT.

λ	RESPONSE
2.040	0.048104
2.265	0.110920
2.440	0.249284
2.555	0.285309
2.670	0.306706
2.795	0.288655
2.915	0.301706
3.040	0.356818
3.180	0.423525
3.310	0.472385
3.435	0.527561
3.575	0.597933
3.710	0.663715
3.840	0.702666
4.125	0.775609
4.345	0.890429
4.565	0.965996
4.800	1.000000
5.015	0.959507
5.260	0.792819
5.510	0.127913
5.750	0.021400

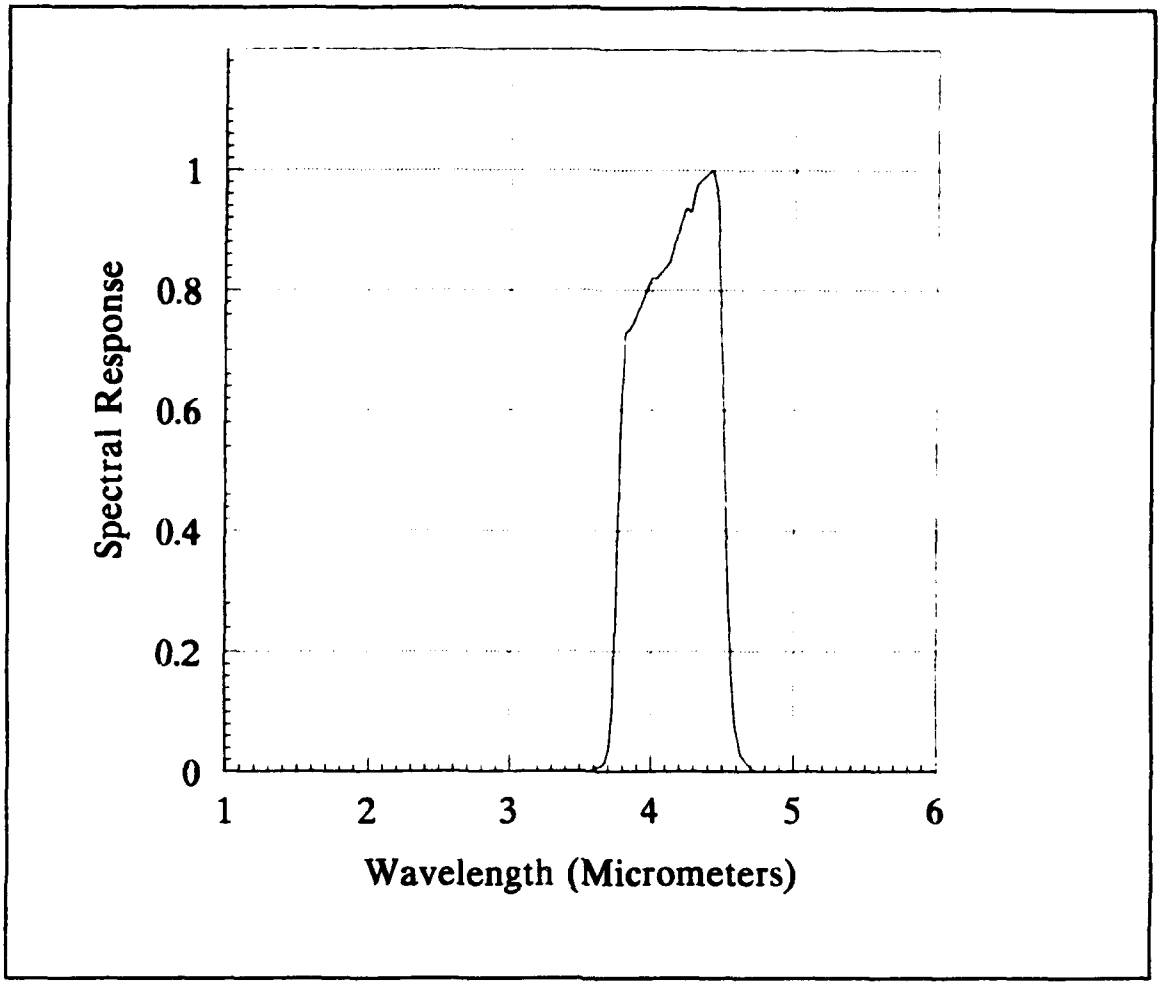

FIGURE B-10. CALCULATED SPECTRAL RESPONSE OF THE 880+ SYSTEM INCLUDING THE YELLOW FILTER.

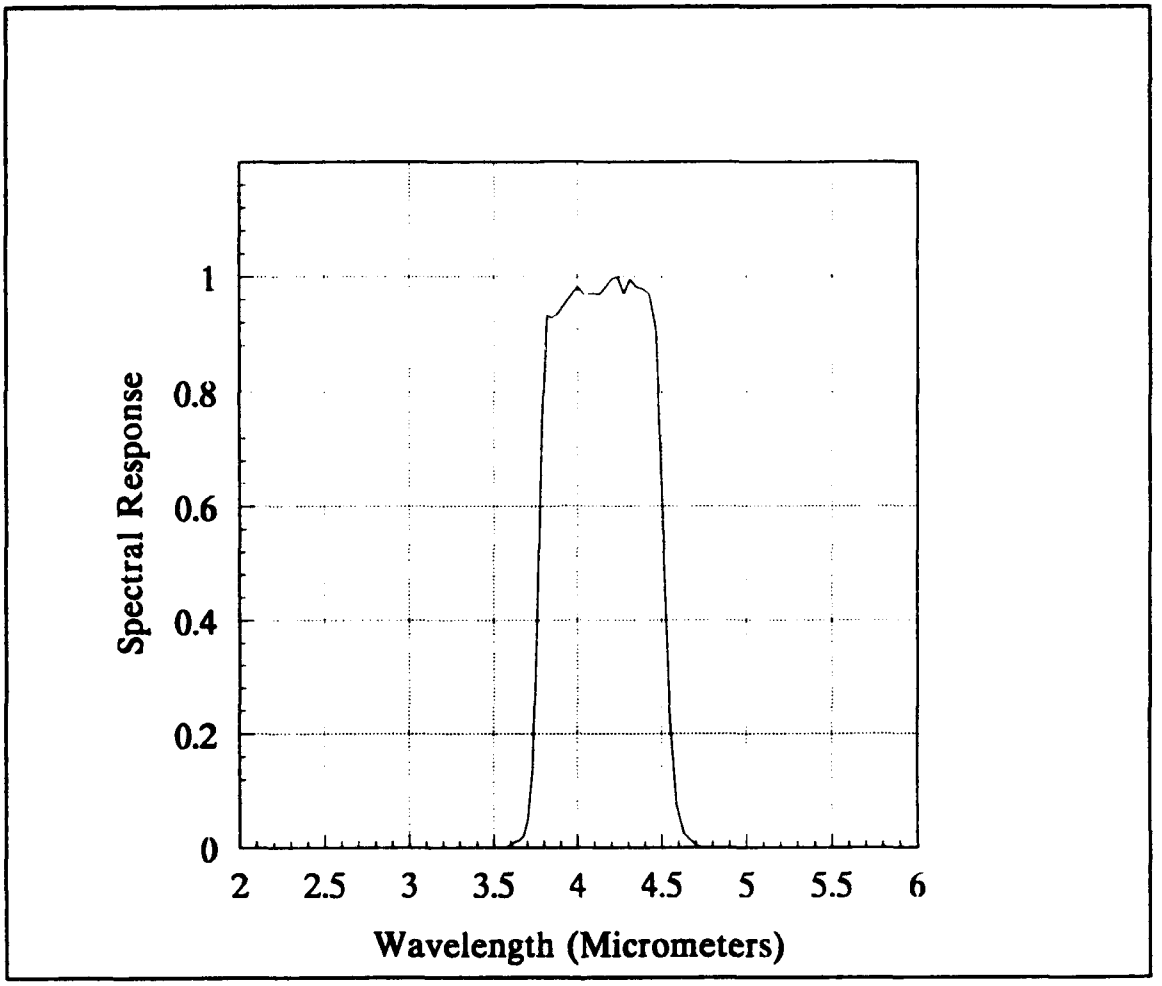

FIGURE B-11. NORMALIZED SPECTRAL TRANSMISSION OF THE YELLOW FILTER.

λ	RELATIVE TRANS.	λ	RELATIVE TRANS.
3.5714	0.0000	4.0984	0.9700
3.5971	0.0050	4.1322	0.9700
3.6232	0.0100	4.1667	0.9820
3.6496	0.0120	4.2017	0.9950
3.6765	0.0200	4.2373	1.0000
3.7037	0.0500	4.2735	0.9700
3.7313	0.1370	4.3103	0.9950
3.7594	0.4100	4.3478	0.9820
3.7879	0.7510	4.3860	0.9780
3.8168	0.9330	4.4248	0.9700
3.8462	0.9280	4.4643	0.9080
3.8760	0.9330	4.5045	0.5970
3.9063	0.9450	4.5455	0.2480
3.9370	0.9580	4.5872	0.0750
3.9683	0.9700	4.6296	0.0250
4.0000	0.9820	4.6729	0.0120
4.0323	0.9700	4.7170	0.0020
4.0650	0.9700	4.7619	0.0000

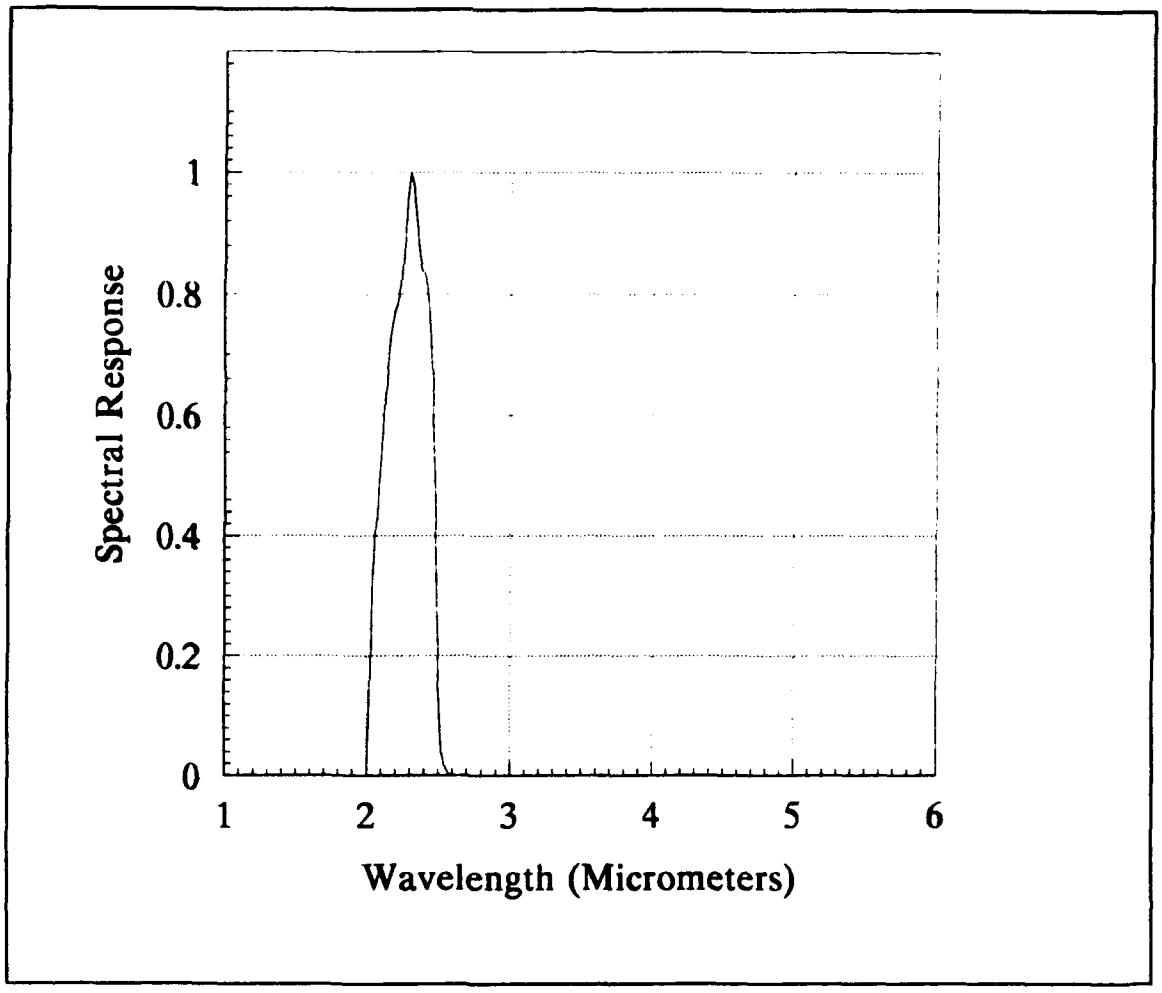

FIGURE B-12. CALCULATED SPECTRAL RESPONSE OF THE 880+ SYSTEM INCLUDING THE BLUE FILTER.

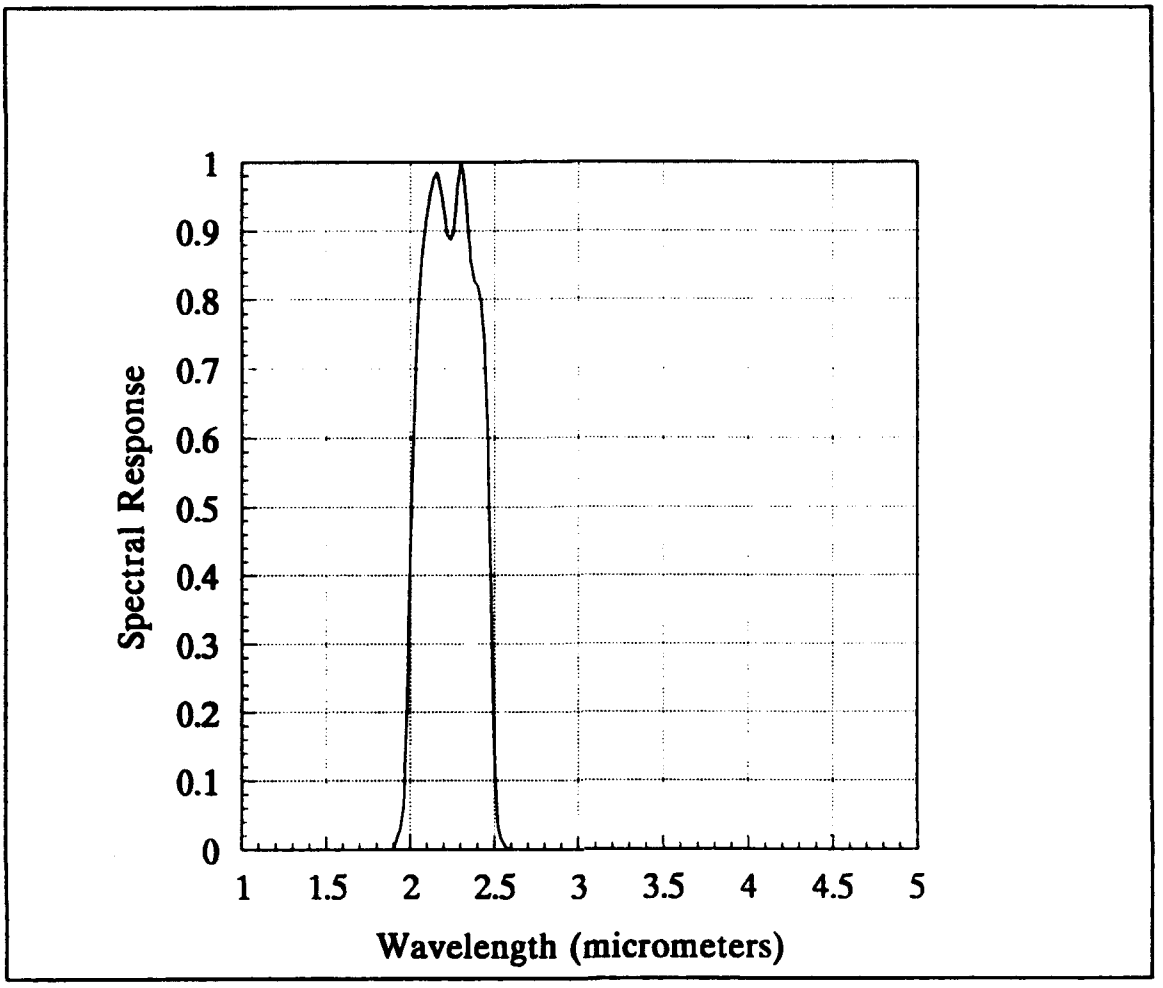

FIGURE B-13. NORMALIZED SPECTRAL TRANSMISSION OF THE BLUE FILTER.

λ	RELATIVE TRANS.	λ	RELATIVE TRANS.
1.900	0.000	2.260	0.902
1.920	0.015	2.280	0.962
1.940	0.030	2.300	1.000
1.960	0.060	2.320	0.977
1.980	0.203	2.340	0.917
2.000	0.439	2.360	0.857
2.020	0.606	2.380	0.827
2.040	0.752	2.400	0.820
2.060	0.834	2.420	0.797
2.080	0.887	2.440	0.737
2.100	0.925	2.460	0.601
2.120	0.955	2.480	0.361
2.140	0.977	2.500	0.135
2.160	0.985	2.520	0.037
2.180	0.962	2.540	0.015
2.200	0.932	2.560	0.007
2.220	0.895	2.580	0.001
2.240	0.887	2.600	0.000

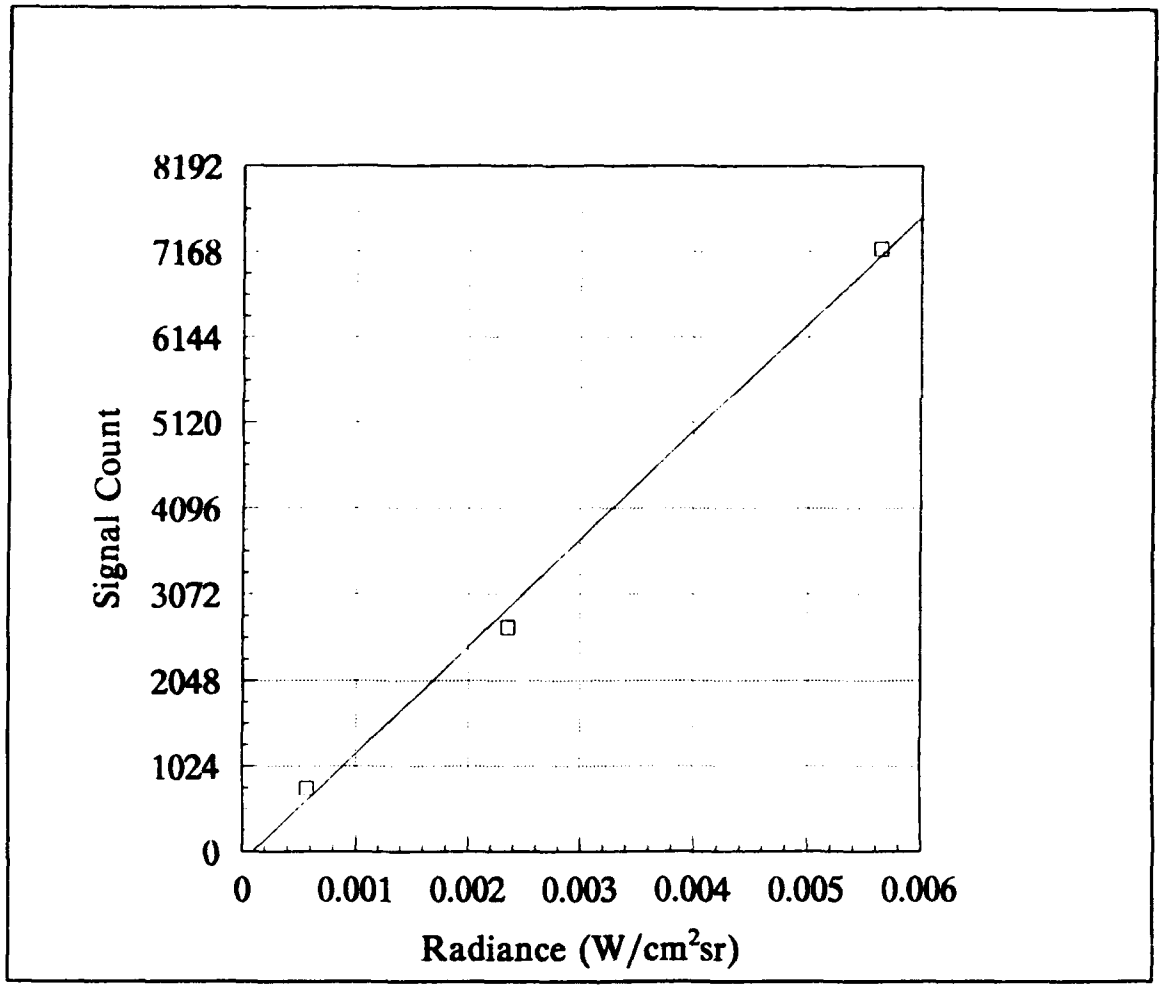

FIGURE B-14. RESPONSIVITY OF THE 880+ WITH THE 7° LENS, NO FILTERS, AND APERTURE 0.

SIGNAL	RADIANCE
759	5.6573e-04
2677	2.3531e-03
7201	5.6426e-03

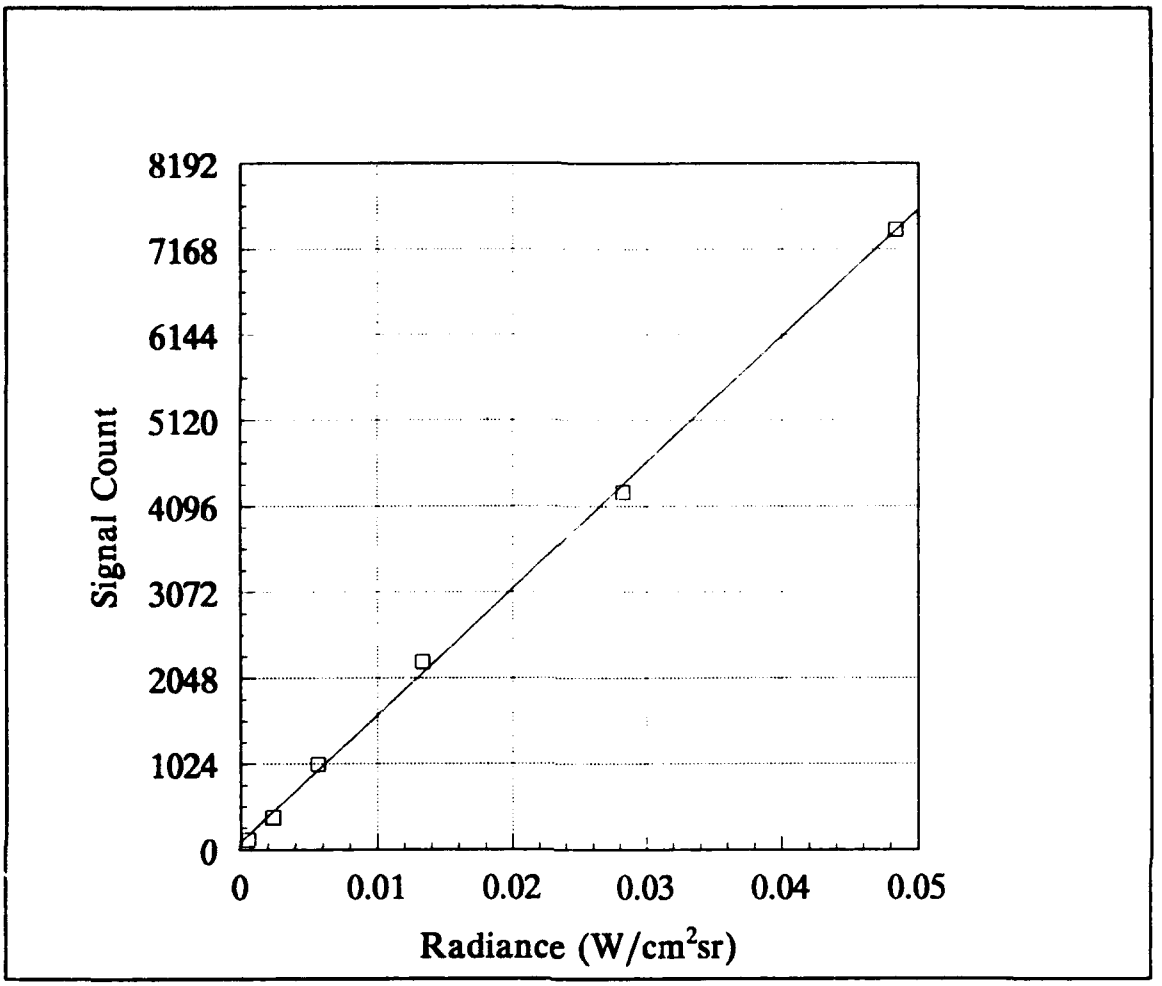

FIGURE B-15. RESPONSIVITY OF THE 880+ WITH THE 7° LENS, NO FILTERS, AND APERTURE 1.

SIGNAL	RADIANCE
117	5.6573e-04
383	2.3531e-03
1017	5.6426e-03
2240	1.3308e-02
4269	2.8240e-02
7401	4.8341e-02

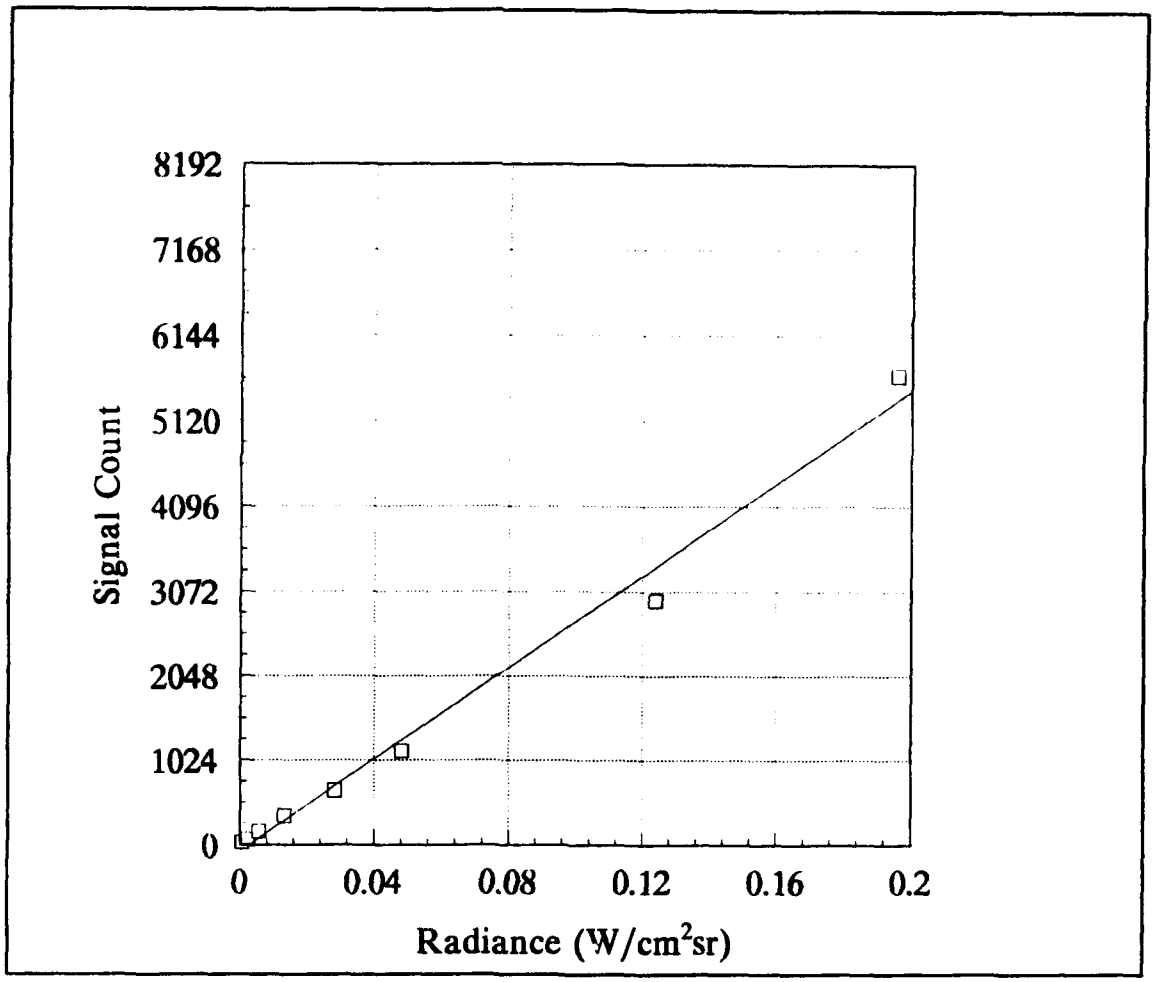

FIGURE B-16. RESPONSIVITY OF THE 880+ WITH THE 7° LENS, NO FILTERS, AND APERTURE 2.

SIGNAL	RADIANCE
30	5.6573e-04
69	2.3531e-03
166	5.6426e-03
351	1.3308e-02
658	2.8204e-02
1131	4.8341e-02
2966	1.2400e-01
5666	1.9599e-01

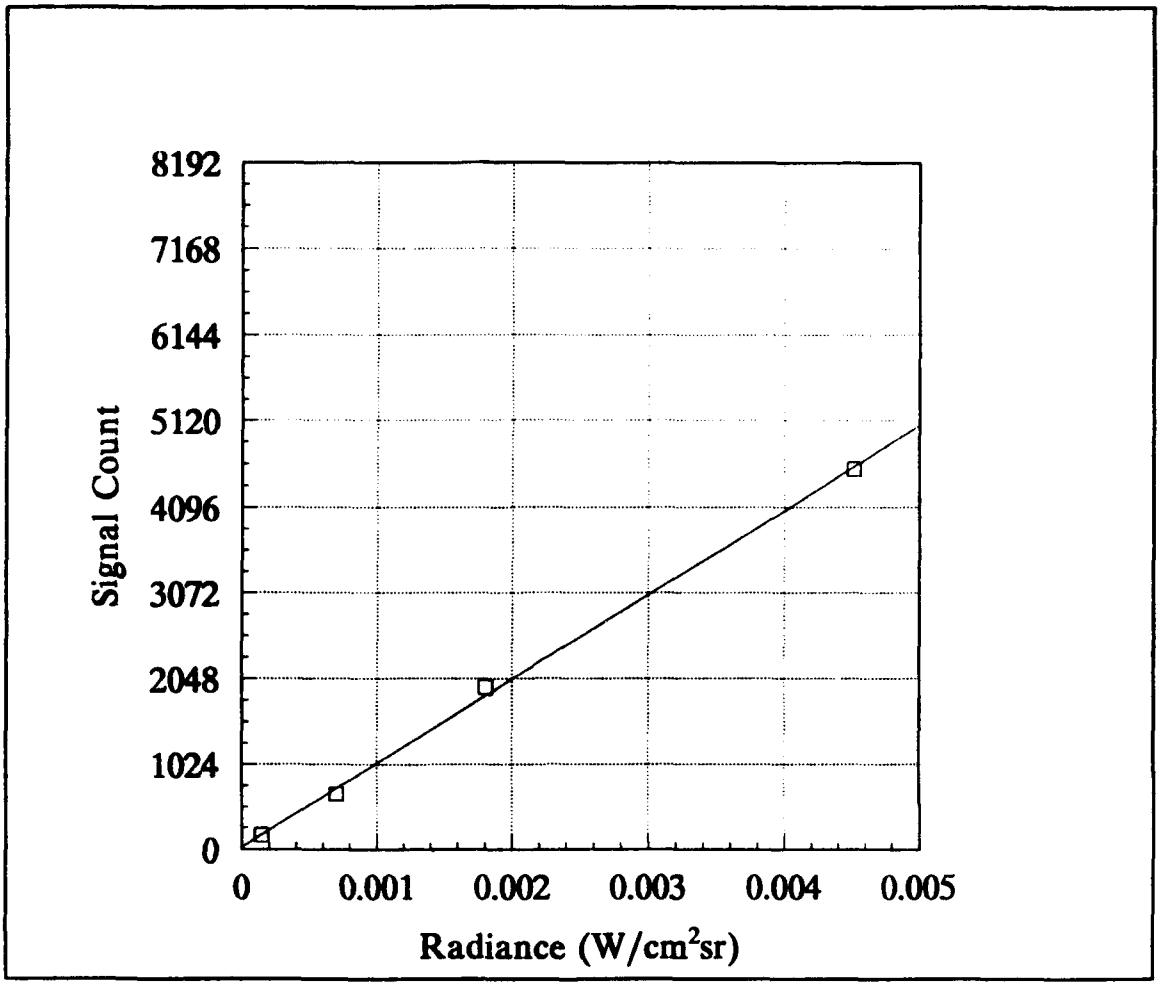

FIGURE B-17. RESPONSIVITY OF THE 880+ WITH THE 7° LENS, YELLOW FILTER, AND APERTURE 0.

SIGNAL	RADIANCE
170	1.4452e-04
666	6.9850e-04
1945	1.8061e-03
4547	4.5109e-03

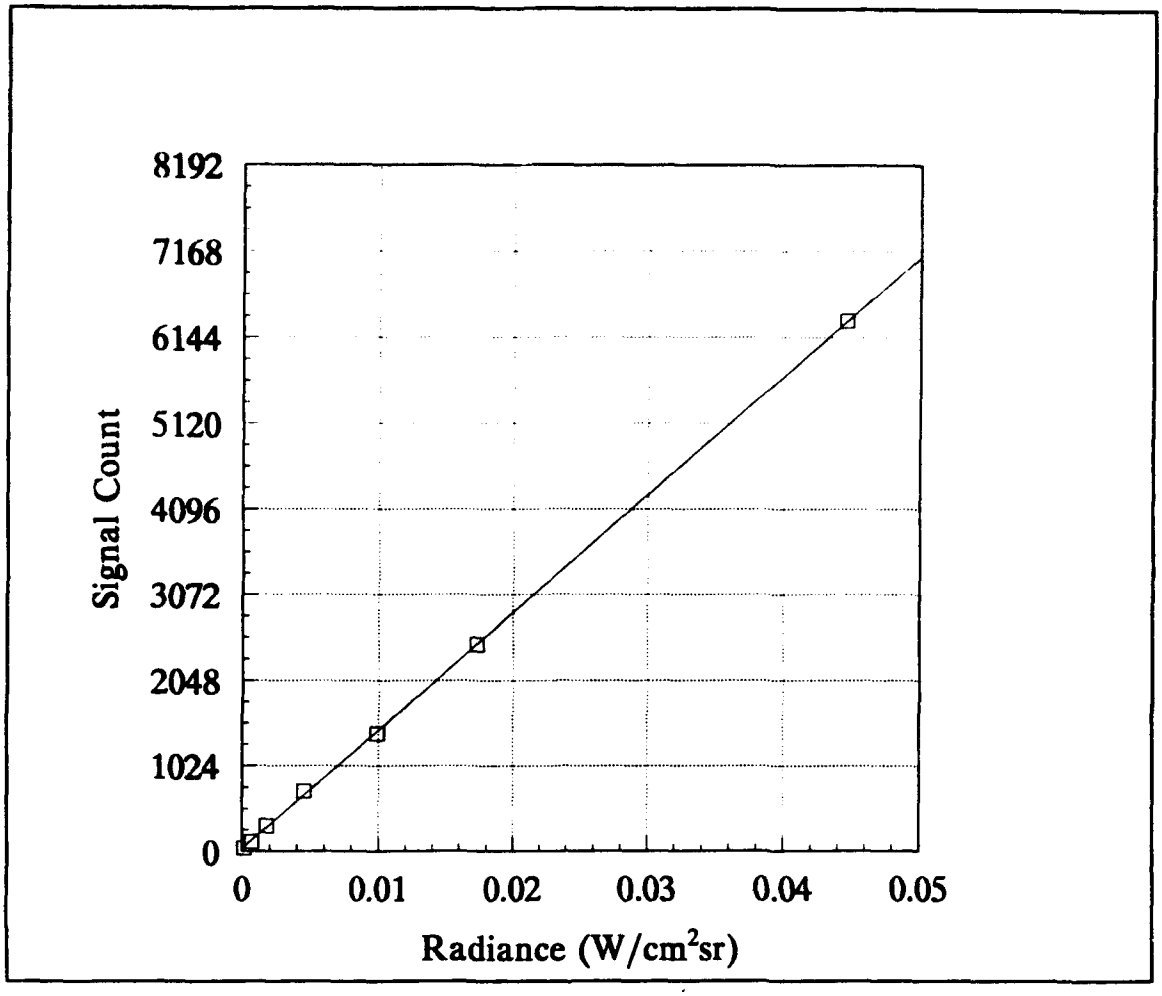

FIGURE B-18. RESPONSIVITY OF THE 880+ WITH THE 7° LENS, YELLOW FILTER, AND APERTURE 1.

SIGNAL	RADIANCE
38	1.4452e-04
113	6.9850e-04
308	1.8061e-03
717	4.5169e-03
1407	9.9286e-03
2471	1.7296e-02
6340	4.4615e-02

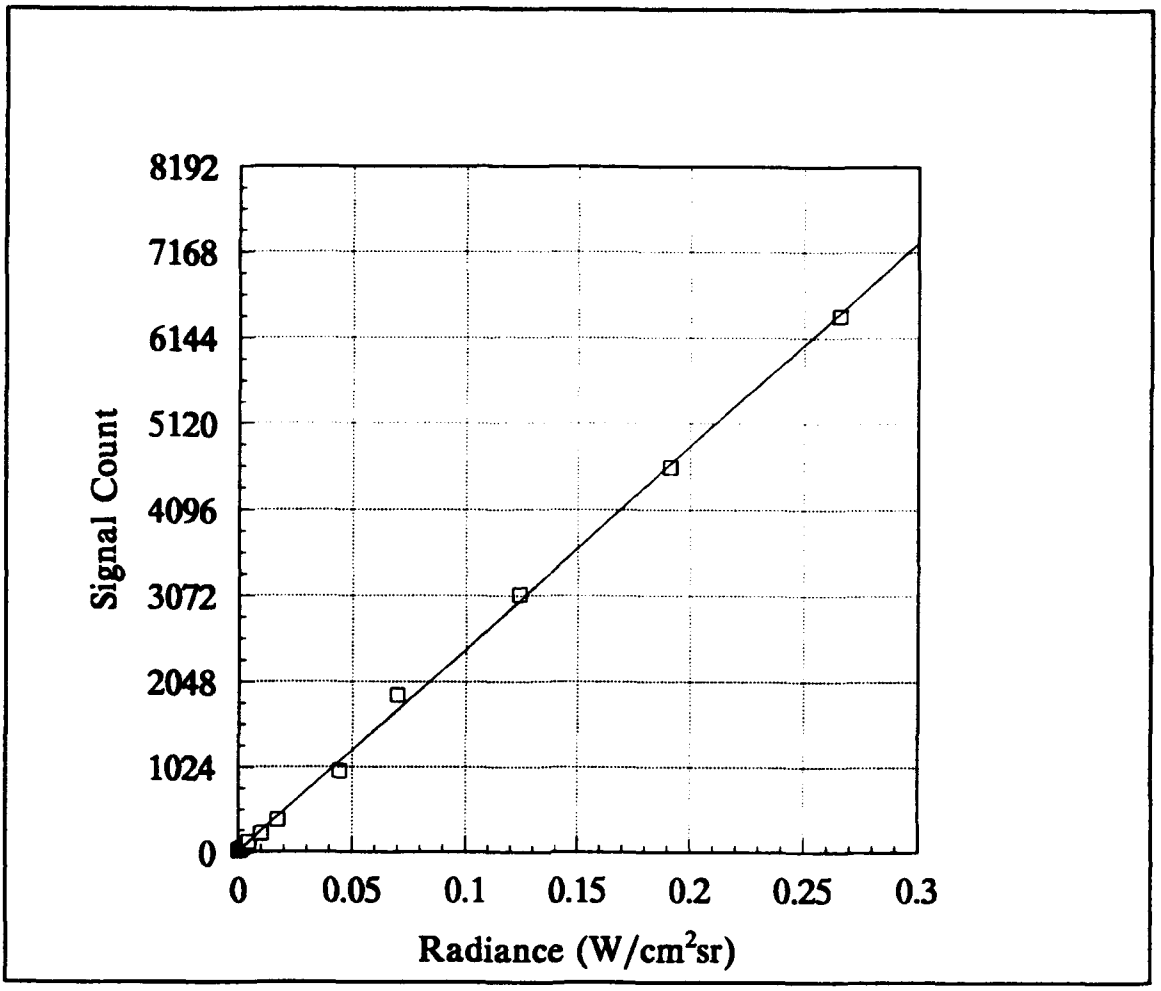

FIGURE B-19. RESPONSIVITY OF THE 880+ WITH THE 7° LENS, YELLOW FILTER, AND APERTURE 2.

SIGNAL	RADIANCE
18	1.4452e-04
28	6.9850e-04
56	1.8061e-03
121	4.5169e-03
223	9.9286e-03
389	1.7296e-02
977	4.4615e-02
1886	6.9897e-02
3084	1.2397e-01
4601	1.9107e-01
6411	2.6545e-01

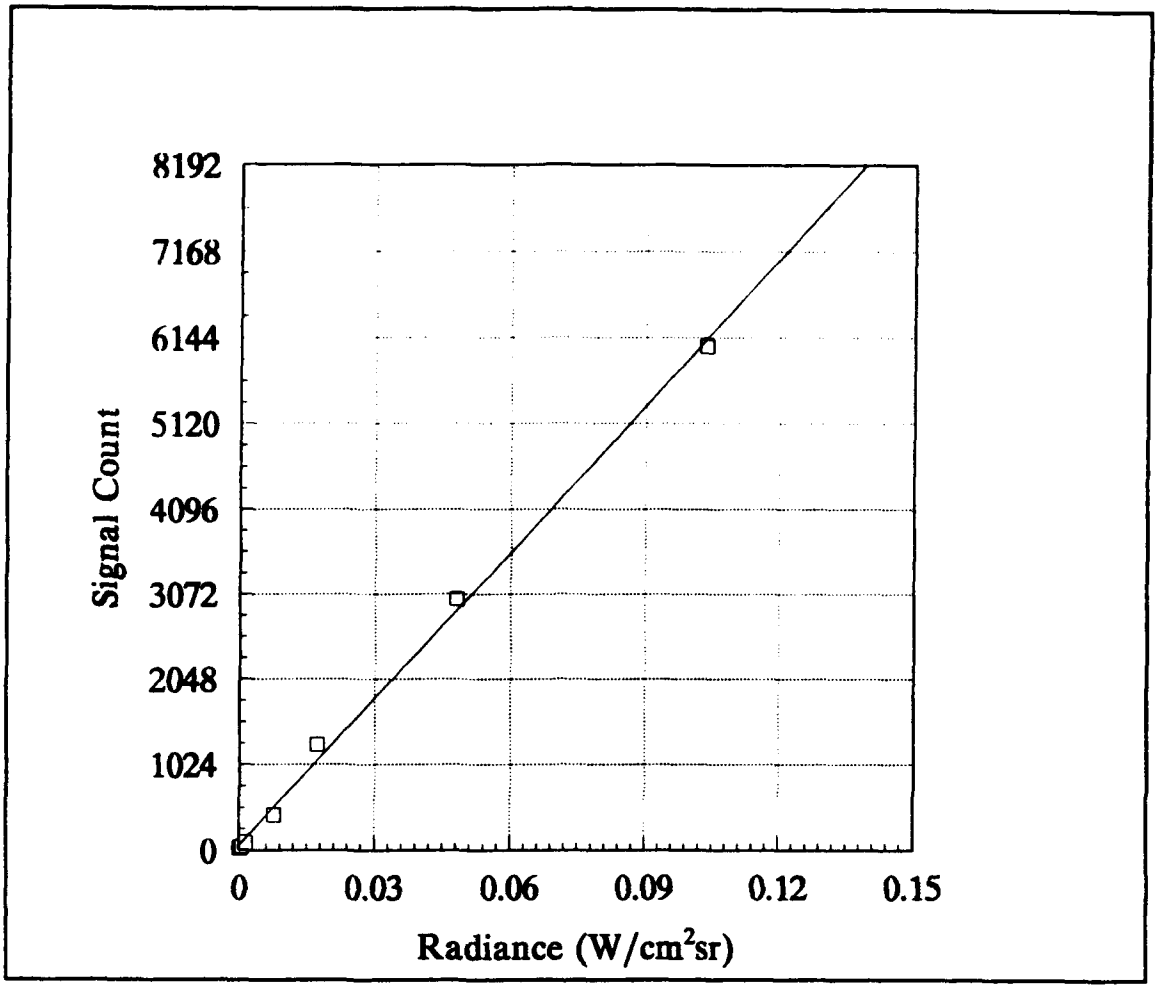

FIGURE B-20. RESPONSIVITY OF THE 880+ WITH THE 7° LENS, BLUE FILTER, AND APERTURE 0.

SIGNAL	RADIANCE
24	1.2498e-04
44	5.1629e-04
93	1.4032e-03
421	7.7220e-03
1263	1.7284e-02
3013	4.8116e-02
6041	1.0364e-01

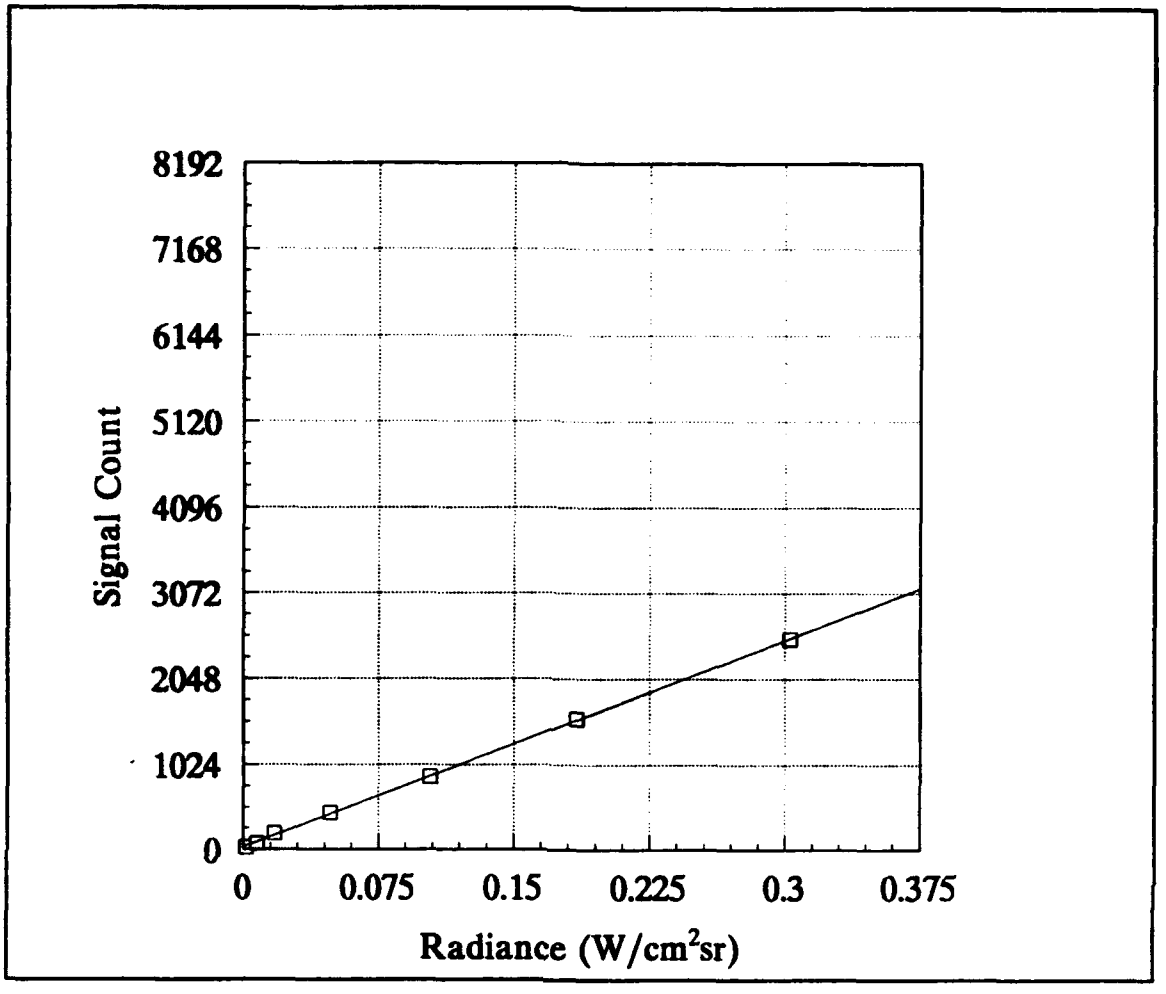

FIGURE B-21. RESPONSIVITY OF THE 880+ WITH THE 7° LENS, BLUE FILTER, AND APERTURE 1.

SIGNAL	RADIANCE
24	1.4032e-03
73	7.7220e-03
194	1.7284e-02
446	4.8116e-02
884	1.0364e-01
1571	1.8476e-01
2523	3.0278e-01

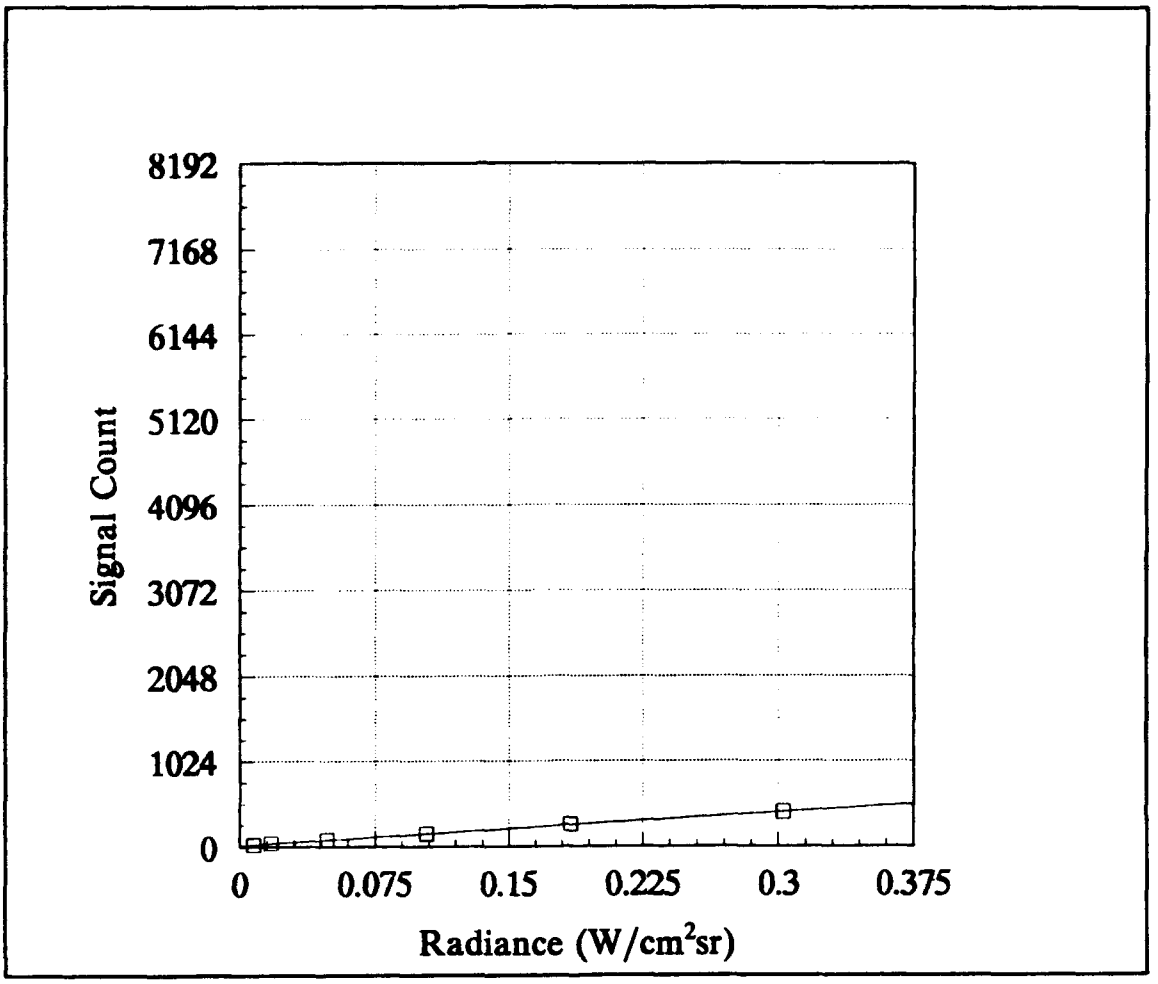

FIGURE B-22. RESPONSIVITY OF THE 880+ WITH THE 7° LENS, BLUE FILTER, AND APERTURE 2.

SIGNAL	RADIANCE
24	7.7220e-03
42	1.7284e-02
83	4.8116e-02
152	1.0364e-01
263	1.8476e-01
413	3.0278e-01

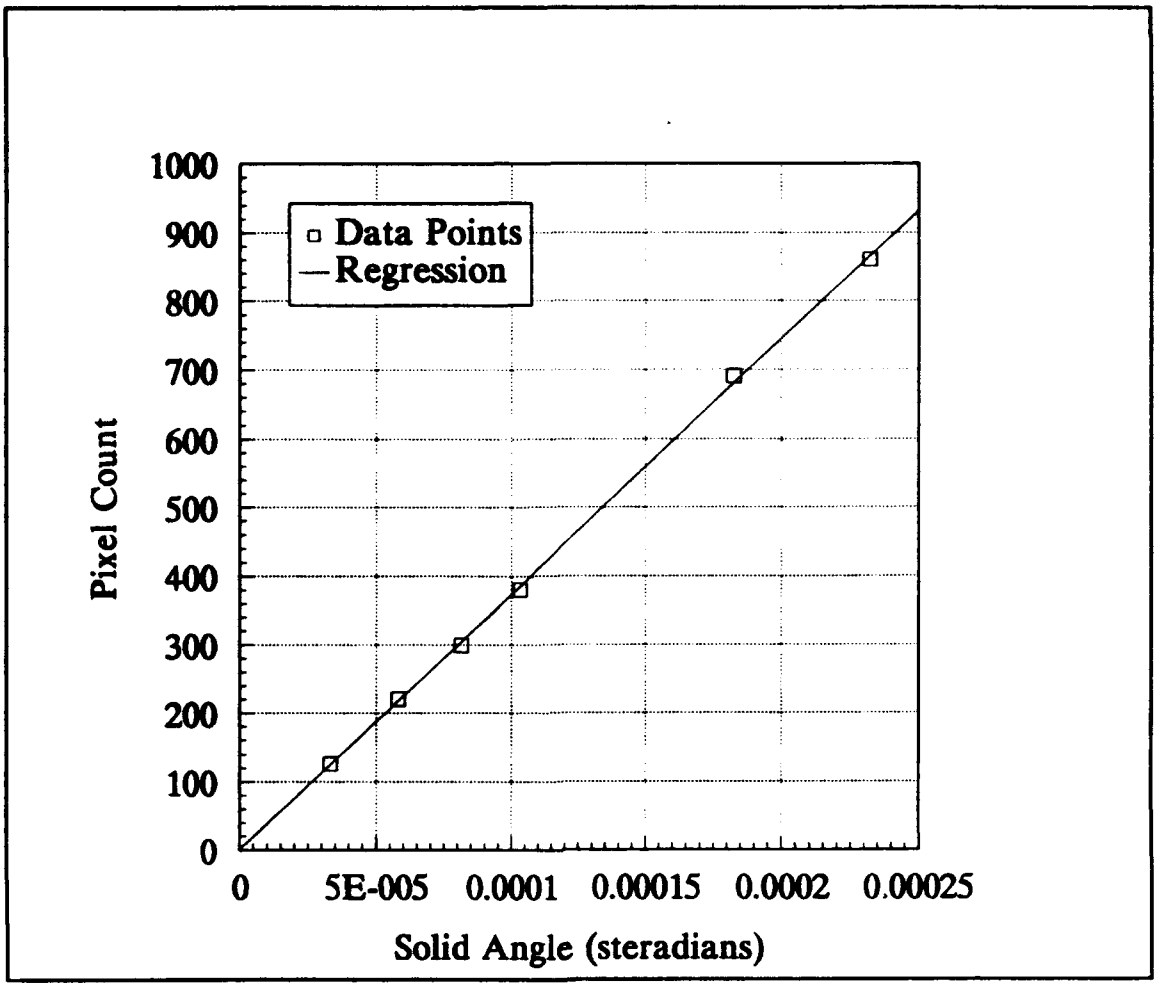

FIGURE B-23. PLOT OF THE SOLID ANGLE SUBTENDED BY THE APERTURE VERSUS THE NUMBER OF PIXELS CONTAINED IN THE IMAGE.

TABLE B-18. DATA FROM THE SPATIAL CALIBRATION. A NUMBER OF SQUARE APERTURES WERE VIEWED WITH THE 880+. THE NUMBER OF PIXELS IN THE IMAGE WAS COUNTED FOR EACH APERTURE. A LEAST-SQUARES REGRESSION OF SOLID ANGLE PER PIXEL WAS PERFORMED ON THE DATA TO GET THE SOLID ANGLE PER PIXEL.

APERTURE AREA (CM^2)	PIXEL COUNT				SOLID ANGLE $\Omega=A/R^2$ SR R=100.0 CM	Ω/PIXEL
	CENTER FOV	TOP FOV	CORNER FOV	AVERAGE		
0.3324	123	133	129	126.3	3.325E-05	6.0436E-07
0.5806	218	223	221	220.7	5.806E-05	4.9329E-07
0.8131	295	305	298	299.3	8.131E-05	4.6112E-07
1.0323	377	379	387	381.0	1.032E-04	4.6216E-07
1.8260	660	686	726	690.7	1.826E-04	4.2396E-07
3.3226	832	850	900	860.7	2.323E-04	4.2679E-07
					SLOPE	4.0432E-07

APPENDIX C

PROGRAMMING AND PROGRAM FLOWCHARTS

This appendix contains a brief description of the computer programs that were created for this project. A flow diagram is provided for each program.

PLRAD.EXE

PLRAD.EXE is a BASIC-coded algorithm that calculates the theoretical spectral radiance for a blackbody of known temperature. The Planck equation is evaluated at specified wavelength intervals and is also integrated over a user-specified waveband. Figure C-1 is a flow diagram of the program PLRAD.EXE.

IMAGER.EXE

IMAGER.EXE was created to provide the means to evaluate images from the 880+ independently from the BRUT. The format of the 880+ image consists of the following: a 512 byte header followed by 78400 bytes of data. The data is organized into 280 rows by 140 columns of two-byte words. The most significant byte (MSB) is the first byte of each two-byte word. The pixel luminance is encoded into the first 13 bits of the word and the 3 high bits must be stripped from the data. Figure C-2 is a flow diagram of IMAGER.EXE.

IMAGER.EXE first reads and decodes the image and then computes a histogram of the pixel gray levels. The bins of the histogram are assigned a specific color. The image and the histogram are then plotted to the screen producing a false color image. The threshold is initially set at the average pixel value over the entire image. The target is located within the image by searching top to bottom and left to right for those pixels above the threshold. This target image is then plotted to the screen with its corresponding histogram. A zoom window, identical to the target image, is also plotted in the center of the screen. Statistics, such as the threshold level and the image and zoom boundaries, are printed on the right of the screen.

After following the initial procedures above, the user can move a cursor within the zoom box to select a pixel level to be used as the threshold. The user may also change the size of the zoom box or the target image to aid in the selection of the threshold. After selecting the threshold, the pixels at or above the threshold are counted and averaged.

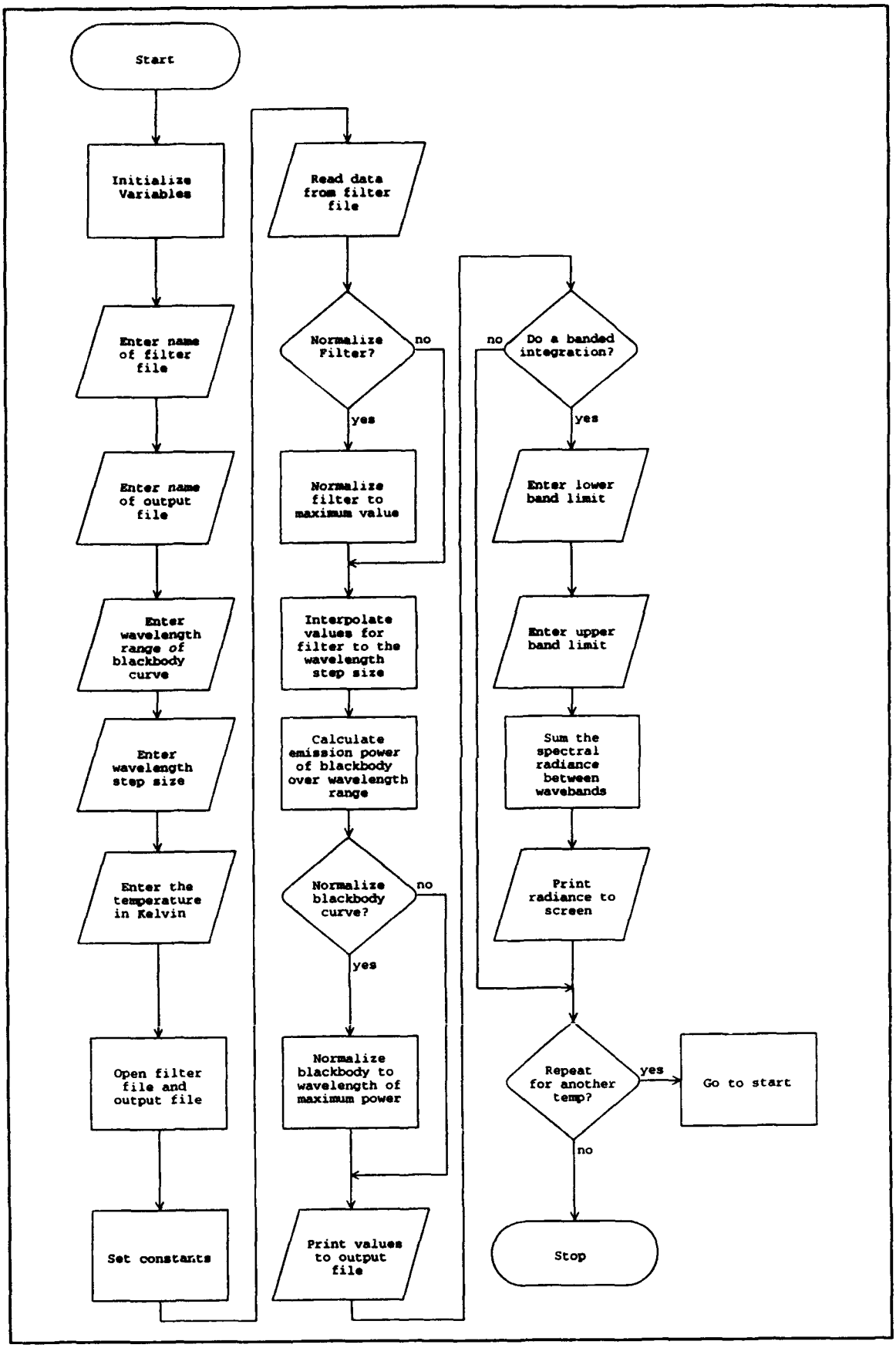

FIGURE C-1. FLOW DIAGRAM OF PLRAD.EXE.

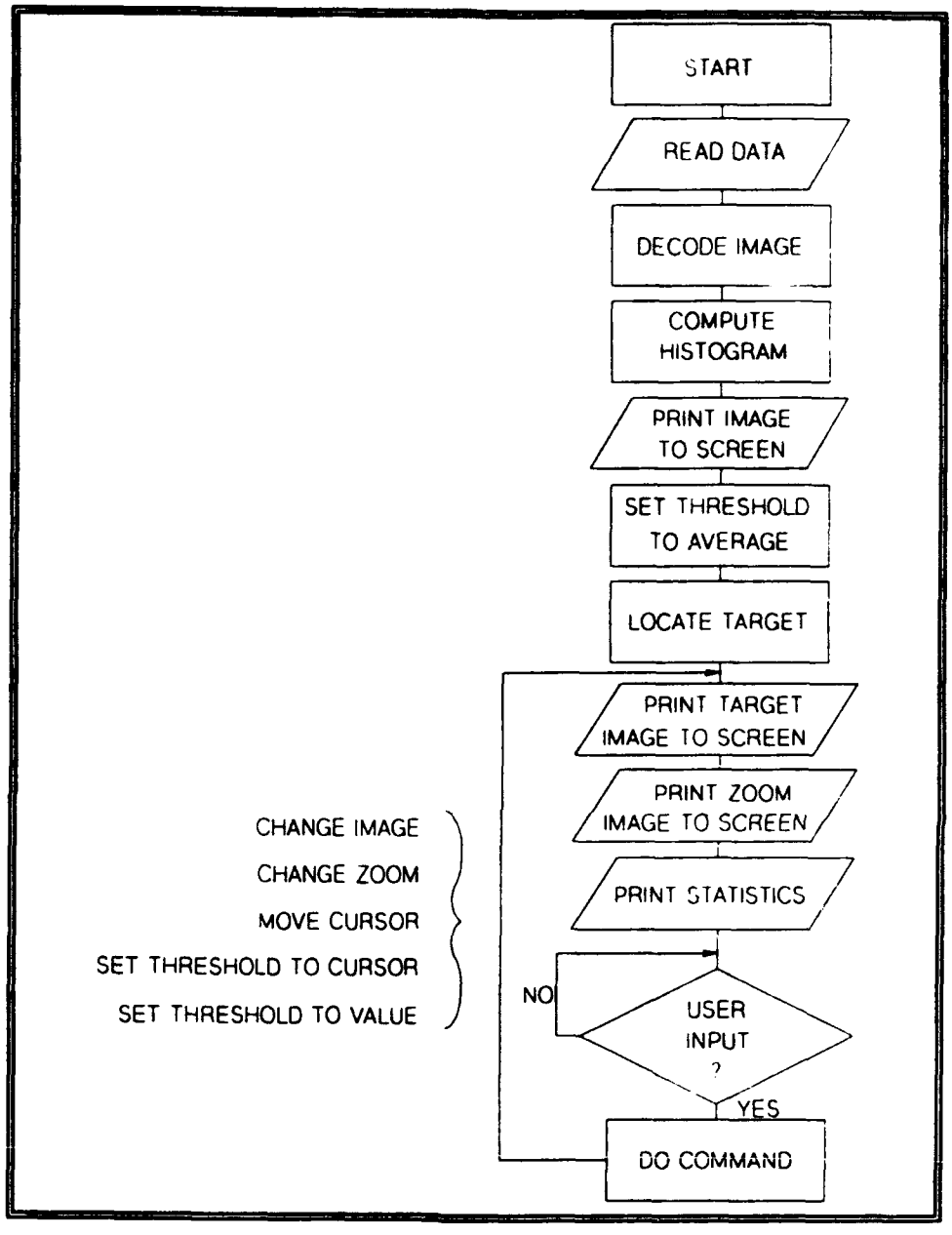

FIGURE C-2. FLOW DIAGRAM OF IMAGER.EXE.